Tran-SET

Transportation Consortium of South-Central States

*Solving Emerging Transportation Resiliency, Sustainability, and Economic Challenges through the Use of Innovative Materials and Construction Methods: From Research to Implementation*

# Evaluation of Bagasse Ash as Cement and Sand Replacement for the Production of Engineered Cementitious Composites (ECC)

**Project No. 19CLSU03**

**Lead University: Louisiana State University**

**Final Report**

**November 2020**

**Disclaimer**

The contents of this report reflect the views of the authors, who are responsible for the facts and the accuracy of the information presented herein. This document is disseminated in the interest of information exchange. The report is funded, partially or entirely, by a grant from the U.S. Department of Transportation's University Transportation Centers Program. However, the U.S. Government assumes no liability for the contents or use thereof.

**Acknowledgements**

The authors would like to acknowledge the financial support for this study by the Transportation Consortium of South-Central States (Tran-SET) and the Louisiana Transportation Research Center (LTRC).

**TECHNICAL DOCUMENTATION PAGE**

| **1. Project No.**<br>19CLSU03 | **2. Government Accession No.** | **3. Recipient's Catalog No.** |
|---|---|---|
| **4. Title and Subtitle** | | **5. Report Date**<br>Nov. 2020 |
| Evaluation of Bagasse Ash as Cement and Sand Replacement for the Production of Engineered Cementitious Composites (ECC) | | **6. Performing Organization Code** |
| **7. Author(s)**<br>PI: Gabriel A. Arce https://orcid.org/0000-0002-3610-8238<br>Co-PI: Marwa M. Hassan https://orcid.org/0000-0001-8087-8232<br>GRA: Sujata Subedi<br>SP: Ana Rivas https://orcid.org/0000-0002-8890-9272<br>SP: Samantha Hidalgo (https://orcid.org/0000-0002-4424-1282<br>SP: Hugo Eguez | | **8. Performing Organization Report No.** |
| **9. Performing Organization Name and Address**<br>Transportation Consortium of South-Central States (Tran-SET) | | **10. Work Unit No. (TRAIS)** |
| University Transportation Center for Region 6<br>3319 Patrick F. Taylor Hall, Louisiana State University, Baton Rouge, LA 70803 | | **11. Contract or Grant No.**<br>69A3551747106 |
| **12. Sponsoring Agency Name and Address**<br>United States of America<br>Department of Transportation | | **13. Type of Report and Period Covered**<br>Final Research Report<br>Aug. 2019 – Nov. 2020 |
| Research and Innovative Technology Administration | | **14. Sponsoring Agency Code** |

**15. Supplementary Notes**
Report uploaded and accessible at Tran-SET's website (http://transet.lsu.edu/).

**16. Abstract**

The objective of this study was to develop novel Engineered Cementitious Composites (ECC) materials implementing sugarcane bagasse ash (SCBA). To this end, the effects on the mechanical and physical properties of ECC materials of: (1) Louisiana raw SCBA (RBA) as a partial and complete replacement of sand (i.e., class S mixtures); (2) Louisiana post-processed SCBA (PBA) as a partial replacement of cement (i.e., class C mixtures); and (3) Ecuador raw SCBA (EBA) as a partial and complete replacement of sand (i.e., class S-E mixtures) were studied. Sand replacement levels with RBA and EBA evaluated were 25, 50, 75, and 100% (by volume), while cement replacement levels with PBA studied were 40, 50, and 60% (by mass). RBA and EBA were subjected to minor processing by drying and sieving to remove moisture and coarse impurities. On the other hand, PBA was produced by further processing of RBA through burning and grinding. RBA and EBA were mainly composed of silica; yet, presented high carbon content and large particle size relative to cement. Conversely, PBA exhibited low carbon content and small particle size. Tests conducted for class S and class C mixtures included compressive strength, uniaxial tensile, surface resistivity, shrinkage, coefficient of thermal expansion, and slant shear tests. In the case of S-E mixtures, tests conducted included compressive strength and flexural strength tests. The use of RBA as sand replacement caused minor reductions in the compressive strength of ECC (up to 11%), yet it produced a dramatic improvement in the tensile ductility (up to 311%). Moreover, the tensile strength of all RBA admixed ECC also improved (up to 22.3%). Implementation of RBA also produced a decrease in surface resistivity and an increase in shrinkage. For class S-E mixtures, the implementation of EBA as sand replacement produced an increase in compressive strength and flexural strength. For class C mixtures, the implementation of PBA as cement replacement produced significant reductions in compressive strength (up to 39.1%) and tensile strength (up to 28.1%). Nevertheless, it increased the tensile ductility of the composites (up to 85%). Furthermore, the surface resistivity and shrinkage of PBA admixed ECC increased with the increment in cement replacement with PBA.

| **17. Key Words** | **18. Distribution Statement** |
|---|---|
| ECC, Bagasse Ash, Concrete, Durability, Repair, Pavements, Engineered Cementitious Composite | No restrictions. This document is available through the National Technical Information Service, Springfield, VA 22161. |

| **19. Security Classif. (of this report)** | **20. Security Classif. (of this page)** | **21. No. of Pages** | **22. Price** |
|---|---|---|---|
| Unclassified | Unclassified | 69 | |

**Form DOT F 1700.7 (8-72)** **Reproduction of completed page authorized.**

# SI* (MODERN METRIC) CONVERSION FACTORS

## APPROXIMATE CONVERSIONS TO SI UNITS

| Symbol | When You Know | Multiply By | To Find | Symbol |
|---|---|---|---|---|
| | | **LENGTH** | | |
| in | inches | 25.4 | millimeters | mm |
| ft | feet | 0.305 | meters | m |
| yd | yards | 0.914 | meters | m |
| mi | miles | 1.61 | kilometers | km |
| | | **AREA** | | |
| $in^2$ | square inches | 645.2 | square millimeters | $mm^2$ |
| $ft^2$ | square feet | 0.093 | square meters | $m^2$ |
| $yd^2$ | square yard | 0.836 | square meters | $m^2$ |
| ac | acres | 0.405 | hectares | ha |
| $mi^2$ | square miles | 2.59 | square kilometers | $km^2$ |
| | | **VOLUME** | | |
| fl oz | fluid ounces | 29.57 | milliliters | mL |
| gal | gallons | 3.785 | liters | L |
| $ft^3$ | cubic feet | 0.028 | cubic meters | $m^3$ |
| $yd^3$ | cubic yards | 0.765 | cubic meters | $m^3$ |
| | NOTE: volumes greater than 1000 L shall be shown in $m^3$ | | | |
| | | **MASS** | | |
| oz | ounces | 28.35 | grams | g |
| lb | pounds | 0.454 | kilograms | kg |
| T | short tons (2000 lb) | 0.907 | megagrams (or "metric ton") | Mg (or "t") |
| | | **TEMPERATURE (exact degrees)** | | |
| °F | Fahrenheit | 5 (F-32)/9<br>or (F-32)/1.8 | Celsius | °C |
| | | **ILLUMINATION** | | |
| fc | foot-candles | 10.76 | lux | lx |
| fl | foot-Lamberts | 3.426 | $candela/m^2$ | $cd/m^2$ |
| | | **FORCE and PRESSURE or STRESS** | | |
| lbf | poundforce | 4.45 | newtons | N |
| $lbf/in^2$ | poundforce per square inch | 6.89 | kilopascals | kPa |

## APPROXIMATE CONVERSIONS FROM SI UNITS

| Symbol | When You Know | Multiply By | To Find | Symbol |
|---|---|---|---|---|
| | | **LENGTH** | | |
| mm | millimeters | 0.039 | inches | in |
| m | meters | 3.28 | feet | ft |
| m | meters | 1.09 | yards | yd |
| km | kilometers | 0.621 | miles | mi |
| | | **AREA** | | |
| $mm^2$ | square millimeters | 0.0016 | square inches | $in^2$ |
| m | square meters | 10.764 | square feet | $ft^2$ |
| m | square meters | 1.195 | square yards | $yd^2$ |
| ha | hectares | 2.47 | acres | ac |
| km | square kilometers | 0.386 | square miles | $mi^2$ |
| | | **VOLUME** | | |
| mL | milliliters | 0.034 | fluid ounces | fl oz |
| L | liters | 0.264 | gallons | gal |
| m | cubic meters | 35.314 | cubic feet | $ft^3$ |
| m | cubic meters | 1.307 | cubic yards | $yd^3$ |
| | | **MASS** | | |
| g | grams | 0.035 | ounces | oz |
| kg | kilograms | 2.202 | pounds | lb |
| Mg (or "t") | megagrams (or "metric ton") | 1.103 | short tons (2000 lb) | T |
| | | **TEMPERATURE (exact degrees)** | | |
| C | Celsius | 1.8C+32 | Fahrenheit | °F |
| | | **ILLUMINATION** | | |
| lx | lux | 0.0929 | foot-candles | fc |
| $cd/m^2$ | $candela/m^2$ | 0.2919 | foot-Lamberts | fl |
| | | **FORCE and PRESSURE or STRESS** | | |
| N | newtons | 0.225 | poundforce | lbf |
| kPa | kilopascals | 0.145 | poundforce per square inch | $lbf/in^2$ |

**TABLE OF CONTENTS**

## LIST OF FIGURES

## LIST OF TABLES

## ACRONYMS, ABBREVIATIONS, AND SYMBOLS

| | |
|---|---|
| ANOVA | Analysis of Variance |
| ASTM | American Society for Testing and Materials |
| DOTD | Department of Transportation and Development |
| ECC | Engineered Cementitious Composites |
| EDS | Energy Dispersive X-ray Spectroscopy |
| DOTD | Louisiana Department of Transportation and Development |
| HPFRCC | High-Performance Fiber-Reinforced Cementitious Composites |
| HRWR | High Range Water Reducer |
| LSU | Louisiana State University |
| LTRC | Louisiana Transportation Research Center |
| LVDT | Linear Variable Displacement Transducer |
| OPC | Ordinary Portland cement |
| PSH | Pseudo Strain Hardening |
| PVA | Polyvinyl Alcohol |
| SAI | Strength Activity Index |
| SBF | Sugarcane Bagasse Fiber |
| SCBA | Sugarcane Bagasse Ash |
| SCM | Supplementary Cementitious Material |
| SEM | Scanning Electron Microscopy |
| XRD | X-ray Diffraction |
| XRF | X-ray Fluorescence |

# EXECUTIVE SUMMARY

The objective of this study was to develop novel Engineered Cementitious Composites (ECC) materials implementing sugarcane bagasse ash (SCBA) to produce cost-effective and practical ECC for repair and new construction of transportation infrastructure in the region. To this end, the effects on the mechanical and physical properties of ECC materials of: (1) Louisiana raw SCBA (RBA) as a partial and complete replacement of sand (i.e., class S mixtures); (2) Louisiana post-processed SCBA (PBA) as a partial replacement of cement (i.e., class C mixtures); and (3) Ecuador raw SCBA (EBA) as a partial and complete replacement of sand (i.e., class S-E mixtures) were studied. Sand replacement levels with RBA and EBA evaluated included 25, 50, 75, and 100% (by volume), while cement replacement levels with PBA studied included 40, 50, and 60% (by mass). The SCBA labeled as RBA was SCBA collected from a Louisiana sugar mill, which was subjected to minor processing by drying (at 65°C for 10-12 hours) and sieving (using a No. 20 sieve) to remove moisture and coarse impurities. On the other hand, the SCBA labeled as PBA was produced by further processing of RBA by burning (at 450°C for 3 hours) and grinding (in a jar mill at 300 rpm for 35 minutes). The SCBA labeled as EBA was produced in a similar manner to RBA; however, this material was collected from a sugar mill located in Ecuador. RBA was mainly composed of silica and exhibited a total pozzolanic component of 52.5%. However, RBA presented high carbon content, large particle size (i.e., 256 $\mu$m average particle size) relative to cement, and a low strength activity index (SAI) of 71.2%; thus, failing to meet ASTM C618 requirements to be classified as a pozzolan. On the other hand, PBA exhibited low carbon content, small particle size (i.e., 28 $\mu$m average particles), satisfactory SAI (i.e., 78.8%), and a high pozzolanic component (i.e., 72.6%) to be classified as a class N pozzolan per ASTM C618. Furthermore, EBA exhibited a significantly higher SAI (i.e., 91.1%) in comparison to the RBA. However, like RBA, EBA exhibited large particle size (i.e., mean particle size of 248 μm) relative to cement and high carbon content. The important difference in SAI between RBA and EBA highlights the effect of SCBA source on the material properties.

PBA was used as a supplementary cementitious material (SCM) in ECC mixtures. In contrast, RBA and EBA were used as a sand replacement since these could not be used as SCMs and exhibited a particle size comparable to that of the microsilica sand commonly used in ECC. Tests conducted to evaluate the class S and class C mixtures synthesized in this study included compressive strength test (ASTM C39), uniaxial tensile test (per JSCE recommendations), surface resistivity test (AASHTO T358), shrinkage test (ASTM C157), and coefficient of thermal expansion test (ASTM C531), and slant shear test. In the case of S-E mixtures produced in Ecuador, tests conducted included compressive strength test (ASTM C109) and flexural strength test (ASTM C293).

For class S mixtures, it was found that the increase in sand replacement with RBA caused minor reductions in the compressive strength of ECC materials at 28 days of curing. This was attributed to the increment in air content observed, which was associated with the higher HRWR dosage required to produce workable ECC mixtures with increasing contents of RBA. Furthermore, the implementation of RBA as sand replacement produced a dramatic improvement in the tensile ductility of the ECCs. Relative to control, the maximum enhancement in tensile strain capacity reported was 311%, which occurred at 100% of sand replacement with RBA. Moreover, the tensile strength of all RBA admixed ECC also improved compared to control, where the maximum reported an increase of 22.3% occurred at 25% of sand replacement with RBA. The increase in the tensile ductility of the composites was attributed to the likely reduction of $J_{tip}$ and enhancement

of fiber dispersion (due to the decrease of the aggregate particle size), as well as the potential increase in $J_b'$ (due to the decrease in fiber/matrix chemical bond from the possible fiber carbon coating effect produced by RBA). On the other hand, the tensile strength enhancement observed was attributed to RBA's filler and/or pozzolanic effect, which likely improved the fiber/matrix frictional bond. Upon completion of the uniaxial tensile test for all class S ECC, the average residual crack width ranged from 51.3 to 58.2 μm; thus, suggesting an excellent durability potential. The surface resistivity of class S ECC materials showed a progressive decrease with the increment in sand replacement with RBA. Yet, the control mixture and S-25 fell in the category of low CIP. Furthermore, ECC mixtures using 50, 75, and 100% RBA as a sand replacement fell in the category of medium CIP. The decrease in surface resistivity with RBA addition was attributed to the increase in air content reported, RBA's porous nature, and RBA's high carbon content. Apart from S-25 at 28 days of curing, all ECC implementing RBA showed an increase in shrinkage compared to control at all ages of curing. The higher shrinkage observed for RBA admixed ECC was attributed to the decrease in aggregate particle size due to the replacement of fine river sand with RBA. However, a clear relationship between RBA content and shrinkage was not evident. Due to its satisfactory mechanical strength, high tensile ductility, and proper fresh state workability, ECC mixture S-75 was selected to evaluate the bond with concrete under the slant shear test. The composite specimen did not fail in the slant surface, suggesting excellent bond characteristics of this novel composite material with concrete.

The implementation of cement replacement with PBA in class C mixtures produced significant reductions in compressive strength. The maximum decrease reported of 39.1% occurred at the maximum cement replacement level evaluated of 60% by weight. The important decrease observed in compressive strength was attributed to the fact that the specimens were evaluated at 28 days of curing; thus, substantially limiting the contribution of the pozzolanic reaction of PBA to the strength gain of the ECC. Nevertheless, the use of PBA as partial cement replacement did generate an enhancement in the tensile ductility of all the PBA admixed ECC. Compared to the control ECC mixture, a tensile strain capacity increase of up to 85% was reported for the ECC material utilizing a 50% cement replacement with PBA. These observations were primarily attributed to a likely decrease in $J_{tip}$ (due to the weakening of the cementitious matrix with PBA addition) and a possible increase in $J_b'$ (associated with the decrease in the fiber/matrix chemical bond due to the reduction in the concentration of calcium ions in the matrix). Furthermore, compared to control, the tensile strength of the class C mixture using 40% of cement replacement with PBA marginally increased (i.e., by 4.1%); yet, mixtures using 50% and 60% of cement replacement with PBA exhibited lower tensile strengths compared to control with the maximum decrement being 28.1% at 60% of cement replacement with PBA. The surface resistivity of PBA admixed ECC mixtures increased with the increment in cement replacement with PBA. However, all class C mixtures, including control, fell into the category of high CIP. This was attributed to the fact that class C mixtures did not use fly ash in its composition. Moreover, the progressive enhancement in surface resistivity with PBA increase was attributed to PBA's filler/pozzolanic effect. Nevertheless, it was recognized that this effect was much less influential as that of fly ash since even at 60% cement replacement with PBA, surface resistivity values for class C mixtures were low compared to those observed for class S mixtures (which did implement fly ash). The lack of fly ash in class C mixtures was also associated to the significant increase in shrinkage values during curing reported for class C mixtures compared to class S mixtures. Moreover, except for C-50 at 7 days of curing, shrinkage values for PBA admixed ECC mixtures observed were higher than control at all curing ages. Furthermore, a distinctive relationship between shrinkage and PBA content was observed at 14 and 28 days of

curing, where the maximum shrinkage increase reported at 28 days of curing was 24.4% for C-60 (compared to control). Since ECC mixture C-50 was the composite exhibiting the highest tensile ductility from all the class C materials, it was selected for slant shear test evaluation. The failure mode of C-50 on a concrete substrate did not occur in the slant surface; therefore, indicating excellent bond properties of this material.

For class S-E mixtures, the implementation of sand replacement with EBA produced an increase in compressive strength of ECC at 7 and 28 days of curing. The maximum increase in compressive reported at 28 days was of 21.0% and occurred at a sand replacement with EBA of 75%. Improvements observed were attributed to the high SAI exhibited by EBA. In the case of flexural strength, similar improvements were observed for EBA admixed ECC materials. The maximum enhancement in flexural strength of 21.5% at 28 days of curing was reported for the ECC mixture using 100% of sand replaced with EBA. These improvements were attributed to EBA's pozzolanic activity and/or filler effect, which likely enhanced the fiber bridging capacity of the EBA admixed ECC mixtures.

The experimental results and analysis show that the beneficial use of raw SCBA as sand replacement in ECC exhibits great promise as it yields composites exhibiting satisfactory mechanical strength and high tensile ductility. As such, future research should be conducted on evaluating the long-term properties and durability of ECCs using raw SCBA as sand replacement. On the other hand, the use of PBA as cement replacement in ECC presents several challenges and significantly underperforms in contrast to other SCMs such as fly ash conventionally used in the manufacture of ECC. Yet, the evaluation of hybrid systems implementing fly ash and PBA may open the possibility of using this agricultural by-product as a partial replacement of cement in ECC.

# 1. INTRODUCTION

Concrete is brittle and possesses a low tensile strength. This allows for the occurrence and propagation of cracks due to loading or changing environmental conditions (*1*). Moreover, cracks in concrete are highly related to the deterioration and failure of concrete pavements, overlay systems, and bridges; hence, the improvements of crack resistance in concrete materials are of particular interest for the transportation sector. Adding fibers to concrete is a well-established practice to mitigate the brittle behavior of concrete by limiting crack growth and propagation. Yet, traditional fiber reinforced concrete (FRC) produces relatively marginal improvements in ductility and tensile strength. Furthermore, FRC continues to exhibit a strain-softening phenomenon after first cracking (single localized crack growth associated with a decrease in load carrying capacity) under tensile stresses, as shown in Figure 1a. For this reason, high-performance fiber-reinforced cementitious composites (HPFRCC) were developed as a superior alternative to mitigate concrete brittleness and its weak behavior under tensile stresses. In contrast to FRC, HPRFRCC exhibit a strain hardening performance after first cracking under tensile stresses. Strain-hardening occurs due to the inelastic deformation of the composite through the formation of multiple micro-cracks (*2*). This inelastic deformation occurs with an increase in load-carrying capacity and is referred to as pseudo-strain-hardening (PSH) to differentiate this mechanism from the strain-hardening phenomena observed in metals (*3*). Early versions of HPFRCC, such as SIFCON (Slurry Infiltrated Fiber Concrete), were designed by using high contents of fiber (4-20% volume fraction) and achieved desirable improvements in tensile strength and ductility (*4*). However, high fiber content limited its application in the field due to constructability issues and cost.

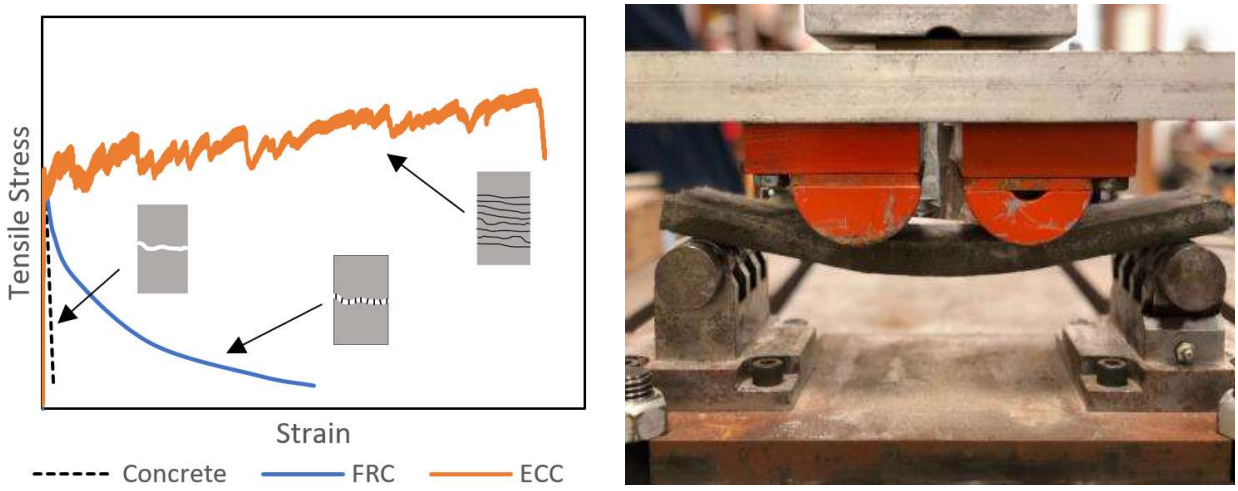


**(a)** **(b)**

**Figure 1. (a) Stress vs. Strain behavior of cementitious materials in tension, (b) High deflection capacity of ECC material developed at LSU.**

Engineered Cementitious Composites (ECC), also known as bendable concrete (Figure 1b), are a novel class of HPFRCC that are designed and optimized based on micromechanics principles to exhibit a high tensile ductility (1 to 8% strain capacity in tension) through a robust PSH behavior at low fiber content (usually 2% volume fraction) (*5*). This makes ECC practical to be implemented in the field using existing equipment and techniques and significantly more cost-effective than early versions of HPFRCC. Research on ECC durability has shown promising results against major types of concrete deterioration, including corrosion, freeze-thaw, alkali-silica reaction, and sulfate attack (*4*, *6*, *7*). Furthermore, ECC exhibits significant self-healing characteristics because of its

tight crack width that allows autogenous healing mechanisms of cementitious materials to be effective; thus, further enhancing the durability potential of this novel composites (*8*, *9*). To date, ECC has been applied in bridge deck link slabs, shear keys, and several repairs (wall retrofit, patch repair of bridge decks, repair of irrigation channels, earth-retaining walls, etc.) of concrete structures with successful performance (*4*, *10–12*). While ECC properties are promising for the repair and new construction of transportation infrastructure, its high cost (in contrast to conventional concrete) limits its widespread application. ECC typically uses a 2% volume fraction of polyvinyl alcohol (PVA) fiber, microsilica sand, and high cement contents, which significantly increase its cost compared to regular concrete. Consequently, the implementation of low-cost materials that can partially or completely replace cement and microsilica sand can provide more cost-effective and practical ECC materials.

In Louisiana, the sugar production industry is of immense relevance generating a yearly economic value of $3 billion (*13*). According to the American Sugarcane League, in 2018, more than 16.9 million tons of sugarcane was harvested in the state yielding 1.8 million tons of sugar and nearly 3.5 million tons of a fibrous by-product sugarcane bagasse fiber (SBF) (*14*). Typically, bagasse is burned by the sugar mills to generate energy and mitigate the fire hazard presented by dry fibrous bagasse (see Figure 2a) (*15*). Depending on the bagasse's burning process, the obtained ash yield ranges between 3% to 9%. This ash by-product is known as sugarcane bagasse ash (SCBA) and is considered an agricultural waste with no economic value. In addition, bagasse ash constitutes a potential environmental hazard, leading to containment and disposal costs to the industry (see Figure 2b). Based on the literature, when properly processed by sieving (to remove coarse particles), controlled burning (to remove excess carbon content), and grinding (to reduce particle size), SCBA can exhibit significant pozzolanic activity due to its chemical composition and small particle size (*16–21*). Typically, processed SCBA consists of more than 60% silicon oxide ($SiO_2$) and 7% aluminum oxide ($Al_2O_3$) by weight. In turn, this makes bagasse ash an excellent candidate for an affordable supplementary cementitious material (SCM) to partially replace cement in the production of ECC.

**(a)** **(b)**

**Figure 2. Land disposal of: (a) Bagasse ash and (b) Bagasse fiber.**

While SCBA can serve as an SCM material when adequately processed, raw bagasse ash (i.e., SCBA obtained directly from the mill without further processing) exhibits high carbon content and low pozzolanic activity. While raw SCBA cannot be utilized as an SCM, this lower quality ash presents excellent potential as a highly fine aggregate material to replace the expensive microsilica sand (which can be more expensive than cement) used in ECC production. This project aims to

evaluate the feasibility of utilizing bagasse ash with different levels of quality as cement and fine aggregate replacement for the manufacture of ECC to reduce its cost, make it more practical, and increase its greenness.

## 1.1 ECC Design

Two primary conditions need to be met for the PSH behavior of ECC materials to occur, the strength criterion and the energy criterion (*22*). The strength criterion (Eq. 1) guarantees adequate fiber-bridging capacity ($\sigma_0$) upon crack initiation and requires the first-cracking strength of the composite ($\sigma_{cs}$) to be less than the fiber-bridging capacity on any plausible crack plane (*22*).

$$\sigma_0 \geq \sigma_{cs} \quad [1]$$

where $\sigma_{cs}$ is determined by the preexisting initial flaw size and matrix fracture toughness ($K_m$).If this criterion is not met (i.e., the insufficient fiber-bridging capacity to carry tensile load upon cracking of the cementitious matrix, the composite would fail due to the fiber rupture or pullout upon crack initiation (*23*).

The second condition, the energy criterion (Eq. 2), guarantees the requirement for steady-state flat crack propagation, as first demonstrated by Marshall and Cox using J-integral analysis (*24*, *25*).

$$J_b' = \sigma_0\delta_0 - \int_0^{\delta_0} \sigma(\delta)\, d\delta \geq J_{tip} = \sigma_{ss}\delta_{ss} - \int_0^{\delta_{ss}} \sigma(\delta) d\delta \quad [2]$$

Where $J_b'$ is the complementary energy of the fiber-bridging relation; $\delta_0$ is the crack opening corresponding to $\sigma_0$; $\sigma(\delta)$ is the fiber-bridging relation; $J_{tip}$ is the crack-tip matrix toughness; $\sigma_{ss}$ is the steady-state cracking stress; and $\delta_{ss}$ is the crack opening corresponding to $\sigma_{ss}$.

Per equation 2, $J_b'$ needs to be equal or greater than $J_{tip}$ for the energy criteria to be satisfied. If the crack-tip matrix toughness $J_{tip}$ (sensitive to the details of the cementitious matrix design) is too high, or inadequate energy absorption occurs in the increasing phase of the $\sigma(\delta)$ curve, then the steady-state crack propagation is hard to be achieved (*26*, *27*). Figure 3 presents a graphical representation of $J_b'$ and $J_{tip}$ on a schematic fiber-bridging curve. From Eqs.1 and 2, successful design of ECC is achieved when, both, the strength and the energy criteria are satisfied. Consistent with the conditions for PSH behavior presented above, if the ratios $J_b'/J_{tip}$ and $\sigma_0/\sigma_{cs}$ named pseudo strain-hardening performance indexes (PSH indexes) are greater than one then, both, the strength and the energy criteria will be met. Otherwise, if any of the two ratios are less than one, the tensile-softening behavior of fiber reinforced concrete (FRC) will prevail (as shown in Figure 1a). It is important to notice that the equality signs on Eq.1 and Eq.2 assume a perfectly homogeneous material; thus, in practice the need for PSH indexes greater than one are required for robust PSH performance (*2*, *24*). Theoretical and experimental evidence suggests that a PSH strength index of 1.3 and a PSH energy index of 2.7 correlates with saturated multiple cracking behaviors of fiber-reinforced cementitious composites (*28*). Saturated PSH behavior refers to the before crack spacing is too small for further crack formation (due to the inability of sufficient stress

transfer from fibers maximum multiple cracking intensity that can occur in fiber-reinforced cementitious composites crack plane (*29*).

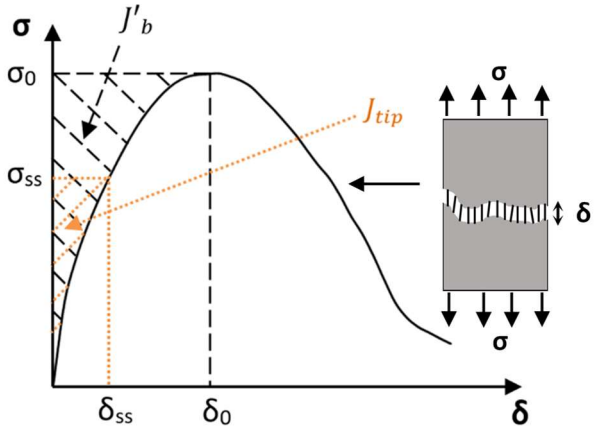


**Figure 3. Fiber bridging relation, $\sigma(\delta)$ curve (adapted from Noorvand et al. (*30*)).**

## 2. OBJECTIVES

The objective of this study is to develop novel Engineered Cementitious Composite (ECC) materials implementing sugarcane bagasse ash (SCBA) to produce cost-effective and practical ECC materials for repair and new construction of transportation infrastructure in the region.

# 3. LITERATURE REVIEW

A comprehensive literature review was conducted to understand the finding from previous studies evaluating the use of SCBA in concrete materials. The literature review primarily focused on the implementation of SCBA as a replacement of fine aggregate and/or cement in cementitious composites. Furthermore, it also reviews previous studies that focused on enhancing ECC mixtures' greenness by replacing microsilica sand and/or cement with sustainable alternative products.

## 3.1. Use of Bagasse Ash in Cementitious Materials

### *3.1.1. Use of Bagasse Ash as Fine Aggregate*

Different studies have been conducted to evaluate the feasibility of using SCBA as a substitute to fine aggregate in concrete mixtures. Modani and Vyawahare (*31*) investigated the influence of replacing fine aggregate with raw bagasse ash (collected from a local sugar factory in India) in concrete mixtures. A total of five mixtures with different replacement levels, i.e., 0%, 10%, 20%, 30%, and 40% by volume of fine aggregate with raw SCBA were produced in this study. The study evaluated fresh concrete properties (i.e., slump cone test and compaction factor test) and hardened concrete properties (i.e., compressive strength, sorptivity, and splitting tensile strength test) for all concrete mixtures produced in the study. The test results revealed that raw SCBA could be used as a partial replacement to fine aggregate without compromising its hardened properties (*31*). Furthermore, a decrease in a slump was observed with the increase in SCBA; however, the loss in workability was not significant at the 10% and 20% aggregate replacement level.

In a similar study, Sua-iam and Makul (*32*) replaced high volumes of fine aggregate in concrete mixtures with raw SCBA (collected from a local sugar mill in Thailand) and/or limestone powder. The influence of bagasse ash as fine aggregate was investigated by producing concrete mixtures with different replacement levels of fine aggregate (i.e., 0%, 10%, 20%, 40%, 60%, 80%, and 100% by volume) with only bagasse ash, only limestone powder and with an equal volume of limestone powder and bagasse ash. The study evaluated all concrete mixtures' workability by conducting slump flow, $T_{50cm}$ slump flow time, V-funnel flow time, and J-ring flow. In addition, the study also assessed the hardened properties (ultrasonic pulse velocity and compressive strength) of each concrete mixtures (*32*). The test results revealed that replacing fine aggregates with 20% limestone powder and 20% bagasse ash yields a mixture with improved workability and hardened properties compared to the control mixture. Nevertheless, the improvement in compressive strength due to the replacement of fine aggregates was marginal (*32*). In terms of the mixtures using only SCBA as a substitute to fine aggregate, a significant decrease in workability with the increase in aggregate replacement level was observed. Similarly, increasing amounts of SCBA generally decreased the strength at all curing ages due to the greater porosity of the material.

Sales and Lima (33) used raw SCBA (collected from sugar mills located in São Carlos, SP, Brazil) as sand replacement in concrete and mortar mixtures. Different replacement levels of sand with SCBA (by mass) including 0%, 10%, 15%, 20%, 30%, 50%, and 100% were evaluated in this study. The influence of SCBA as a sand replacement in mortars and concrete were investigated by evaluating compressive strength, tensile strength, and elastic modulus of each mixture. The experimental characterization of raw SCBA revealed that SCBA presents similar physical properties to that of natural sand. Furthermore, test results revealed that, when used as a partial

replacement to sand, SCBA produces mortars and concrete with similar mechanical properties as mixtures with natural sand (i.e., control) (33).

A study by Humberto et al. (34) assessed the properties of mortars using low volumes of SCBA as a partial replacement to sand in mortars. The raw SCBA used in the study was collected from sugar mills located in the south of Brazil. The collected ash was minimally processed by sieving with a 0.6 mm sieve to produce the SCBA to be used in concrete mixtures. The study produced five mixtures with different fine aggregate replacement levels with SCBA (i.e., 0%, 5%, 10%, 15%, and 20% by volume). All produced mortars were characterized in the plastic state by evaluating water retention, air content, and bulk density. Similarly, the influence of SCBA on hardened properties was determined in terms of compressive strength, tensile strength by bending test, axial compressive strength, flexural and longitudinal Young's modulus, and capillary coefficient. The experimental test results showed that raw SCBA could be used as a partial replacement to sand without compromising compressive strength. In addition, statistical analysis revealed that SCBA did not significantly change the properties of SCBA admixed mortars compared to the control mixture (34).

The aforementioned studies have scrutinized the different replacement levels of fine aggregate with untreated SCBA in concrete. These studies showed that the use of raw SCBA as a partial or complete substitution to fine aggregate is possible. However, the improvement in the mechanical properties is minimal.

### *3.1.2. Use of Bagasse Ash as a Supplementary Cementitious Material*

Various studies have been conducted to determine the feasibility of using SCBA as a partial replacement to cement in concrete mixtures. While many studies revealed that SCBA produced in sugar mills does not exhibit pozzolanic properties due to high carbon content, few researchers have reported that post-processing of raw SCBA by further burning, grinding, or a combination of these can yield materials of SCM quality (*16*, *20*, *35*, *36*). Ganesan et al. (*16*) investigated the feasibility of using post-processed SCBA as an SCM in concrete. The SCBA collected from the sugar mill, located in southern India's, was further burned at 650°C for 1 hour under laboratory conditions and grounded to a mean particle size of 5.4 $\mu$m before using as a substitute to cement in concrete mixtures. The effects of post-processed SCBA on concrete properties were determined through compressive strength, water absorption, splitting tensile strength, permeability, and resistance to chloride ion penetration tests. The experimental results revealed that post-processed SCBA could replace up to 20% of cement without compromising its compressive strength (*16*). The study also showed that the increase in SCBA content (i.e., up to 25% by cement mass) reduces water permeability and increases the resistance to chloride permeation and diffusion of the concrete mixture.

In a similar study, Amin (*37*) studied the effects of using post-processed SCBA as a partial substitute to cement in concrete mixtures. The post-processed SCBA was produced by further burning (at 650°C for 1 hour) and grinding SCBA collected from multiple sugar mills located in Pakistan. Seven different cement replacement levels with post-processed SCBA ranging from 0% to 30% (at 5% increments) were evaluated in this study. The study evaluated different concrete properties such as compressive strength, splitting tensile strength, and chloride diffusion for all mixtures produced in the study. The experimental results revealed that up to 20% cement replacement with SCBA, no significant reduction in compressive strength was observed. In

addition, the partial replacement of cement with SCBA resulted in the development of high early strength and showed an improvement in resistance to chloride ion penetrability by 50% (*37*).

Montakarntiwong et al. (*38*) investigated the compressive strength of concrete utilizing various types of bagasse ash with different fineness and loss on ignition (LOI)). Four different types of bagasse ash with two levels of LOI (referred to as high and low LOI) and two levels of fineness (i.e., unground and ground) were considered in the study. Concrete mixtures using 0%, 20%, 30%, and 40% by weight of cement replaced with SCBA were produced in the study. Based on the experimental findings, up to 30% and 20% of cement can be replaced with ground bagasse ash with low LOI and high LOI, respectively (*38*). At these replacement levels, concrete mixtures exhibited compressive strengths equivalent to the control mixture.

Bahurudeen and Santhanam (*39*) investigated the influence of production methodology on the pozzolanic activity of SCBA. This study performed microstructural characterization and evaluated the pozzolanic performance of various types of SCBAs produced with different processing methodologies (i.e., grinding, burning, or combination of these). When used as a replacement to cement in mortar mixtures, the as-received SCBA negatively influenced compressive strength and did not meet the minimum requirement of pozzolanic activity index (i.e., 75%) to be classified as a pozzolan (*40*). As such, it was concluded that raw SCBA without any processing could not be used as SCMs cementitious composites. However, post-processing of SCBA by different methodologies, including burning (at 700°C), sieving (through 300 $\mu$m), and grinding (to particles finer than 53$\mu$m) showed higher strength activity index (SAI) than raw SCBA. In addition, the study also investigated the influence of combining different processing methodology on pozzolanic reactivity, i.e., SCBA produced by burning at 700°C and then ground to cement fineness (300 $m^2$/kg), and SCBA produced by sieving raw SCBA through 300 $\mu$m sieve and then ground to cement fineness. Among these processing methodologies, sieved and ground samples exhibited higher SAI (i.e., 106%) than burned and ground SCBA samples (i.e., 90%) at 28 days of curing. The study concluded that sieving (through a 300 $\mu$m sieve) and grinding (to cement fineness) is the optimum production methodology to yield high pozzolanic activity index with minimum processing energy (*39*). This post-processed SCBA showed excellent results in comparison to any other processing methodologies evaluated in this study.

Subedi et al. (*21*) compared the pozzolanic activity of SCBAs produced from three different methodologies: (i) SCBA produced in sugar mills from uncontrolled burning (i.e., raw SCBA); (ii) SCBA produced from post-processing of raw SCBA; and (iii) SCBA produced by controlled burning of bagasse fibers under laboratory conditions. Experimental results showed that while controlled burning of sugarcane bagasse fiber under laboratory conditions yields SCBA with low carbon content and high strength activity index, raw SCBA obtained in the field presented high carbon content and low strength activity index (i.e., 69%). This is the case since SCBA produced in the sugar mill produces uncontrolled burning, which produces large temperature gradients and fails to eliminate all the organic carbon in the SCBA. Furthermore, it was shown that post-processing of raw SCBA by further burning and grinding resulted in similar pozzolanic properties to those of controlled SCBA. Considering the low SCBA yield of the controlled burning of bagasse fibers, the study concluded that post-processing of raw SCBA by further burning at 450°C for 3 hours and grinding is the optimum processing methodology due to its high SCBA yield and high strength activity index (i.e., 90%).

The aforementioned studies showed that post-processed SCBA could be used as a partial substitution to cement in regular concrete. As such, the utilization of SCBA as an SCM alternative in the production of concrete mixtures can potentially benefit an underutilized agricultural waste and enhance the cost-effectiveness and greenness of ECCs.

## 3.2. Development of Green and Cost-Effective ECC

### *3.2.1. Aggregates Used in ECC Materials*

The wide application of ECC materials has been mainly hindered by its high cost and relatively low practicality. ECC material's high cost is primarily driven by the use of manufactured microsilica sand and 2% volume fraction of polyvinyl alcohol (PVA) fiber; yet, the use of high cement content is also a contributing factor to ECC's high cost relative to conventional concrete. Contradictorily to conventional practice in concrete materials, ECC mixtures are intentionally designed to facilitate crack initiation and propagation in the cementitious matrix. This promotes the necessary PSH behavior, which endows these composites with its ductile strain-hardening characteristics. As such, ECC mixtures forgo the use of coarse aggregate to lower the matrix fracture toughness (i.e., $K_m$); thus, resulting in composites using only fine aggregate. In order to minimize $K_m$ and yield high tensile ductility, typically highly fine sands such as manufactured microsilica sand (with particle size smaller than 250 μm) are used. However, microsilica sand is highly expensive (more expensive than cement) and consumes more energy during production in contrast to natural fine aggregates. In addition, microsilica sand is not widely available, which limits the applicability of ECC materials in construction. As such, to improve ECC materials practicality and cost-effectiveness, various studies have been conducted to determine the feasibility of using alternatives to microsilica sand in ECC mixtures.

Mustafa et al. (*41*) evaluated the use of five types of fine aggregate in ECC mixtures: microsilica sand with maximum aggregate size (MAS) of 200 μm (as control); crushed dolomitic limestone sand with MAS of 1.19 mm and 2.38 mm; and gravel sand with MAS of 1.19 mm and 2.38 mm. The study performed compressive strength, uniaxial tensile, flexural, and drying shrinkage tests for all the ECC materials. It was observed that coarser aggregates slightly reduce the ductility of the composites, which was attributed to the adverse effect of coarser aggregate on fiber dispersion and the likely increase of $K_m$. However, it was shown that increasing the replacement of cement with fly ash was effective in mitigating the adverse effect of coarser sands on composite ductility. In addition, the use of coarser sands was shown to be effective in reducing drying shrinkage. It was concluded that ECC materials using sands coarser than microsilica sand could be successfully manufactured (*41*).

Noorvand et al. (*30*) studied the use of two different types of river sand, coarse (MAS of 1.18 mm) and fine (MAS of 0.6 mm), on the mechanical properties of ECC. Furthermore, the study also evaluated the use of crumb rubber as a partial replacement of sand (20% sand replacement with crumb rubber by volume) in ECC. The experimental results demonstrated that the different sand types produced a minor influence on ECC's mechanical properties (*30*). On the other hand, the replacement of sand with crumb rubber was highly effective in enhancing the tensile ductility of ECC; however, significant decrements in strength were observed due to the defect-like nature of crumb rubber.

Lepech et al. (*42*) evaluated the complete substitution of virgin silica sand (with an average particle size of 110 $\mu$m and maximum particle size of 300 $\mu$m) with waste foundry sand from the calcinator baghouse (FCS) and foundry green sand (FGS). FCS is captured by foundry dust collection systems and is nearly identical in appearance and mechanical properties to virgin sand. Green foundry sand is a waste from lost foam metal casting with the particle size distribution coarser than the virgin sand. The flowability test (flow table test) showed that using these green sand alternatives improved flowability in the fresh state. However, the complete substitution of virgin sand with FGS reduced the tensile strain capacity by over 50% compared to the control ECC. This was attributed to the presence of carbon residue in FGS along with the PVA oil coating (1.2% by weight), which substantially reduced the fiber-bridging capacity of the composites; thus, leading to a decrease in the complimentary energy ($J_b'$) of the fiber-bridging relation of 80%. Furthermore, the FSG produced a decrease in matrix toughness of nearly 40%. In balance, these counteracting mechanisms resulted in a reduced PSH energy index; thus, negatively influencing the tensile ductility. To address the significant decrease in interface properties, the study also produced an ECC mixture containing FGS and PVA fiber (with oil coating at 0.3%). This mixture increased the tensile strain capacity from 1.5% to 3.5%. This was credited to the presence of carbon in FGS and low oil coating of PVA fiber, which created an optimum balance in reducing matrix toughness and improvement in fiber/matrix interface properties. As such, this study revealed that it is possible to use these waste materials as sand replacement in ECC mixtures without compromising its mechanical properties if the ingredients are carefully tailored to yield PSH behavior (*42*).

The aforementioned studies showed that more conventional types of sands (coarser than microsilica sand) could be used to produce ECC materials. However, achieving high tensile ductility while implementing these sands can be more challenging and requires careful tailoring of the ECC composition. It is worth mentioning that the implementation of coarser sands in ECC mixtures can negatively affect fiber distribution and result in lower composite ductility, especially when manufacturing ECC at a large-scale in the field where high shear planetary mixers like the once typically used in the laboratory may not be readily available. This effect has been reported in a recent study, where fiber clumping was observed during the construction of an ECC ultra-thin whitetopping overlay using a conventional ready-mix truck *(43)*. The ECC mixture used in the project implemented conventional fine river sand and did not show fiber clumping when manufactured in the laboratory using a planetary mixer. As such, the use of aggregate with particle size comparable to that of microsilica sand is preferable to minimize the possibility of fiber distribution problems. Consequently, finding alternative aggregate materials that are locally available, cost-effective, and of comparable size to micorsilica sand is of significant importance to enhance the greenness and practicality of ECC materials without compromising its mechanical performance.

### *3.2.2. Use of Green Binder in ECC Mixtures*

Due to the absence of coarse aggregate in its composition, ECC mixtures consist of high cement content compared to the regular concrete (i.e., 2-3 times higher) (*44*). Consequently, this compromises the environmental sustainability of ECC materials as cement production is both energy- and emission-intensive. For instance, it has been quantified that the cement industry is responsible for about 8% of the global $CO_2$ anthropogenic emissions (*45*). In addition, cement production generates a significant amount of pollutants and particulate matter (*45*). As such, to reduce the environmental impact of ECC materials, it is imperative to partially or completely replace cement with supplementary or alternative cementitious materials without compromising

its mechanical properties. To date, different researchers have produced ECC mixtures with green binders/fillers. These studies have reduced the cement usage in three different ways: (i) partial replacement of cement with SCMs such as fly ash and ground granulated blast furnace slag (GBBFS) and agricultural by-products such as rice husk ash (*44*, *46*, *47*); (ii) partial replacement of cement with relatively inert fillers such as iron ore tailings (IOTs) and limestone powder (*48*, *49*) and (iii) complete replacement of cement with geopolymers and alkali-activated binders (*9*, *50–52*). Among all these methods and materials, partial substitution of cement with fly ash is widely adopted to produce ECC mixtures with enhanced greenness (*22*, *53*, *54*). Fly ash is a by-product of coal-fired electric generating plants. It is estimated that nearly 38.2 million tons of fly ash are produced in the US in 2017, where only 63% of this material is utilized (*55*). The use of fly ash as a partial substitute to cement enhances the material greenness by consuming an industrial waste stream and reducing cement consumption. In addition, the partial substitution of cement with fly ash reduces the cost of ECC and produces favorable effects on ECC's properties, including the reduction in drying shrinkage, average crack width, and heat of hydration (*56*).

Wang and Li (*53*) evaluated PVA-ECC mixtures with class F fly ash as a partial substitute to cement (FA/C ratio ranging from 0.1 to 1.5 by mass). The study investigated the influence of fly ash content on ECC's matrix and fiber/matrix interface properties. The study revealed that increasing the fly ash content decreases the matrix fracture toughness (between 21% to 50%), fiber/matrix chemical bond (between 59% to 70%), and frictional bond (between 0% to 25%); thus, enhancing the tensile performance of ECC materials. The study concluded that waste products could be utilized as SCMs if the governing micromechanics parameters are controlled.

Yang et al. (*57*) evaluated PVA-ECC mixtures with high amounts of cement replacement with class F fly ash (FA/C ratio ranging from 1.2 to 5.6 by mass). The study revealed that ECC materials' tensile ductility generally increases with increments in cement replacement with fly ash. This was credited to a decrease in the matrix fracture toughness and the fiber/matrix chemical bond. The average crack width and drying shrinkage also decreased at higher levels of cement replacement with fly ash, which are beneficial to structural durability. The average crack width reduction was attributed to an observed improvement in the fiber/matrix frictional bond at high replacement levels of cement with fly ash. On the other hand, compressive strength showed a negative trend with the increase in fly ash content.

Zhang et al. (*58*) studied the influence of replacing cement with class F fly ash on mechanical properties and self-healing behavior of micro-cracked ECC mixtures. The study concluded that using class F fly ash as a partial replacement to cement reduces the composites' compressive strength but increases its ductility. However, a significant improvement in the pore structure was observed for ECC mixtures using fly ash due to its fine and spherical-shaped particles. Furthermore, the study also revealed that high volume fly ash decreases the crack width; thus, exhibiting excellent self-healing behavior.

Amin et al. (*59*) partially substituted cement with post-processed SCBA in ECC mixtures. The post-processed SCBA was produced by burning SCBA collected from a sugar mill located in Pakistan at 650°C for 1 hour under laboratory conditions and followed by grounding. The finely ground SCBA was used as a partial replacement to cement at different proportions (i.e., 10%, 20%, and 30%) on ECC properties. The results showed that the ECC mixture utilizing 10% of SCBA as a substitute to cement exhibited higher compressive strength than control. Furthermore, this ECC mixture exhibited better tensile performance among all other mixtures evaluated in the study.

However, the reported tensile strain for the best-performing SCBA admixed ECC was 457μ (0.0457%), which is significantly lower than the ductility of a typical ECC mixture. As such, the characteristic robust PSH behavior of ECC was not achieved.

Based on these studies, it is evident that the use of silica-rich pozzolanic materials as a partial replacement of cement can be beneficial in the manufacturing of ECC materials. As such, the utilization of locally available pozzolanic materials can improve the tensile performance, cost-effectiveness, durability, and greenness of these composites.

# 4. METHODOLOGY

## 4.1. ECC Materials Produced with Louisiana SCBA

### *4.1.1. Materials*

In this study, the SCBA material was collected from a Louisiana based sugar mill (Figure 4). This material was used to produce the two different types of Louisiana SCBAs evaluated in this study, i.e., raw SCBA and post-processed SCBA. Table 1 presents a summary of the tests conducted to characterize the SCBAs. The production methodologies for both types of SCBAs are explained in detail in the following sub-sections.

**Figure 4. Raw SCBA collection in Louisiana's sugar mill**

#### *4.1.1.1 Louisiana Raw SCBA*

The SCBA collected from the sugar mill is generated from the uncontrolled burning of bagasse fibers. As such, the collected SCBA included large amounts of unburned fibrous particles, as presented in Figure 5. Raw SCBA, used as a substitute to sand in ECC mixtures, was produced by drying (at 65°C for 10-12 hours) and sieving (using a No. 20 sieve) the SCBA collected at the sugar mill. While drying was performed to remove moisture, sieving was performed to remove coarse impurities (i.e., unburnt fibers, gravel, etc.). The raw SCBA material obtained after drying and sieving were labeled as RBA. The processing methodology of RBA is illustrated in Figure 5.

**Table 1. Bagasse ash produced from different methodologies.**

| Material | SCBA Source | Calcination Temperature (°C) | ID | Tests Performed (No. of Replicas) |
|---|---|---|---|---|
| Raw SCBA | Louisiana | - | RBA | SEM (1); EDS (3); XRD (1); Particle Size Analysis (1); Chapelle's Test (3); Strength Activity Index (6); Density and Specific Gravity (2) |
| Post-processed SCBA | Louisiana | 450 | PBA | |
| Raw SCBA | Ecuador | - | EBA | SEM (1); EDS (1); XRD (1); Particle Size Analysis (1); Strength Activity Index (6); |

#### *4.1.1.2 Louisiana Post-Processed SCBA*

The methodology for the production of post-processed SCBA is presented in Figure 5. The processing methodology in this study was adopted from Subedi et al. (*21*). After drying and sieving (according to section 4.1.1 guidelines), RBA was further processed by burning and grinding under controlled laboratory conditions. In the burning phase, the RBA was calcinated at 450°C for 3 hours to remove any unburned fibrous particles and decrease the carbon content. The burning of RBA changed the color of SCBA from black to brown, indicating a significant decrease in carbon content. After completion of the calcination process, the materials were allowed to cool inside the oven until the temperature reached 90°C. Subsequently, the SCBA was grounded in a jar mill at 300 rpm for 35 minutes. The post-processed SCBA was labeled as PBA.

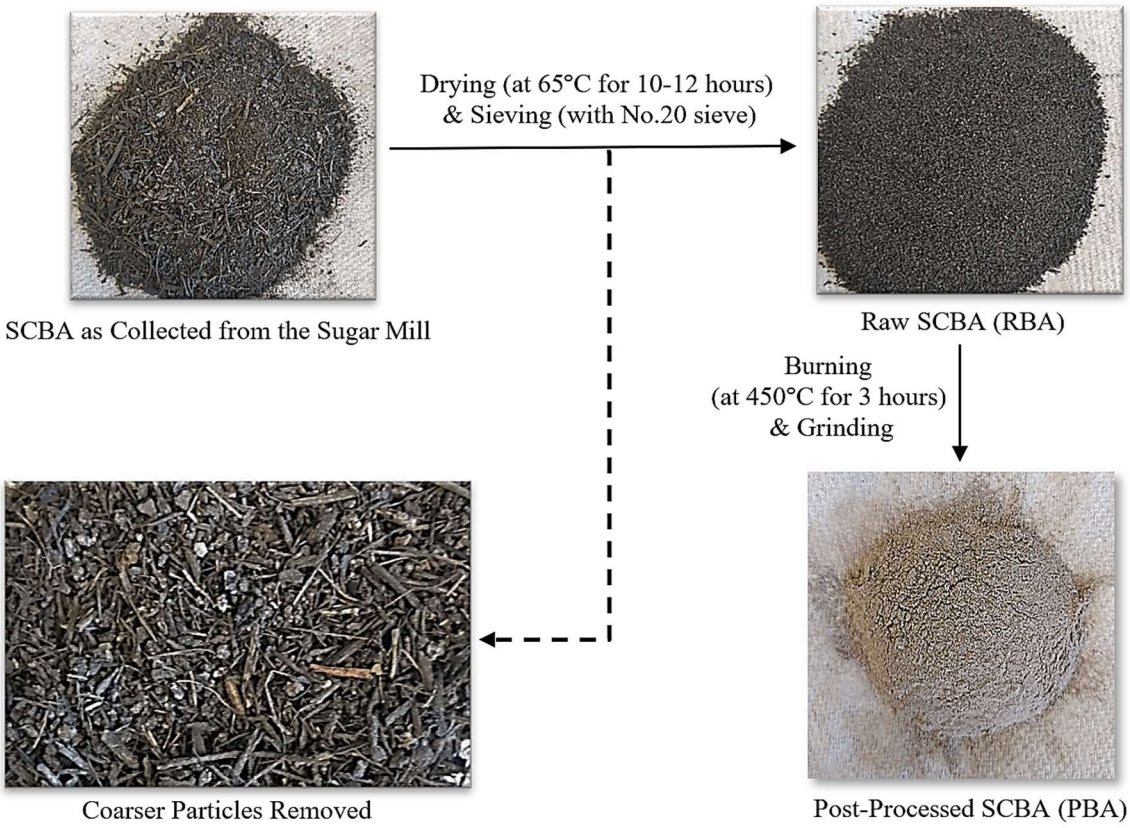


**Figure 5. Processing methodology for RBA and PBA**

#### *4.1.1.3 Cement*

Ordinary Portland Cement (OPC) Type I conforming to the ASTM C150 standard was used for all mixtures manufactured in the study (*60*). The chemical composition of the cement is presented in Table 2. The specific gravity of the cement was 3.15.

#### *4.1.1.4 Fly ash*

Class F fly ash conforming to ASTM C618 was utilized in all ECC mixtures produced in this study. The chemical composition of the fly ash obtained from X-ray fluorescence (XRF) analysis is presented in Table 2. Furthermore, the particle size of fly ash obtained from laser diffraction

analysis is presented in Figure 6. The fly ash used in this study exhibited a mean particle size of 22.8 $\mu$m.

**Table 2. Cement and fly ash chemical composition (by weight).**

| Oxide | CaO | $SiO_2$ | $Al_2O_3$ | $Fe_2O_3$ | $K_2O$ | $Na_2O$ | MgO | $SO_3$ | $CO_2$ | $SiO_2$+ $Al_2O_3$+ $Fe_2O_3$ |
|---|---|---|---|---|---|---|---|---|---|---|
| Cement (%) | 63.77 | 19.06 | 4.55 | 3.00 | 0.37 | 0.00 | 2.27 | 3.43 | - | 26.6 |
| Fly Ash (%) | 7.97 | 57.94 | 20.03 | 3.67 | 1.24 | 2.14 | 2.02 | 0.49 | - | 81.6 |

### *4.1.1.5 Sand*

For the ECC mixtures produced in this study, silica sand, i.e., fine river sand (specific gravity of 2.62) with a mean particle size of 474 $\mu$m and a $D_{90}$ (90% passing size) of 786 $\mu$m was used as fine aggregate. Figure 6 presents the particle size distribution of fine river sand obtained from the laser diffraction particle size analyzer. Standard graded sand conforming to ASTM C778 (*61*) was used for the Strength Activity Index evaluation.

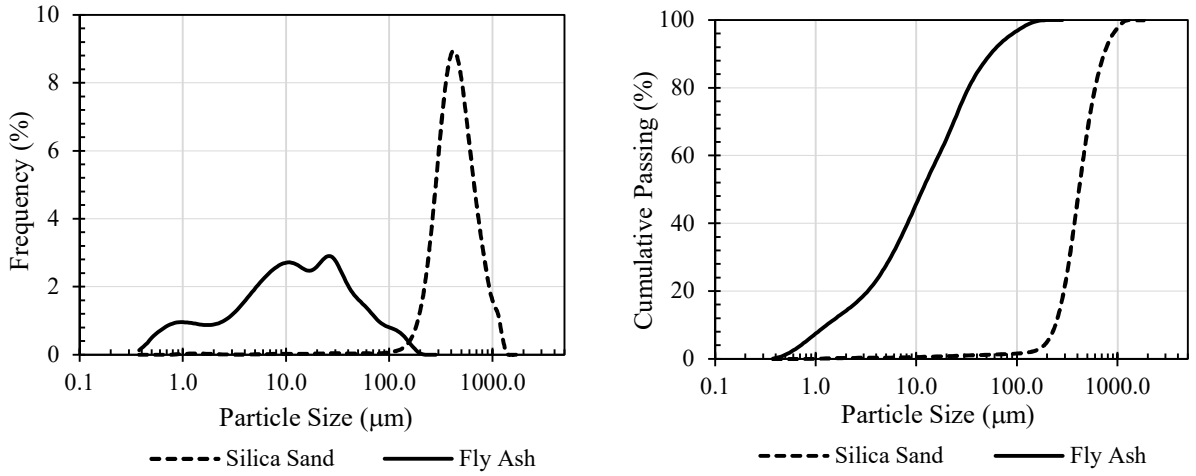


**Figure 6. Sand particle size distribution: (a) Particle size distribution frequency, and (c) Cumulative passing percent particle size distributions**

### *4.1.1.6 Polyvinyl Alcohol (PVA) fibers*

The PVA fibers utilized were non-oil-coated RECS-15 fibers from NYCON, US. The properties of the PVA fiber is summarized in Table 3.

**Table 3. PVA fiber properties**

| Fiber Type | Length (mm) | Diameter ($\mu$m) | Young's Modulus (GPa) | Tensile Strength (MPa) | Elongation (%) |
|---|---|---|---|---|---|
| RECS-15 | 8 | 38 | 40 | 1600 | 6 |

### *4.1.1.7 Superplasticizer*

A polycarboxylate based High-Range Water Reducer (HRWR) (ADVA 195) was utilized in this study for all ECC mixtures. HRWR was used to obtain the proper workability of the fresh mixtures.

In this study, the HRWR dosage was limited to 1.5% of cement content (by weight) due to its influence on other material characteristics such as air content.

### *4.1.2. SCBA Characterization*

Raw SCBA (RBA) and post-processed SCBA (PBA) produced in this study were thoroughly characterized. The different analyses conducted are explained in the following subsections.

#### *4.1.2.1 Microstructure and Chemical Composition*

The chemical composition and morphology of SCBA can significantly influence ECC's properties when used as SCM or as sand replacement. As such, these characteristics of RBA and PBA were evaluated. The chemical composition of RBA and PBA was obtained from energy-dispersive X-ray spectroscopy (EDS) by using a Quanta™ 3D Dual Beam™ FEG FIB-SEM, with EDAX Pegasus EDS/EBSD detectors, as shown in Figure 7. Furthermore, to gain insight into the morphology of the SCBAs, backscattered scanning electron microscopy images (BSE-SEM) were obtained using the same equipment. It should be noted that the EDS spectra for both SCBAs were collected at a current of 4 pA and a voltage of 20kV under area mode. Similarly, BSE-SEM images were obtained at 20kV.

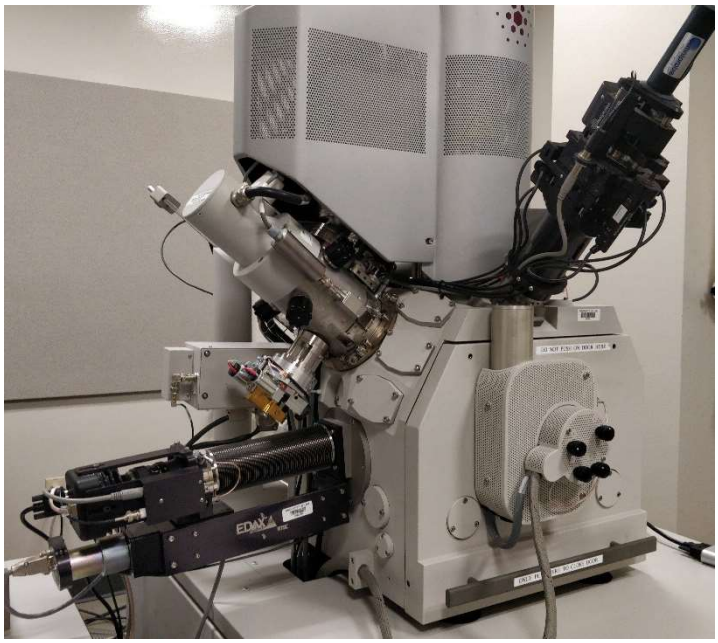

**Figure 7. Quanta™ 3D DualBeam™ FEG FIB-SEM for SEM-EDS.**

#### *4.1.2.2 Particle Size Analysis*

The particle size of fine aggregate or SCMs has a substantial effect on the matrix and fiber/matrix interface properties of ECC materials. While the RBA used as a sand replacement was not grounded, the PBA produced for SCM utilization was ground in a jar mill at 300 rpm for 35 minutes to achieve a finer particle size distribution; and enhance its reactivity potential. The particle size of the SCBAs was analyzed using the Beckman Coulter LS200 laser diffraction analyzer, as shown in Figure 8. The equipment used for the analysis can detect particles ranging from size 0.4 $\mu$m to 2000 $\mu$m. Both SCBA materials were analyzed in a microvolume module where the particles were agitated for 60 seconds, and water was used as a dispersing medium.


**Figure 8. Beckman Coulter LS 200 for particle size analysis.**

### *4.1.2.3 X-Ray Diffraction (XRD)*

The mineralogical phase composition (i.e., amorphous and crystalline phases) of ingredients used in ECC materials can significantly affect its properties. As such, the mineralogical composition of both SCBAs was obtained via XRD analysis. XRD analysis was conducted on a powder sample by using Panalytical Empyrean X-ray Diffractometer, as presented in Figure 9. It is worth mentioning that the XRD analysis was conducted by using CuK$\alpha$ radiation at 40mA and 45kV. Both samples were scanned from a range of 10° to 80° 2θ at a step size of 0.026°. Furthermore, for quantifying the mineralogical phase composition, the HighScore Plus software (*62*) was used. Furthermore, quartz ($SiO_2$) powder was used as an amorphous standard and was analyzed in the same conditions as the SCBA samples.

**Figure 9. Panalytical Empyrean X-ray Diffractometer for XRD analysis.**

### *4.1.2.4 Density, Specific Gravity, and Absorption Test*

In this study, the density of PBA was determined as per ASTM C188 (*63*), and the specific gravity and absorption of RBA were determined as per ASTM C128 (*64*). To measure the density of PBA per ASTM C188, a Le Chatelier flask and kerosene were used. Initially, kerosene was filled up to

a mark between 0 and 1-mL on the flask's stem, as shown in Figure 10. After the addition of kerosene, the first reading on the flask was taken. Next, about 50 grams of PBA were added to the flask. After the SCBA was introduced, the stopper was placed, and the flask was whirled to remove any air bubbles. Once air bubbles were no longer observed, the final reading on the flask was taken. The material's density was computed using Eq. 3, where the volume of the kerosene displaced is the difference between the initial and the final readings of the flask.

Density ($g/cm^3$) = mass of the cement (g)/volume of the kerosene displaced ($cm^3$) [3]

**Figure 10. Le Chatelier's flask**

The specific gravity and absorption of RBA were determined as per ASTM C128 (*64*). Initially, a 1-liter capacity of pycnometer was filled with water up to its calibration capacity and the mass was recorded. Next, the pycnometer was partially filled with water and 200 ± 10 g of RBA (in saturated-surface-dry conditions, SSD) was introduced into the pycnometer. Subsequently, the pycnometer was filled with additional water up to 90% of the pycnometer capacity. The pycnometer was then agitated to remove the air bubble at the surface of the water. When no further air bubbles were observed, the pycnometer was filled with water up to its capacity, and the mass was recorded. Next, the SCBA from the pycnometer was dried at 110±5°C until it reached a constant mass. After it reached a constant mass, the sample was allowed to cool for 0.5 hours, and the final mass reading was taken. The specific gravity and absorption were computed as per Eq. 4 and 5, respectively.

$$\text{Bulk Specific Gravity} = \frac{S}{B+S-C} \quad [4]$$

$$\text{Absorption} = \frac{S-A}{A}\ x\ 100 \quad [5]$$

where,

A = mass of oven-dry RBA in air, in grams;

B = mass of pycnometer filled with water, in grams;

C = mass of pycnometer with RBA and water to calibration mark, in grams; and

S = mass of SSD RBA added to the pycnometer, in grams.

#### *4.1.2.5 Chapelle's Test*

Chappelle's test method is a chemical method to determine the pozzolanic reactivity of natural and artificial pozzolans (*65*). It is an accelerated method, standardized by the ABNT- Associação Brasileria de Normas Técnicas (NBR 15895: 2010) (*66*), and quantifies the calcium consumption associated with the vitreous or amorphous phase of a pozzolanic material (*65*). For Chapelle's test, one gram of SCBA and two grams of CaO are added to 250ml of distilled water. The mixture is then placed at 90±10°C for 16 hours. The consumption of CaO is determined utilizing sucrose extraction and titration with hydrochloric acid using phenolphthalein as an indicator. For Chapelle's method, three sets of replicas were performed for each type of SCBA. The results are expressed as milligrams of lime (CaO) reacted or fixed per gram of pozzolan and computed using Eq. 6.

$$\text{Mg CaO per gram of material} = \frac{(28*(v_3-v_2)*2*2)}{m_4*m_2} \quad [6]$$

where,
$m_2$ = grams of pozzolanic material = 1g;
$m_3$ = grams of CaO mixed with pozzolanic material = 2g;
$m_4$ = grams of CaO in the blank test = 2g;
$v_2$ = milliliters of HCl 0.1M consumed by the sample solution;
$v_3$ = milliliters of HCl 0.1M consumed by the blank solution;

#### *4.1.2.6 Strength Activity Index*

For both SCBAs, pozzolanic activity was determined as per ASTM C311 (*67*). The control mortar mixture was prepared with the specified sand to cement (S/C) and water to cement ratios of 2.75 and 0.48, respectively. The sand used for the SAI test was a standard graded sand meeting ASTM C778 requirements (*68*). For RBA and PBA mortar mixtures, 20% of the cement (by mass) was replaced with the corresponding SCBA material per ASTM C311 requirements. For mixtures with SCBAs, the amount of water required was determined such that the same flow within ±5% tolerance was obtained compared to control. It should be noted that for each mixture, a total of six 50 mm (2") cube specimens were cast. After 24 hours of casting, the cube specimens were removed from the molds and were cured in a saturated lime water tank for 28 days. At the end of the curing phase, the compressive strength of the mortar cubes was determined as per ASTM C109 standard (*69*). The test setup is presented in Figure 11. The strength activity index was computed as the percentage strength of the SCBA admixed test cubes compared to the control cubes. In addition, a set of cube specimens were prepared by replacing 20% of cement in the control mixture with inert silica sand. This was performed to have a reference for a material with no pozzolanic activity for comparative purposes. It should be noted that a minimum of 75% SAI is required to be classified as a pozzolan as per ASTM C618 (*70*).

**Figure 11. Compressive strength testing setup for 50.8-mm (2-in) mortar cubes.**

### *4.1.3. Testing of Louisiana SCBA Admixed ECC*

The initial phase of this study focused on the physical and chemical characterization of SCBA materials (RBA and PBA). In this following phase, the mechanical properties of ECC mixtures with RBA as a sand replacement and PBA as a cement replacement were evaluated. The mechanical and physical properties of all the produced ECC mixtures were experimentally investigated. Properties evaluated included compressive strength, tensile strength and strain capacity, surface resistivity, shrinkage, and coefficient of thermal expansion.

#### *4.1.3.1 Mixture Proportioning*

Two types of ECC mixtures were prepared: (i) RBA admixed ECC (i.e., class S) with sand partially or completely replaced with RBA; and (ii) PBA admixed ECC (i.e., class C) with cement partially replaced with PBA. For class S mixtures, the investigated sand replacement levels with RBA were 0%, 25%, 50%, 75%, and 100% by volume. For class C mixtures, the investigated cement replacement levels with PBA were 0%, 40%, 50%, and 60% by mass. Furthermore, for both mixtures classes, water to binder ratio (W/B) and fiber content were kept constant at 0.32 and 1.5% (volume fraction). For class S mixtures, class F fly ash was utilized as a partial replacement to cement. For comparative purposes, the fly ash-to-cement ratio (F/C) ratio was kept constant at 2.2 for all class S mixtures. For class C mixtures, the sand-to-binder ratio was 0.36 for all mixtures. The details of the different mixture proportions are summarized in Tables 4 and 5 for class S and class C mixtures, respectively. In summary, a total of five different class S mixtures and four different class C ECC mixtures were produced.

**Table 4. Class S ECC mix design proportion by weight.**

| Mix ID | Cement ($kg/m^3$) | Fly Ash ($kg/m^3$) | Water ($kg/m^3$) | Sand ($kg/m^3$) | RBA ($kg/m^3$) | RBA (%)[a] | Fibers ($kg/m^3$) | HRWR (%)[b] | Air Content (%) |
|---|---|---|---|---|---|---|---|---|---|
| S-0 | 358.9 | 789.5 | 367.5 | 416.2 | 0 | 0 | 19.5 | 0 | 1.4 |
| S-25 | 358.9 | 789.5 | 367.5 | 312.2 | 92.2 | 25 | 19.5 | 0.13 | 2.9 |
| S-50 | 358.9 | 789.5 | 367.5 | 208.1 | 184.3 | 50 | 19.5 | 0.45 | 3.5 |
| S-75 | 358.9 | 789.5 | 367.5 | 104.1 | 276.4 | 75 | 19.5 | 0.80 | 5.3 |
| S-100 | 358.9 | 789.5 | 367.5 | 0 | 368.6 | 100 | 19.5 | 1.5 | 5.8 |

[a] % of sand replacement by volume; [b] % of HRWR by weight of cement; [c] % of fiber content by volume

**Table 5. Class C ECC mix design proportion by weight.**

| Mix ID | Cement ($kg/m^3$) | PBA ($kg/m^3$) | PBA (%)[a] | Water ($kg/m^3$) | Sand ($kg/m^3$) | HRWR (%) [b] | $V_f$ (%)[c] | Fibers ($kg/m^3$) |
|---|---|---|---|---|---|---|---|---|
| C-0 | 1271.2 | 0.0 | 0 | 406.8 | 457.6 | 0 | 1.5 | 19.5 |
| C-40 | 736.1 | 490.8 | 40 | 441.6 | 441.6 | 0.6 | 1.5 | 19.5 |
| C-50 | 608.1 | 608.1 | 50 | 389.1 | 437.8 | 1.0 | 1.5 | 19.5 |
| C-60 | 482.3 | 723.4 | 60 | 385.8 | 434.1 | 1.5 | 1.5 | 19.5 |

[a] % of cement replacement by mass; [b] % of HRWR by weight of cement; [c] % of fiber content by volume

### *4.1.3.2 Specimen Preparation*

All ECC mixtures produced in this study were mixed in the following steps. Initially, powder components (cement, fly ash, sand, and RBA for class S mixtures, cement, PBA, and sand for class C mixtures) were mixed at a slow speed (i.e., 60 rpm) in a planetary mixer for three minutes. Subsequently, water and HRWR were added within one minute and mixed for three minutes at medium speed (i.e., 110 rpm). Finally, PVA fibers were introduced slowly to the wet mix (within two minutes) and mixed for an additional five minutes at high speed (i.e., 200 rpm). The mixing procedure is illustrated in Figure 12a. After completing the mixing process, three cylindrical specimens, six dog-bone shaped specimens, and four prismatic specimens (for shrinkage (length change) evaluation) were cast per each ECC mixture. Figure 12b presents the ECC specimens in the molds right after casting. After molding, all specimens were sealed with plastic coverings to avoid moisture loss. After 24 hours, cylindrical specimens and dog-bone shaped specimens were demolded and allowed to cure in a saturated lime water tank, according to ASTM C511 (*71*). The prismatic specimens for shrinkage determination were demolded and cured in saturated lime water following the ASTM C157 standard (*72*).


**(a)**

**(b)**

**Figure 12. ECC specimen preparation (a) ECC mixing process (b) ECC specimen cast in molds**

### *4.1.3.3 Compressive Strength Test*

The compressive strength of all ECC materials was determined as per ASTM C39 on 101.6-mm x 203.2- mm (4-in x 8-in) cylinders (*73*). It is important to mention that three replicas were evaluated for each mixture. The compressive strength was determined at a loading rate of 15MPa/min using hydraulic pressure. Figure 13 presents the test setup for the compressive strength test.

**Figure 13. Compressive strength test setup.**

### *4.1.3.4 Uniaxial Tensile Test*

The tensile performance of all ECC materials was determined as per the recommendation of the Japan Society of Civil Engineers (*74*). The test was conducted at 28 days of curing on dog-bone shaped specimens (as shown in Figure 14a). The test was conducted using a 250kN capacity servo-hydraulic machine where a displacement controlled constant axial load was applied. For all specimens, the gage length was kept constant at 80 mm, and one LVDT was attached to each side of the specimen to evaluate its deformation. The test setup is presented in Figure 14b. It is important to mention that a total of 6 replicas were tested for each mixture.

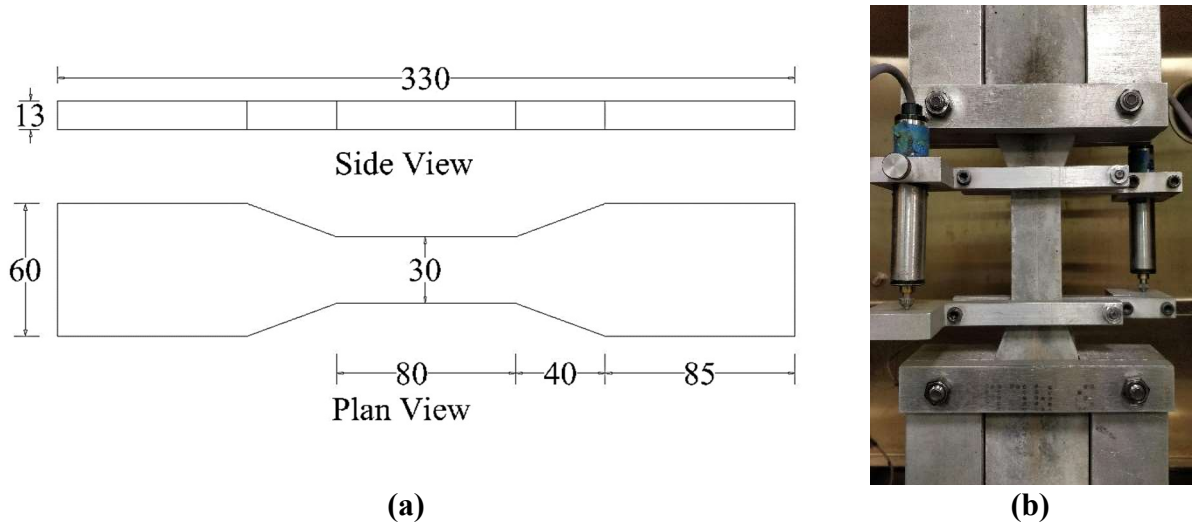


**Figure 14. Uniaxial tensile test: (a) Dimensions of dog-bone shaped specimen in mm and (b) Uniaxial tensile test setup**

#### *4.1.3.5 Surface Resistivity*

Permeability is the most important factor influencing the durability of concrete materials. A permeable concrete allows deleterious substances to enter into the material; thus, deteriorating the concrete structure and decreasing its service life. As such, to gain insight into the permeability of ECC mixtures, a surface resistivity test as per AASHTO T358 "Standard Method of Test for Surface Resistivity Indication of Concrete's Ability to Resist Chloride Ion Penetration" was performed (*75*). The test method determines the electrical resistivity of the material, which has shown to strongly correlate with the chloride ion penetrability of concrete materials. In this context, higher surface resistivity indicates a lower chloride ion penetrability and vice versa. It is worth mentioning that the surface resistivity is a non-destructive test. As such, the cylinders used to evaluate compressive strength were first utilized to measure surface resistivity. A Wenner four-pin array with a 38 mm spacing was used to measure the surface resistivity. Prior to the surface resistivity evaluation, the cylinders were taken out from the lime saturated water tank, and the excess water at the surface was removed by using a wet towel. Next, the initial surface resistivity measurement was taken at a random location along the center of the longitudinal axis of the cylinders, as shown in Figure 15. This location was defined as 0°. Subsequently, the specimens were rotated counterclockwise, and readings were taken at 90°, 180°, and 270°. For each specimen, a total of eight readings (i.e., two measurements per location) were taken. The average surface resistivity from three replicas was then obtained and multiplied by the curing correction factor (i.e., 1.1 for saturated lime water curing). The surface resistivity value of each mixture was then used to categorize ECC materials' chloride ion penetrability, according to AASHTO T358, as shown in Table 6.

**Figure 15. Surface resistivity test setup.**

**Table 6. Chloride ion penetrability (*75*).**

| Chloride Ion Penetrability | 4 in. X 8 in. Cylinder (KΩ-cm), a=1.5"* | 6 in. X 12 in. Cylinder (KΩ-cm), a=1.5"* |
|---|---|---|
| High | <12.0 | <9.5 |
| Moderate | 12.0-21.0 | 9.5-16.5 |
| Low | 21.0-37.0 | 16.5-29.0 |
| Very Low | 37.0-254.0 | 29.0-199.0 |
| Negligible | >254.0 | >199 |

*Note: a= Wenner probe spacing

### *4.1.3.6 Shrinkage*

Shrinkage is an important characteristic of concrete materials, which affects dimensional stability. When shrinkage is excessive, it can produce cracking, leading to early deterioration of concrete structures. Furthermore, shrinkage is a fundamental factor for concrete materials used in repair applications as it can produce stresses at the old/new concrete interface leading to debonding and failure of the repair. In this study, shrinkage during curing conditions was measured according to ASTM C157 (*72*). This was done by using prismatic specimens measuring 25 mm (1 inch) square cross-section and 254 mm (10 inches) in length (*72*). The test specimens were demolded after 23±0.5 hours of casting as per ASTM C157 (*72*). After demolding, specimens were immersed in a lime saturated water tank for 30 minutes at 23 ± 2°C, according to ASTM C157 (*72*). At the end of 30 minutes, the initial readings were taken using a digital length comparator, as shown in Figure 16. Next, the specimens were immersed again in the lime saturated water container. Subsequent readings were taken at 7, 14, and 28 days of curing. The relative length change for each specimen was computed as the ratio between the reading difference (i.e., reading at the desired age of curing and the initial readings) and the gage length, i.e., 250 mm., as shown in Eq. 7 (*72*).

$$\Delta L_x = \frac{CRD - initial\ CRD}{G}\ X\ 100 \quad [7]$$

where,

$\Delta L_x$= Length change of specimen at any given curing %;

CRD = Difference between the comparator reading of the reference bar and the specimen at any given age; and

G = Gage length (250 mm [10 inch]).

**Figure 16. Digital length comparator with the test specimen.**

### *4.1.3.7 Crack Width Analysis*

Wide cracks in concrete materials allow for the ingress of deleterious substances into concrete structures, which can adversely affect the durability. Unlike regular concrete, ECC materials exhibit tight cracks (usually between 60 to 100 $\mu$m). As such, structures constructed with ECC materials are likely to be more durable than regular concrete, as these tight cracks do not significantly increase the permeability of the material and allow self-healing characteristics of cementitious materials to be effective. For this reason, the cracking behavior of all ECC mixtures produced in this study was studied. Light microscopy was used to collect images of residual cracks in the dog-bone shaped specimens after completing the uniaxial tensile test. The microscope utilized in this study was a Zeiss SteREO Lumar V12 Microscope, as presented in Figure 17. A minimum of three specimens was evaluated for each material. The crack width was measured from the collected images by using digital image analysis software.

**Figure 17. Zeiss SteREO Lumar V12 Microscope**

### *4.1.3.8 Slant Shear Test (SST)*

For materials to be used for the repair of concrete structures, it is essential to determine the material's bond strength with a concrete substrate. The bond strength of SCBA admixed ECC materials were determined following a similar procedure to that of ASTM C882 standard. The bond strength was determined using 4" x 8" cylinders with a substrate layer composed of regular concrete and a top layer composed of SCBA admixed ECC mixture, as shown in Figure 18a. The concrete substrate was cast by filling 50% of the cylinder volume and tilting it at a 30° angle from the horizontal using a specimen holder, as shown in Figure 18b. Right after casting, the cylinders were covered with a plastic lid to prevent moisture loss. After 24 hours, the cylinders with the hardened concrete substrate were placed in saturated lime water for 28 days (without removing the concrete substrate from the molds). The concrete material used as a substrate was a Louisiana DOTD Type-B pavement mixture. This concrete material had a W/C ratio of 0.45 and a cement content of 297 kg/m$^3$. Mixture design details are presented in Table 7. After allowing the concrete substrate to cure for 28 days in saturated lime water, SCBA admixed ECC mixtures were poured on top of the concrete substrate to fill the remaining half-section of the cylinders. After 24 hours of casting, the cylinders were demolded and placed in saturated lime water for 28 days. At the end of the curing phase, the specimens were tested for compressive strength as per ASTM C39 to determine the composite cylinder's (presented in Figure 18c) maximum load at failure. It is important to note that only one mixture was utilized to test for bond strength for each class of ECC mixture (i.e., class S and class C). These materials were the best performing for each ECC mixture class. The bond strength was calculated by using Eq. 8.

$$\tau_n = \frac{P}{A}\sin(\alpha) * \cos(\alpha) \quad [8]$$

where: $\tau$ = shear stress, P = ultimate load, A = cross sectional area, and $\alpha$ = angle of the bonded interface from horizontal (30°).

**Table 7. Mix proportion of concrete mixtures used in SST**

| Target Compressive Strength MPa (psi) | Cement (kg/m$^3$) | Coarse Aggregate (kg/m$^3$) | Fine Aggregate (kg/m$^3$) | Water (kg/m$^3$) |
|---|---|---|---|---|
| 27.6 (4000) | 296.7 | 1124.1 | 744.3 | 133.5 |

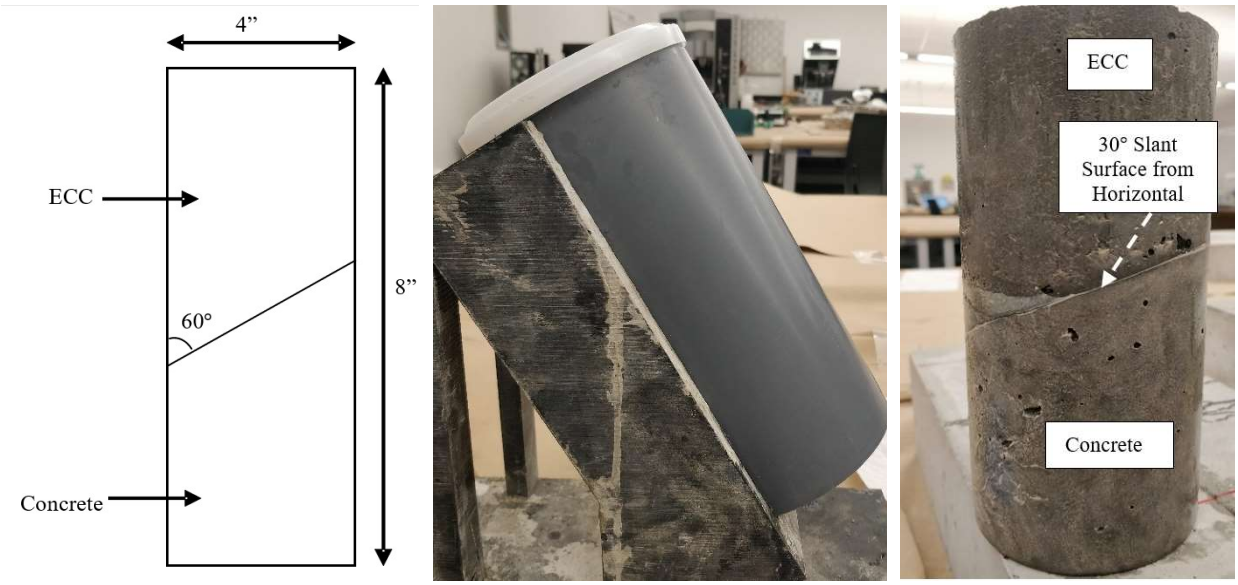


**Figure 18. Slant shear test: (a) Cylinder dimension (b) Specimen in a mold (c) Composite cylinder with two material layers**

#### *4.1.3.9 Coefficient of Thermal Expansion*

The coefficient of thermal expansion (CTE) of materials to be used for repair applications of concrete structures is of great relevance since compatibility between the repair material, and the concrete substrate minimizes the possibility of debonding failure. Furthermore, the CTE is also a relevant property regarding the potential occurrence of cracking in concrete materials subjected to large temperature fluctuations under restrained conditions. In this study, the CTE was determined as per ASTM C531 using the mortar bars (*76*). The specimens used to determine the CTE were dry specimens (i.e., they were placed at room temperature, i.e., 23 ± 2°C). The dry specimen's length was measured using the digital length comparator, as shown in Figure 16. Subsequently, the specimens were placed at 100°C for at least 16 hours. After 16 hours, the specimens were removed from the oven to measure the length of the specimens. Next, the specimens were again placed at room temperature for 16 hours, and the length was measured. This process (23°C to 100°C to 23°C) was repeated until the specimen reached a constant length at both temperatures. The CTE was then determined by using Eq. 9. It is worth mentioning that the results from four replicas for each mixture were averaged and reported in this study.

$$C = (A - B - Y)/T(Y - X) \quad [9]$$

$A$ = length of the bar, including studs, at elevated temperature, in. (mm),
$B$ = length of stud expansion, in. (mm), = X × T × k (where k is the linear coefficient of thermal expansion per °F (°C) of the studs); K= 7.2 × $10^{-6}$ per °F (4 × $10^{-6}$ per °C); T= 100°C.
$Y$ = length of the bar, including studs, at a lower temperature, in. (mm),
$T$ = temperature change, °F (°C) and
$X$ = length of the two studs at a lower temperature, in. (mm).

## 4.2. ECC Materials Produced with Ecuador SCBA

### *4.2.1. Materials*

#### *4.2.1.1 Ecuador Raw SCBA*

In addition to the investigation of RBA properties, this study also characterized raw SCBA produced in the Ingenio San Carlos sugar mill located in Guayas, Ecuador. The raw SCBA was produced in a similar method, as described in section 4.1.1.1. Figure 19a presents the Ecuador raw SCBA used as a substitute of silica sand in ECC mixtures. The specific gravity of the produced SCBA was 2.19. The raw SCBA produced in Ecuador was labeled as EBA. The produced EBA was thoroughly characterized by SEM-EDS, X-ray diffraction (XRD), and laser diffraction particle size analysis. In addition, the pozzolanic activity of EBA was evaluated by the Strength Activity Index (SAI) method, according to ASTM C311. The EBA was used as a partial and complete replacement to river sand in ECC mixtures. The ECC mixtures using EBA as a substitute to silica sand were produced in Ecuador using readily available ingredients in the country. These mixtures are referred to as class S-E mixtures.

**(a)** **(b)** **(c)**

**Figure 19. Materials used in ECC mixtures: (a) Raw SCBA produced in Ecuador, i.e., EBA (b) Zeolite (c) PP Fiber**

#### *4.2.1.2 Other Ingredients*

The materials used in the production of class S-E ECC mixtures were Type I OPC (specific gravity of 3.15), zeolite (specific gravity of 2.17) as a partial replacement to cement, fine river sand (specific gravity of 2.64), water, high-range water-reducing admixture (HRWR), and Polypropylene (PP) fibers. The particle size distribution of zeolite and river sand determined by laser diffraction particle size analysis and sieve test are presented in Figures 20a and 20b, respectively. The zeolite exhibited a mean particle size of 47.5 $\mu$m (with maximum nominal particle size of 227.5 $\mu$m). Furthermore, the fine river sand exhibited a maximum particle size of 2360 $\mu$m.

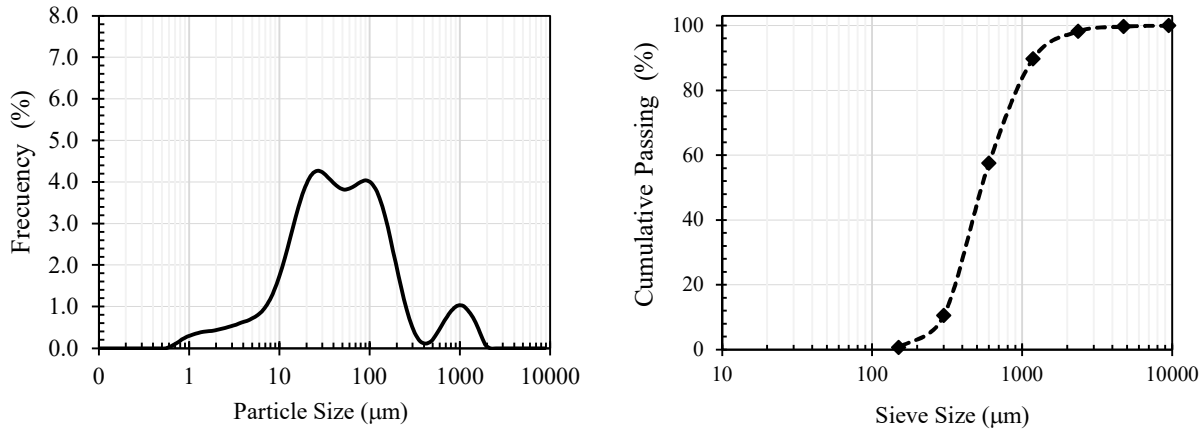


**Figure 20. Cumulative passing particle size distribution: (a) Zeolite particle size distribution (b) Fine river sand gradation**

The PP fibers utilized in ECC mixtures were provided by SIKA Ecuador. The Sika-fibers have a length of 19 mm, a Young's modulus of 14.7 GPa, a maximum elongation of 20-30%, and a specific gravity of 0.91. Figures 19b and 19c show images of the Zeolite and PP fibers used in ECC mixtures, respectively.

### *4.2.2. Testing of Ecuador SCBA Admixed ECC*

#### *4.2.2.1 Mixture Proportioning and Specimen Preparation*

The raw SCBA produced in Ecuador (EBA) was used as a substitution to fine river sand to produce class S-E mixtures. To investigate the influence of sand replacement with EBA on the properties of ECC, a total of five ECC mixtures were prepared. The dosages of sand replacement investigated were 0%, 25%, 50%, 75%, and 100% by volume. The zeolite-to-cement ratio (Z/C), water-to-binder ratio (W/B), and the fiber content of all EBA admixed ECC mixtures were kept constant at 2.2 (by weight), 0.32 (by weight), and 2.2% (volume fraction), respectively. The details of the ECC mixture proportions are illustrated in Table 8.

**Table 8. EBA admixed ECC mixture proportions**

| Mix ID | Cement ($kg/m^3$) | Zeolite ($kg/m^3$) | Water ($kg/m^3$) | Sand ($kg/m^3$) | RBA ($kg/m^3$) | RBA (%)[a] | HRWR (%)[b] | $V_f$ (%)[c] |
|---|---|---|---|---|---|---|---|---|
| S-E-0 | 356.4 | 784.0 | 364.9 | 366.4 | 0 | 0 | 0 | 2.2 |
| S-E-25 | 356.4 | 784.0 | 364.9 | 274.8 | 83.4 | 25 | 0.13 | 2.2 |
| S-E-50 | 356.4 | 784.0 | 364.9 | 183.2 | 166.9 | 50 | 0.45 | 2.2 |
| S-E-75 | 356.4 | 784.0 | 364.9 | 91.59 | 250.3 | 75 | 0.80 | 2.2 |
| S-E-100 | 356.4 | 784.0 | 364.9 | 0 | 333.7 | 100 | 1.5 | 2.2 |

[a] % of sand replacement by volume; [b] % of HRWR by weight of cement; [c] % of fiber content by volume

The ECC mixtures were produced in a planetary mixture by following the same procedure, as explained in section 4.3.2. At the end of the mixing process, three cubes and three beams were cast for each mixture for 7- and 28-day testing. All the specimens were covered with plastic and left in the mixing room (specimens were covered to prevent moisture loss) for 24 hours before demolding. After demolding, all specimens were placed in a lime saturated water tank, according to ASTM C192 (*77*).

#### *4.2.2.2 Compressive Strength*

The compressive strength of the EBA admixed ECC mixtures were assessed according to ASTM C109 (*78*) on 50 x 50 x 50 mm cube specimens. For each mixture, three specimens were tested at 7 and 28 days of curing, utilizing hydraulic pressure with a constant loading rate of 0.25 MPa/s.

#### *4.2.2.3 Flexural Strength*

A test method as per ASTM C293 (*79*) was performed to determine the modulus of rupture of specimens. For each mixture, three 76.2 x 35.1 x 300 mm beams were cast and cured as per ASTM C192 (*80*) to be evaluated at 28 days of curing. A simple beam with center-point loading was used to determine the flexural strength.

# 5. ANALYSIS AND FINDINGS

## 5.1. Louisiana SCBA Characterization

### *5.1.1. Microstructure and Chemical Composition*

Figure 21a shows the RBA used as a substitute to silica sand in class S mixtures, and Figure 21b presents its morphology obtained from backscattered electron SEM (BSE-SEM) imaging. RBA particles were found to exhibit a variety of shapes and sizes (i.e., fibrous particles, irregular porous particles, spherical particles, and prismatic particles). It is worth mentioning that the SCBA in sugar mills is produced from the uncontrolled burning of SBF, and therefore, a high temperature gradient exists within the sugar mill boilers. As such, fibrous particles observed in the BSE-SEM image occurred likely due to SBF's incomplete combustion at low burning temperature zones within the boiler. Moreover, prismatic particles observed, which are typically associated with crystalline silica, did likely occur due to SBF's calcination at high temperature zones (i.e., usually above 700°C) (*35*). However, the presence of prismatic particles in RBA may also be partially credited to soil contamination (i.e., soil adhered to SBF during harvesting). A previous study revealed that spherical particles in SCBA are formed due to the melting of silica at high temperatures (*35*). As such, the spherical particles in RBA are credited to the SBF portion, experiencing the highest temperatures at the sugar mill boiler. Finally, in accordance with previous literature, it is believed that the irregular porous particles observed in RBA are rich in silica (*81*). It should be noted that RBA's black color is indicative of the high carbon content of this material.

Figure 21c presents the PBA used as a substitute to cement in ECC mixtures, and Figure 21d presents its BSE-SEM image. As mentioned earlier, PBA was produced by burning RBA at 450°C. A distinctive effect of burning on PBA is observed from its appearance the SCBA changed from black to brown color. This change indicates the removal of a significant amount of carbon from the material. Furthermore, residual unburnt fibers observed in RBA were burned during the post-processing phase. This in turn, resulted in the absence of fiber-like particles in PBA's BSE-SEM image. Similar to RBA, PBA consisted of irregular prismatic and porous particles. Furthermore, as in RBA, the prismatic particles are attributed to crystalline silica, while the irregular particles are associated with amorphous silica. It is worth mentioning that the main differences between these two materials, in terms of morphology, were the presence/absence of unburnt fibrous particles and particle size.

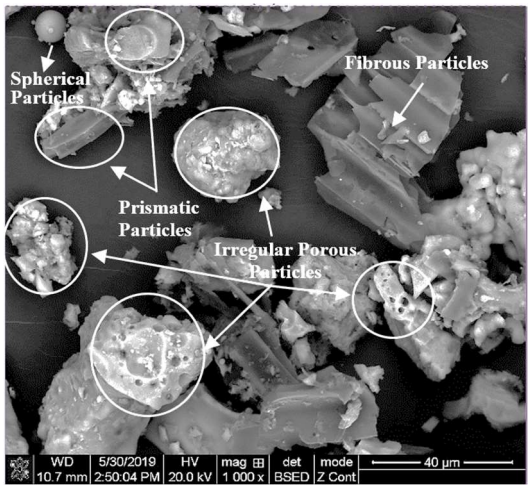

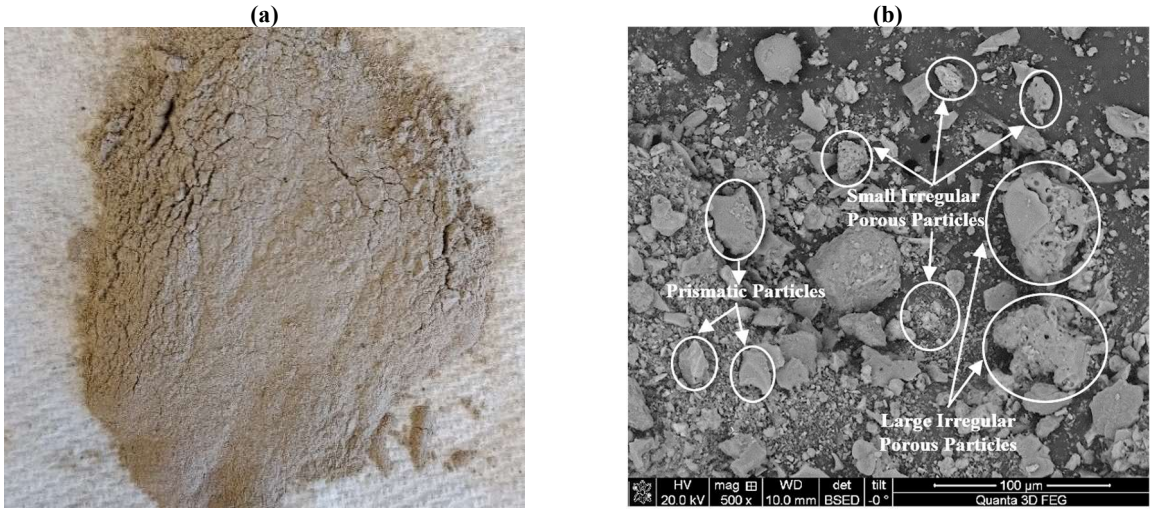


**Figure 21. SCBAs' characterization (a) RBA (b) BSE-SEM image of RBA (c) PBA (d) BSE-SEM image of PBA**

To obtain insight into the chemical composition of both SCBAs, EDS spectra were collected during the SEM imaging process. The oxide composition of both SCBAs is presented in Table 9a. It is observed that RBA mainly consists of silicon dioxide ($SiO_2$) and carbon (presented as $CO_2$ equivalent in Table 9a). Regarding PBA, a significant amount of $SiO_2$ (i.e., 70.1%) and a minimal amount of carbon (i.e., 6.8%) were present. The sum of the pozzolanic component ($SiO_2$+$Al_2O_3$+$Fe_2O_3$) for RBA and PBA was 52.5% and 83.9%, respectively. While RBA met ASTM C618 (*82*) minimum pozzolanic requirement (i.e., 50%) to be classified as Class C pozzolan, PBA met the requirement (i.e., 70%) to be classified as Class F and N pozzolan. Moreover, as per ASTM C618, the maximum allowable limit for $SO_3$ is 4% for class N pozzolan and 5% for class F and C pozzolan, which was met by both SCBAs (*82*).

In order to verify the EDS results obtained for both SCBAs, XRF analysis was conducted. In contrast to the EDS system, the XRF equipment cannot detect elements lighter than magnesium. As such, the detection of carbon is not possible. For the XRF analysis, 0.6 grams of powdered samples were fused with a mix of Li-iodide, Li-metaborate, and Li-tetraborate at 1000°C in a Clarisse LENeo fluxer to glass beads. The XRF results for both SCBAs are presented in Table 9b. For RBA, the total pozzolanic component reported from the XRF analysis (i.e., 88.75%) was much higher than that reported from the EDS analysis. This was attributed to the absence of carbon detectiont in the XRF analysis. In contrast, for PBA, the XRF analysis showed a lower pozzolanic component (i.e., 72.62%) compared to the EDS analysis results. Yet, PBA continued to meet the minimum pozzolanic component requirement (i.e., 70%) to be classified as Class F and N pozzolan, according to ASTM C618.

**Table 9. SCBA oxide composition (by weight) (a) EDS analysis (b) XRF**

**(a)**

| Material | CaO | $SiO_2$ | $Al_2O_3$ | $Fe_2O_3$ | $K_2O$ | $Na_2O$ | MgO | $SO_3$ | C (as $CO_2$ equivalent | $SiO_2$+ $Al_2O_3$+ $Fe_2O_3$ | ASTM C618 Requirement |
|---|---|---|---|---|---|---|---|---|---|---|---|
| RBA(%) | 3.8 | 42.8 | 5.5 | 4.2 | 3.6 | 0.1 | 0.5 | 0.1 | 38.1 | 52.5 | Class C Pozzolan |
| PBA (%) | 3.6 | 70.1 | 8.2 | 5.6 | 4.1 | 0.0 | 0.4 | 0.0 | 6.8 | 83.9 | Class F and N Pozzolan |

**(b)**

| Material | CaO | $SiO_2$ | $Al_2O_3$ | $Fe_2O_3$ | $K_2O$ | $Na_2O$ | MgO | $SO_3$ | $SiO_2$+ $Al_2O_3$+ $Fe_2O_3$ | ASTM C618 Requirement |
|---|---|---|---|---|---|---|---|---|---|---|
| RBA(%) | 3.1 | 78.6 | 7.6 | 2.5 | 4.5 | 0.7 | 1.2 | 0.0 | 88.7 | Class C Pozzolan |
| PBA (%) | 5.1 | 63.5 | 6.5 | 2.6 | 4.1 | 0.6 | 1.5 | 0.2 | 72.6 | Class F and N Pozzolan |

### *5.1.2. Particle Size Analysis*

The particle size distribution of RBA, unground PBA, and ground PBA, obtained from Laser diffraction particle size analysis, is presented in Figure 22. Furthermore, Table 10 presents the mean, median, D10, D25, D50, D75, and D90 particle size. It is observed that the mean particle size of RBA is 256 $\mu$m, indicating that the RBA is much finer than the fine river sand (i.e., mean particle size of 474 $\mu$m) used in this study. Furthermore, the $D_{90}$ particle size of RBA was 539 $\mu$m, while for the fine river sand, it was 786 $\mu$m. As mentioned earlier, the use of aggregate with fine particle size is preferable in ECC mixtures to enhance the PSH behavior. Consequently, the fine particle size of RBA makes this material promising for sand replacement in ECC mixtures.

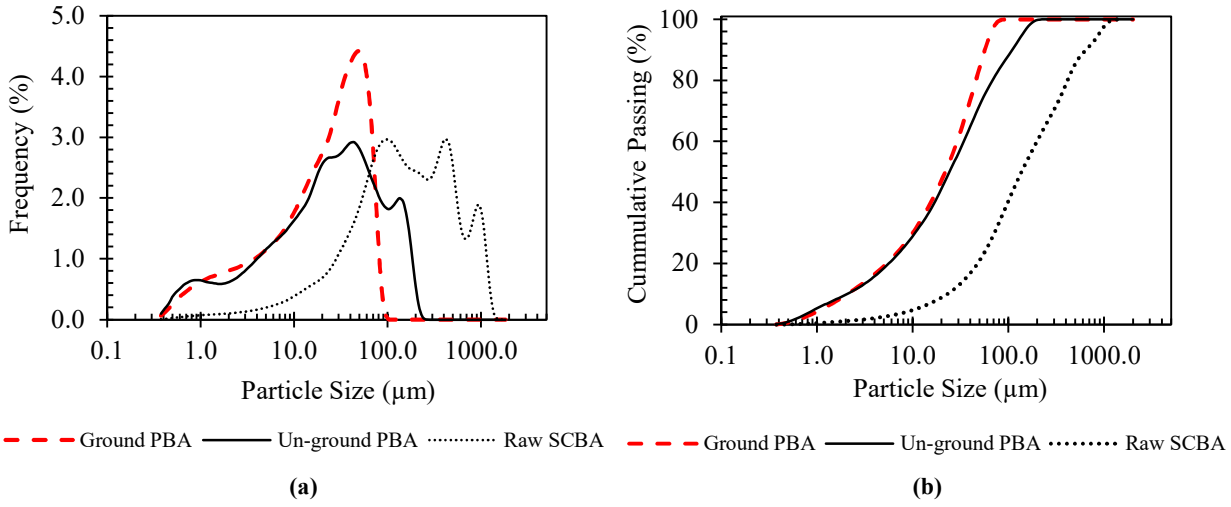


**Figure 22. SCBAs particle size analysis: (a) Particle size frequency distribution and (b) Cumulative particle size distribution.**

In contrast to RBA, un-ground PBA particles were much finer; thus, highlighting a significant effect of post burning on reducing the particle size. This phenomenon is credited to the calcination of coarse fibrous impurities observed in RBA during the post burning treatment. In the case of ground PBA, a significant effect of grinding was observed on the particle size distribution. For instance, the mean particle size of un-ground PBA was 44 $\mu$m, which was reduced to 28 $\mu$m for ground PBA. This was mainly attributed to the effectiveness of grinding in eliminating the coarser particles, i.e., $D_{90}$ size for un-ground PBA was 120 $\mu$m and 62 $\mu$m for ground PBA. It should be noted that the particle size distribution of the ground PBA was similar to that of fly ash. The fly ash exhibited a mean particle size of 22.7 $\mu$m and is presented in Figure 6.

**Table 10. Size distribution for ground samples.**

| ID | Mean ($\mu$m) | Median ($\mu$m) | D10 ($\mu$m) | D25 ($\mu$m) | D50 ($\mu$m) | D75 ($\mu$m) | D90 ($\mu$m) |
|---|---|---|---|---|---|---|---|

| | | | | | | | |
|---|---|---|---|---|---|---|---|
| RBA | 256 | 171 | 22 | 67 | 171 | 341 | 539 |
| Un-ground PBA | 44 | 27 | 2 | 9 | 27 | 61 | 120 |
| Ground PBA | 28 | 24 | 2 | 8 | 24 | 45 | 62 |

### *5.1.3. X-ray Diffraction (XRD)*

Figures 23a and 23b present the XRD pattern of RBA and PBA, respectively. For both SCBAs, a characteristic quartz peak is present, which is indicative of the presence of crystalline silica in the form of quartz. It is also important to note that both SCBAs exhibited very similar XRD patterns. The patterns observed included an amorphous bump between 2θ angles of 10° and 40° and a dominant peak at a 2θ angle of 26.6°.

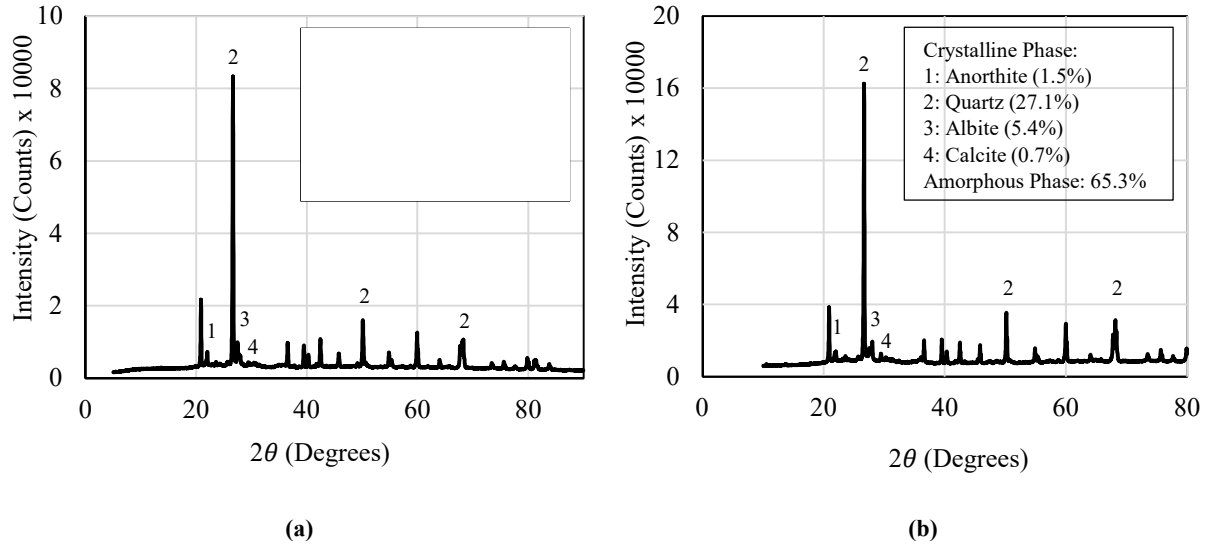


**Figure 23. X-ray diffraction patterns: (a) RBA and (b) PBA**

The different phases present in SCBA materials were quantified by using Rietveld analysis conducted using Highscore plus software. It is important to mention that the quartz powder was used as an amorphous standard. The analysis results yielded 52.9% of amorphous component, 38.9% of quartz, and 5.5% of albite for RBA and 65.3% of the amorphous component, 27.1% of quartz, and 5.4% of albite for PBA. For both SCBA materials, the quartz content may be attributed to the crystallization of amorphous silica during calcination of SBF at the sugar mill and the presence of soil adhered to the SBF during sugarcane harvest. In contrast, the presence of an amorphous phase can be attributed to the presence of amorphous silica and/or unburnt SBF.

### *5.1.4. Density, Specific Gravity, and Absorption*

The specific gravity and absorption of RBA determined as per ASTM C128 was 2.32 and 2.0%, respectively. In contrast, the density and absorption of the fine river sand was 2.62 and 0.4%, respectively. This shows that RBA is lighter than the fine river sand and has a greater water absorption capacity. In the case of PBA, the density as determined per ASTM C188 was 2519 kg/m$^3$. It is worth mentioning that the reported density is the average of two readings and the standard deviation was 27 kg/m$^3$, which was within 30 kg/m$^3$ permitted standard deviation as per ASTM C 188. This indicates that PBA density is much lower than that of cement (i.e., the density of 3150 kg/ m$^3$); yet, comparable to that of fly ash (i.e., a specific gravity of 2.29).

### *5.1.5. Chapelle's Test*

The summary of the pozzolanic activity test, as per Chapelle's method, is presented in Table 11. From Table 11, a clear distinction in the pozzolanic activity for RBA and PBA can be observed, While RBA exhibited a calcium consumption of 201.5 mg/g of RBA, PBA exhibited a Chapelle activity (i.e., CaO consumption) of 309.9 mg/ g of PBA. In addition, this result is in line with the previous studies, which exhibited higher reactivity for post-processed SCBA material (*18*, *83*).

**Table 11. Chapelle's test results.**

| Material | CaO consumption (mg/g) | Standard Deviation (mg/g) | Coefficient of Variation (%) |
|---|---|---|---|
| RBA | 201.5 | 74.1 | 36.8 |
| PBA | 309.9 | 181.1 | 58.4 |

### *5.1.6. Strength Activity Index (SAI)*

The compressive strength results of mortar cubes (Control, RBA, PBA, and sand) and corresponding SAI values are presented in Figures 24a and 24b, respectively. It is observed that replacing cement with either of the SCBAs reduced the compressive strength significantly. For instance, the control mixture's compressive strength was 42.7 MPa, which was reduced to 30.8 MPa for RBA mixtures and 33.7 MPa for PBA mixtures. Nevertheless, for both SCBA admixed mortars, the compressive strength was higher than the sand mixture (i.e., compressive strength was 27.23 MPa).

From Figure 24b, the effect of post-processing of RBA to produce PBA is clearly observed in the SAI results. For RBA, the SAI value was 72.1%, which increased to 78.8% for PBA. This result agrees with the pozzolanic component reported from EDS analysis, which was higher for PBA. Besides, the particle size of PBA was finer than RBA, indicating that PBA may exhibit an enhanced reactivity and act as a filler material. As such, the increase in SAI for PBA may be attributed to the enhanced pozzolanic activity and/or filler effect. Even though the SAI for RBA was low, it exhibited higher SAI than the sand admixed mortar cubes (i.e., 63.7%). This result suggests that RBA is likely to exhibit a minor pozzolanic activity and/or filler effect. However, this was not sufficient for RBA to meet the minimum SAI requirement of 75% to be classified as a pozzolan (*84*). While RBA did not meet the SAI requirement, PBA did. As such, PBA presents the potential to be used as an SCM in ECC mixtures.

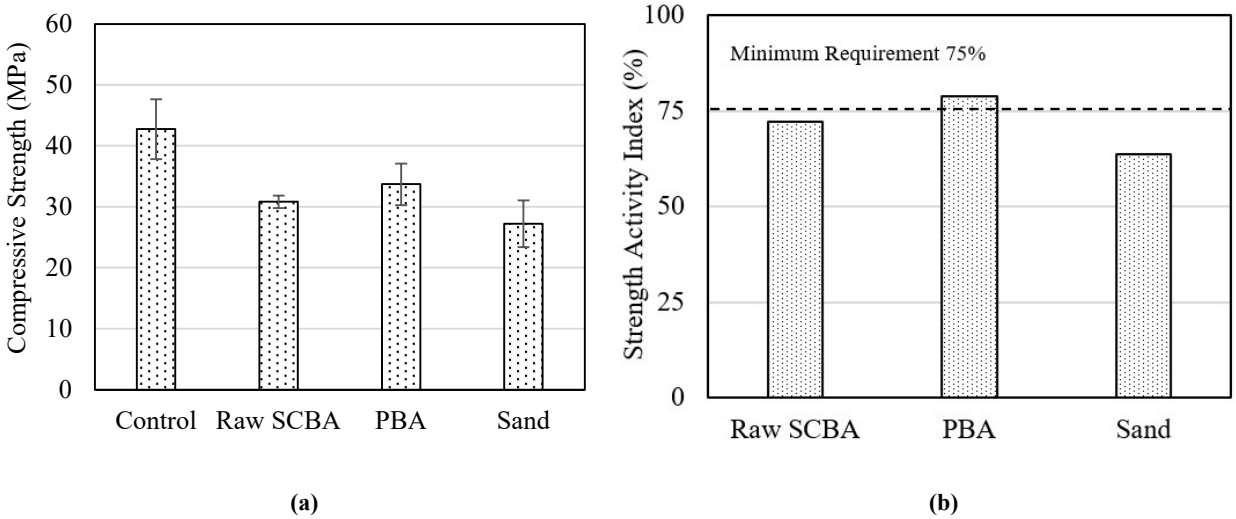


**Figure 24. (a). Compressive strength (b) Strength activity index for RBA and PBA**

## 5.2. Ecuador SCBA Characterization

### *5.2.1. Microstructure and Chemical Composition*

The SEM image of raw SCBA produced in Ecuador (EBA) was obtained using an FEI- Inspect and Phenom 1255 Scanning Electron Microscope (SEM) operated at 10 kV. EDS/EBSD detectors were utilized to investigate the morphology and elemental composition of EBA. Figure 25 presents a backscattered electron images of SCBA, with EDS analysis of particle labeled A (shown in Figure 25b). From the SEM images it can be observed that EBA consists of a combination of particles with different shapes and sizes. The majority of the observed particles were porous particles. Figure 25c presents a magnified image of the particle labeled as A (in Figure 25a). The presence of porous particles is a consequence of the calcination process in sugar mills, during which the organic material is burned, leaving behind mainly porous-amorphous particles rich in silica, as showed by the EDS analysis. Particles with a defined shape like prism are also observed (particle B in Fig 25d). They could correspond to crystalline phases.

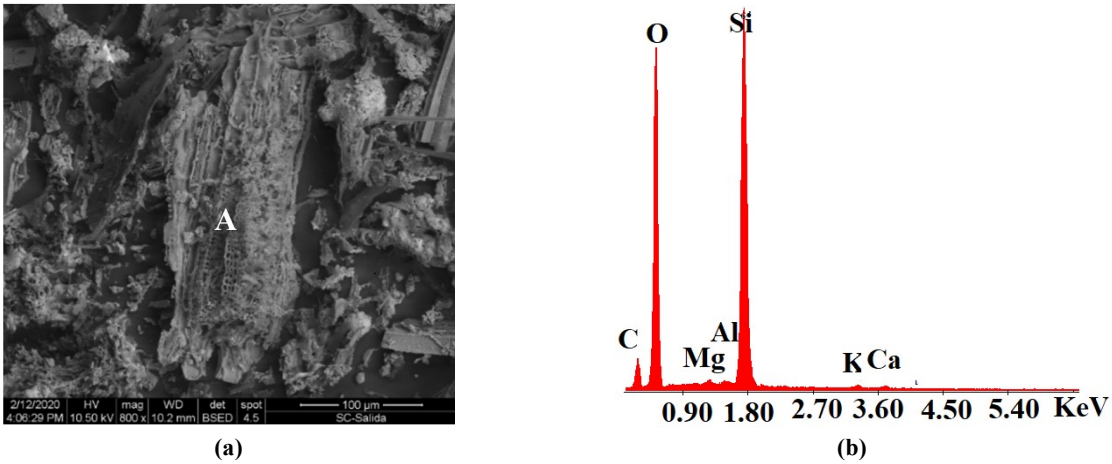

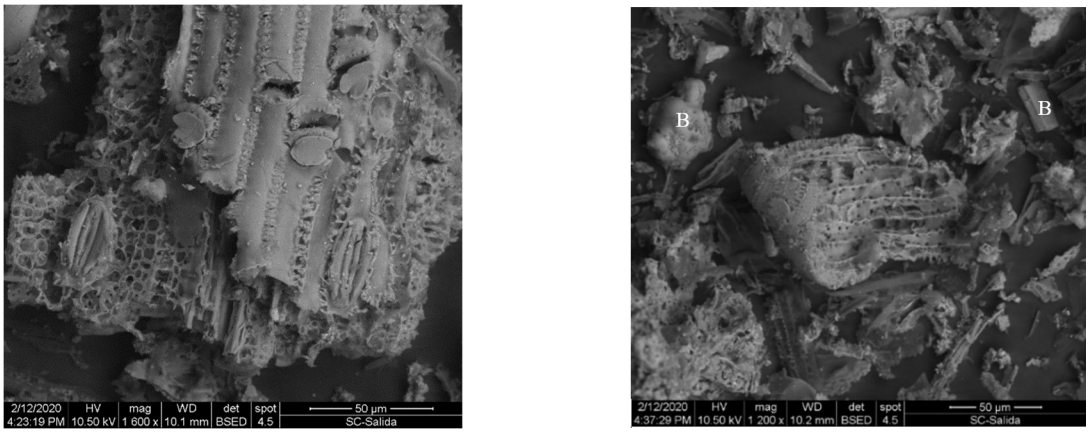


**(c)** **(d)**

**Figure 25. BSE-SEM images of EBA (a) General view with EDS analysis of particle A, (b) EDS spectra for particle A, (c) details of porous particles, and (d) Different shapes particles with a prismatic one**

### *5.2.2. XRD and Particle Size Analysis*

XRD analysis was performed by using Co radiation at 30 mA and 45 kV, with a step size of 0.05 in the range of 5° to 80° $2\theta$. Figure 26a presents the XRD pattern of raw SCBA. The quantitative XRD analysis of SCBA samples reported the presence of 46.1 % of amorphous component, 15.7% of quartz, Anorthite 9.1%, Graphite 7.2%, and 21.9% of Albite in EBA. Furthermore, the particle size distribution of EBA obtained from Mastersizer 2000 Laser Diffraction Particle Size Analyzer is presented in Figure 26b. From Figure 26b, it is observed that EBA consists of finer particles in comparison to that of silica sand. For instance, the mean particle size of raw SCBA was 248 $\mu$m (maximum nominal particle size of 618 $\mu$m), and the mean particle size for river sand was 992 $\mu$m. It is worth mentioning that the particle size of EBA was similar to RBA (i.e., mean particle size of 256 $\mu$m)

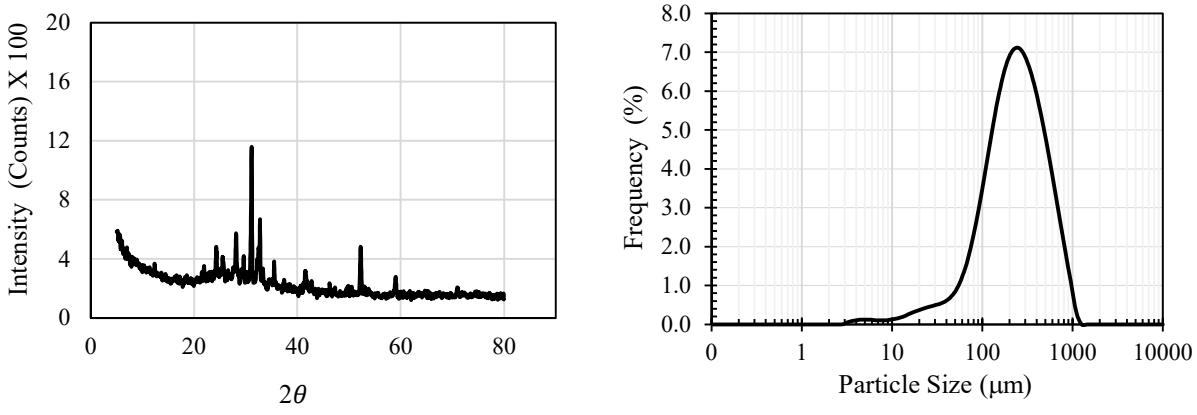


**(a)** **(b)**

**Figure 26. EBA characterization: (a) XRD pattern and (b) Particle Size distribution**

### *5.2.3. Strength Activity Index (SAI)*

The compressive strength and corresponding SAI for EBA is presented in Figure 27a and 27b, respectively. It is observed that replacing cement with EBA reduced the compressive strength. For instance, the compressive strength for the control mixture was 43.33 MPa at 28 days of curing,

which reduced to 39.47 MPa for the EBA mixture. However, this value was significantly higher than the compressive strength for sand mixtures (i.e., the compressive strength of 29.94 MPa). The corresponding SAI value for EBA was 84.4% and 91.1% at 7 and 28 days of curing, respectively. EBA met the ASTM requirement for SAI to be classified as a pozzolan, which may be attributed to the high silica content observed in Figure 25b. It is worth mentioning that the SAI exhibited by EBA is significantly higher than the RBA's SAI. This indicates that different sources of SCBA can significantly influence the pozzolanic properties of raw SCBA. Nevertheless, this difference may also be attributed to the burning process of the SBF in the sugar mill.

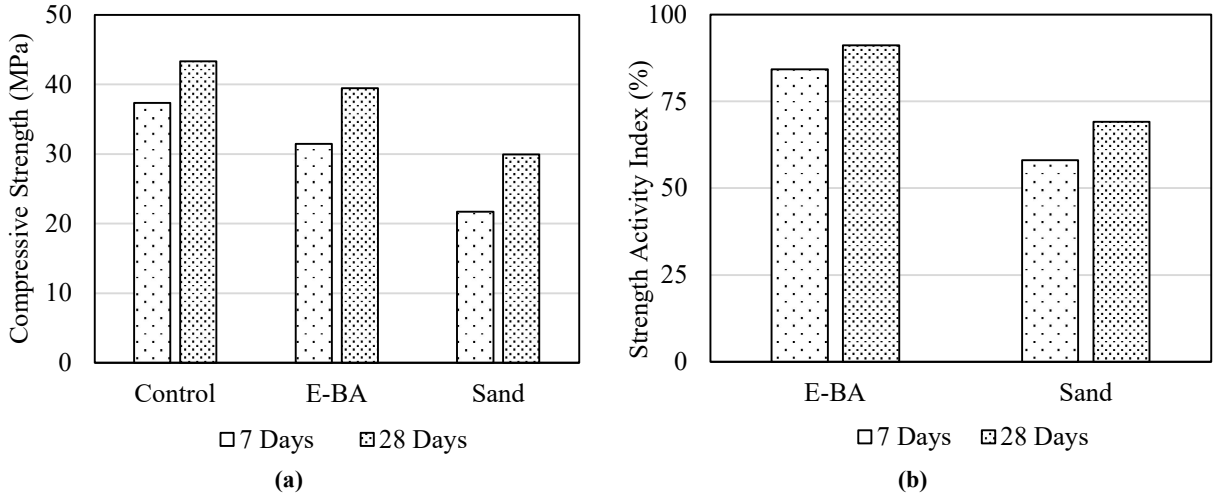


**Figure 27. (a) Compressive strength and (b) Strength activity index for EBA**

## 5.3. Testing of Louisiana SCBA Admixed ECC Mixtures

### *5.3.1. Compressive Strength*

#### *5.3.1.1 Class S Mixtures*

The compressive strength test results for class S mixtures are presented in Figure 28a. In general, a negative trend in compressive strength with the increase in RBA was observed. However, the decrease in compressive strength was small. For instance, relative to the control mixture (with 33.6 MPa compressive strength), the maximum decrease observed was 11.0% (i.e., 29.9 MPa) for the ECC mixture using 75% of RBA as a substitute to silica sand (S-75). For the other mixtures, the reductions in compressive strength relative to the control mix were 0.4% for S-25 (i.e., 33.2 MPa), 5.7% for S-50 (i.e., 31.6 MPa), and 10.4% for S-100 (i.e., 30.1 MPa). An Analysis of Variance (ANOVA) was conducted to determine if the differences in the average compressive strength for class S mixtures were significant. The statistical analysis conducted at a significance level of 0.05 (presented in Appendix A Table A1) showed a significant difference in mixtures' compressive strength (i.e., p-value =0.0006). Furthermore, a Tukey pairwise comparison (presented in Appendix A Figure A1) showed that differences between the control ECC mixture and ECC mixtures using RBA at 75 and 100% replacement level, mix combination of S-25 and S-75, and mix combination of S-25 and S-100 were statistically significant.

It is worth mentioning that the increase in the RBA content reduced the workability of fresh mixtures. As such, HRWR dosage was increased proportionally to achieve good workability. It is well documented in the previous literature that the increase in HRWR dosage directly influences

air content (i.e., air content increases with the increase in HRWR dosage) (*85*, *86*). Due to the increase in HRWR dosage, the air content reported in Table 4 shows an increasing trend with the increase in RBA content. For instance, the air content for control mixtures was 1.4%, which increased to 5.8% for S-100. As per the ACI report, an increase in 1% of air content can decrease compressive strength by approximately 5% (*87*). As such, for 1.5%, 2.1%, 3.9%, and 4.4% increase in air content for S-25, S-50, S-75, and S-100, the expected reduction in compressive strength was approximately 7.5, 10.5, 19.5, and 22%, respectively. However, the actual decrease in the compressive strength reported above was much lower than the expected decrease. This may be attributed to RBA's pozzolanic and/or filler effect, which improved the pore structure and mitigated the reduction in compressive strength.

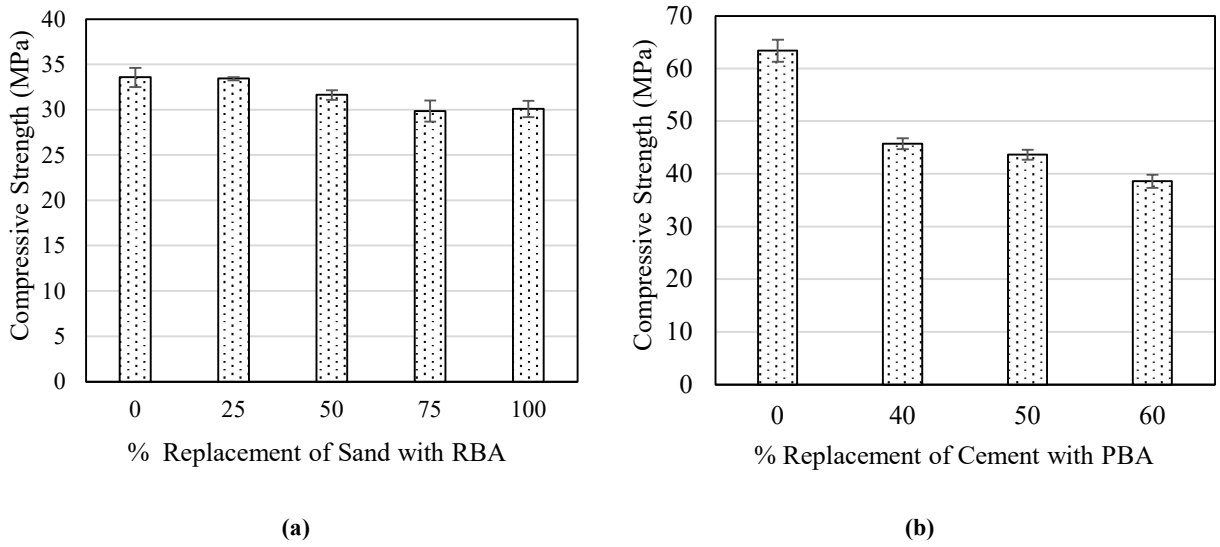


**Figure 28. Compressive strength of ECC cylinders (a) Class S mixtures (b) Class C mixtures**

### *5.3.1.2 Class C Mixtures*

The compressive strength test results for class C mixtures are presented in Figure 28b. A significant decrease in compressive strength with the increase in PBA content is observed for class C mixtures. In comparison to the control mixture (with compressive strength of 63.4 MPa), the decrease in strength for C-40, C-50, and C-60 was 27.9% (i.e., 45.7 MPa), 31.2% (i.e., 43.6 MPa), and 39.1% (i.e., 38.6 MPa), respectively. As per ANOVA (presented in Appendix A Table A2), a significant difference in the compressive strength of class C mixtures was encountered (p-value <0.0001). Moreover, as per Tukey pairwise comparison, the differences in compressive strength between all pairwise comparisons, except C-40 compared to C-50, were statistically significant.

From the EDS and XRD analysis, it is evident that PBA has a substantial amount of amorphous $SiO_2$; and, therefore, were likely to exhibit some pozzolanic activity. However, while the hydration reaction occurs as soon as the water is added to the cement, the pozzolanic reaction occurs at a relatively later age. As such, since the cylinders were tested at 28 days of curing, it is likely that the pozzolanic reaction of PBA did not significantly contribute to the strength of the ECC mixture. It is worth mentioning that the pozzolanic reaction occurs when calcium hydroxide (CH), formed as a by-product of the cement hydration reaction, reacts with amorphous $SiO_2$ present in the pozzolanic materials to produce calcium silicate hydrate (CSH). CSH enhances the pore structure and contributes to the strength of the mixture. Apart from the pozzolanic effect, the unreacted

particles can remain in the matrix as a filler and further contribute to pore structure refinement. As such, at a later age of curing, PBA-admixed mixtures are expected to result in higher compressive strength. To this end, future studies should be conducted to evaluate the compressive strength of PBA admixed ECC mixtures at various curing ages beyond 28 days.

It is worth mentioning that all ECC mixtures (class S and C mixtures) have a compressive strength exceeding that of normal concrete (i.e., 30 MPa). In addition, all of the mixtures met the LaDOTD minimum 28-day compressive strength (i.e., 4000 psi ≈ 27.6 MPa) requirement for concrete materials to be used for pavement construction and repair.

### *5.3.2. Density of Hardened ECC Mixtures*

Figures 29a and 29b present the hardened density of all class S and class C ECC materials. As it can be observed, a progressive decrease in hardened density with the increase in SCBA content occurred. For instance, the density for class S control mixture (S-0) was 1917 kg/m$^3$, which decreased to 1771 kg/m$^3$ for S-100 (i.e., a decrease of 7.6%). Similarly, for the class C control mixture, the density was 2092 kg/m$^3$, which decreased to 1912 kg/m$^3$ for C-60 (i.e., a decrease of 8.6%). For class S mixtures, the density reduction occurred since RBA is lighter than the fine river sand replaced. In addition, the increase in air content reported in Table 4 was also a contributing factor to the decrease in density. For class C mixtures, the decrease in density was credited to the lower specific gravity of PBA (i.e., 2.5) in comparison to that of cement (i.e., 3.1). It is relevant to note that the densities of all the ECC materials evaluated were lower than the density of conventional concrete (i.e., 2400 kg/m3). This, in turn, highlights the higher strength to weight ratio of these composites in contrast to conventional concrete.

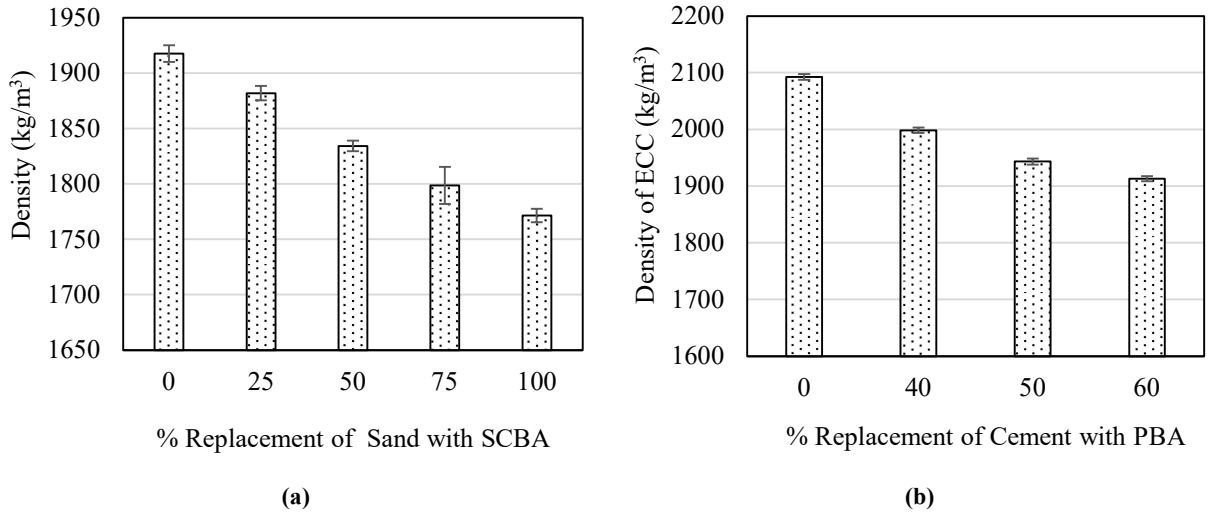


**Figure 29. Density of hardened ECC material: (a) RBA-ECC mixtures (b) PBA-ECC mixtures**

### *5.3.3. Tensile Properties*

#### *5.3.3.1 Class S Mixtures*

The tensile stress-strain curves for all class S mixtures are presented in Figure 30a-e. It is worth mentioning that Figure 30a-e presents the tensile stress-strain curves for all six replicas of each mixture. As it is observed, all class S mixtures exhibited PSH behavior after first cracking (i.e.,

first peak), producing significant amounts of deformation with an increase in load-carrying capacity.

The average first-cracking strength and tensile strength are presented in Figures 31a. Furthermore, the average tensile strain capacity at peak tensile stress is presented in Figure 31b. The tensile strength of all RBA admixed mixtures exhibited a higher value than the control ECC. Relative to the control mixture (with a tensile strength of 3.73 MPa), the highest increase in tensile strength was 22.3% (i.e., 4.56 MPa) for S-25. Moreover, for S-50, S-75, and S-100, the tensile strength incremented by 5.1% (i.e., 3.92 MPa), 7.7% (i.e., 4.02 MPa), and 8.5% (i.e., 4.05 MPa) relative to control. As per ANOVA (presented in Appendix B Table B1), statistically, significant differences were encountered between the mixtures' average tensile strength (p-value=0.0099). Furthermore, as per Tukey pairwise comparison, the tensile strength differences between S-25 and control (i.e., S-0), and S-25 and S-50 were found to be statistically significant.

It is worth mentioning that the tensile strength of ECC mixtures is determined by both the frictional bond ($\tau_0$, influenced by the fiber/matrix interfacial transition zone stiffness and particle packing density) (*57*) and the chemical bond between the fiber and the matrix. Due to the presence of hydroxyl groups (-OH) in PVA fibers, they are hydrophilic in nature. As such, at the interfacial transition zone (ITZ), a thin layer of metal hydroxide (usually $Ca(OH)_2$) is formed, resulting in a strong chemical bond ($G_d$) (*26*). A previous study revealed that the presence of carbon in the matrix tends to coat PVA fibers and weaken the chemical and frictional bond (*44*). From the EDS analysis reported in Table 9a, it is evident that RBA has significant amounts of carbon. As such, it is believed that an increase in RBA can produce a reduction in the chemical and frictional bond, which in turn eases fiber pullout without fiber rupture. Furthermore, the increase in air content reported in Table 4 is also a factor that should diminish the fiber/matrix interaction; thus, contributing to the decrease of the tensile strength. However, it is hypothesized that RBA's filler and/or pozzolanic effect resulted in a net improvement in the fiber/matrix frictional bond, which outweighed the aforementioned phenomena; thus, resulting in the overall increase in the tensile strength of RBA admixed ECC mixtures.

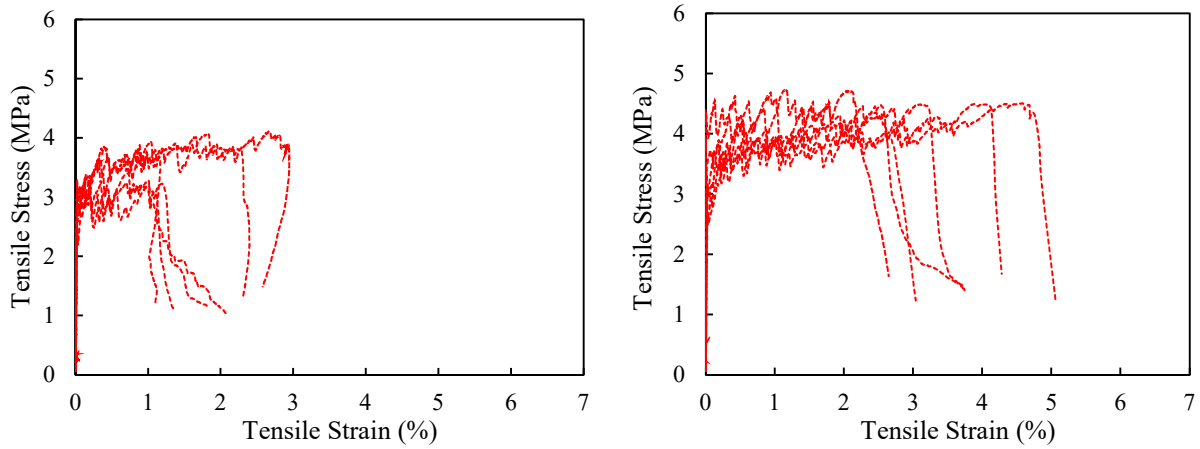


**(a)** **(b)**

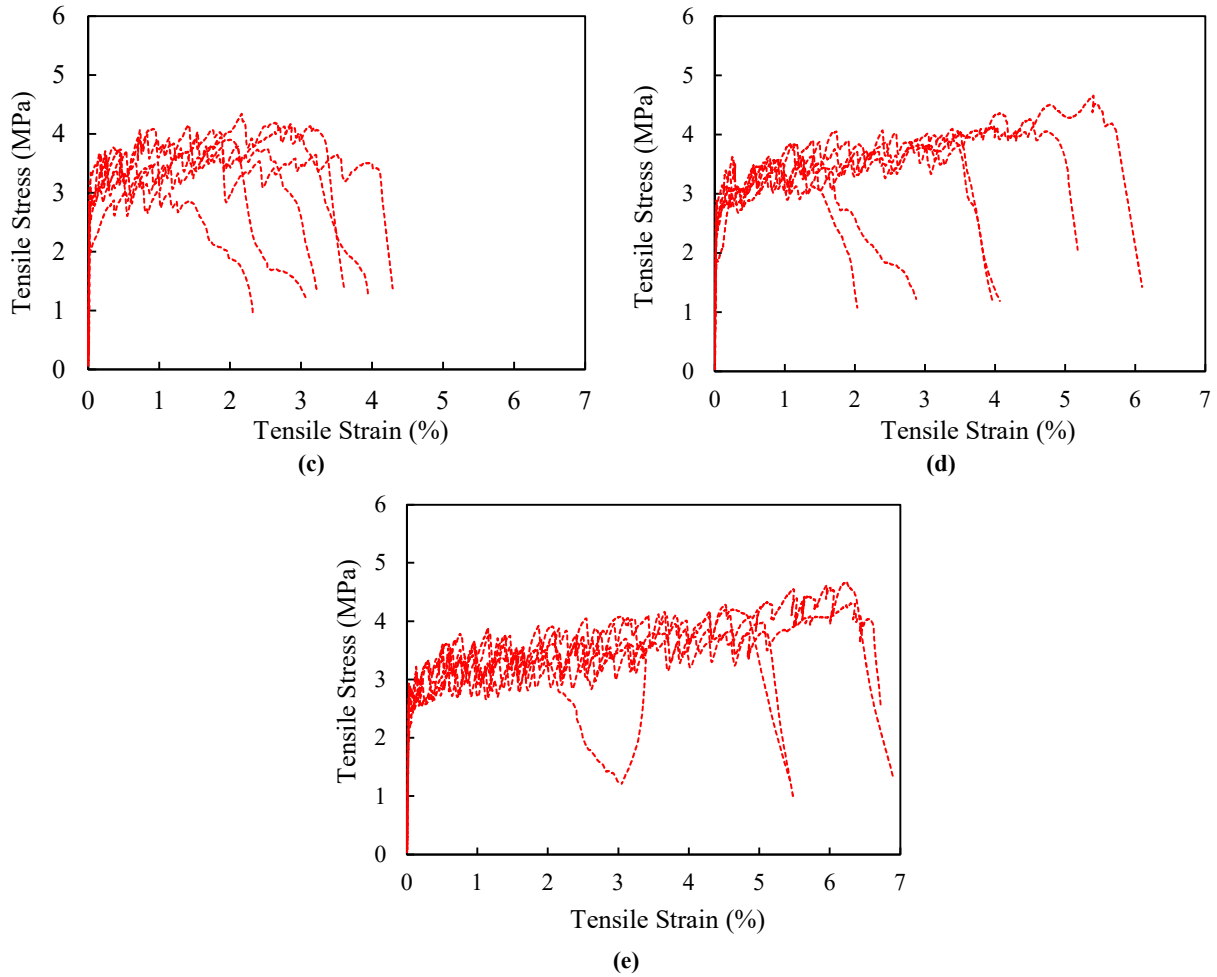


**Figure 30. Tensile stress - strain curves for: (a) S-0, (b) S-25, (c) S-50, (d) S-75, and (e) S-100**

Figure 31b presents the average tensile strain capacity of class S mixtures. A progressive enhancement in the tensile strain capacity with the increase in sand replacement level with RBA is observed. Relative to the control mixture (with a tensile strain capacity of 1.04%), the increase in tensile strain capacity for S-25, S-50, S-75, and S-100 were 139% (i.e., 2.49% strain capacity), 99% (i.e., 2.07% strain capacity), 182% (i.e., 2.94% strain capacity), and 311% (i.e., 4.28% strain capacity), respectively. The ANOVA presented in Appendix B Table B2 showed significant differences between the tensile strain capacities (i.e., p-value = 0.0311) of class C mixtures. Furthermore, the Tukey pairwise comparison indicated that the only significant difference encountered was between S-0 and S-100.

The increase in tensile strain capacity of RBA admixed mixtures are attributed to different phenomena, including the decrease in matrix toughness ($J_{tip}$), the increase in complementary energy ($J_b'$), and an enhancement in fiber distribution. From previous studies, it is evident that the increase in the aggregate particle size increases the fracture path's tortuosity; thus, resulting in higher matrix fracture toughness (*88*, *89*). From the particle size analysis presented in Table 10, it can be seen that RBA has a much finer particle size compared to the fine river sand used. As such, $J_{tip}$ probably tends to decrease with the increase in RBA content; thus, supporting an increment in the PSH energy index (i.e., $J_b'/J_{tip}$). Furthermore, the increase in air content increases the number

of voids in the matrix, which can be critical flaws in the matrix. Air voids disrupt the matrix's continuity and can result in the initiation cracks at a relatively low stresses, leading to the enhancement in tensile ductility. It is worth mentioning that a positive relationship is observed between the air content and tensile ductility of class S mixtures. Apart from the particle size of RBA and air content, the potential carbon coating effect of RBA on PVA fibers, as discussed earlier, can have a significant influence on the tensile ductility of ECC mixtures. A decrease in the chemical bond due to carbon coating can lead to an increase in $J_b'$; thus, enhancing the tensile ductility. As such, it is hypothesized that the decrease in the chemical bond has a relevant effect in enhancing the tensile ductility. Lastly, from a previous study, it is evident that the fiber distribution significantly affects the tensile ductility (*90*) as fiber clumping results in lower effective fiber volume ($V_f$), leading to lower $\sigma_0$ and $J_b'$. In ECC mixtures, it is recommended to use aggregate smaller than the average fiber spacing to avoid fiber clumping. Since RBA is finer than the river sand, it is likely that with the increase in the RBA content, a more uniform fiber distribution state was achieved; thus, leading to improved ductility of the mixtures. This may also be a factor in the enhancement in the tensile strength observed for mixtures containing RBA.

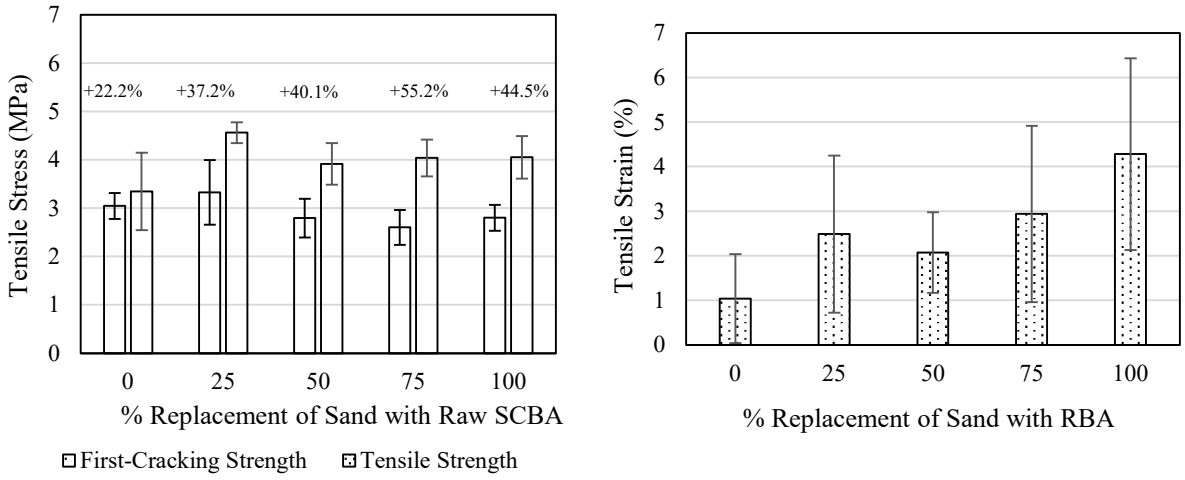


**(a)** **(b)**

**Figure 31. Uniaxial tensile test results: (a) First-cracking strength and tensile strength and (b) Strain at peak strength**

### *5.3.3.2 Class C Mixtures*

The tensile stress-strain curves for all class C mixtures produced in this study are presented in Figures 32a-d. It is observed that the mixtures did not exhibit a robust pseudo-strain hardening behavior. In fact, some specimens exhibited behavior similar to that of conventional FRC where the single crack localized failure occurred. From the tensile stress-strain curve for C-40 (Figure 32b), it is observed that one of the specimens exhibited a significantly different tensile-strain behavior (i.e., very low first-cracking and tensile strength as well as a relatively higher strain capacity) than all other specimens. As such, this specimen was considered as an outlier and was not considered for the computation of the average first-cracking strength, tensile strength, and strain capacity of C-40.

Figure 33a presents the average first-cracking strength and tensile strength for all class C mixtures. The results indicated that the partial replacement of cement with PBA produced a slight enhancement in the first-cracking and tensile strength at the 40% cement replacement level; yet, it produced decrement in the strengths at 50% and 60% replacement levels. The highest increase in

the tensile strength for C-40 (i.e., 4.81 MPa tensile strength) compared to the control mixture (i.e., 4.62 MPa tensile strength) was of 4.1%. On the other hand, the decrease in tensile strength for C-50 and C-60 was of 10.4% (i.e., 4.1 MPa) and 28.1% (i.e., 3.3 MPa), respectively, compared to the control mixture. As per ANOVA analysis (presented in Appendix B Table B3), the average tensile strength differences among class C mixtures were statistically significant (p-value=0.001). Furthermore, the Tukey pairwise comparison showed that the only significant differences in tensile strength was between the C-60 and ECC mixtures C-0 and C-40 mixtures.

As mentioned earlier, the tensile strength of ECC mixtures is determined by the frictional and chemical bond where the chemical bond with PVA fibers is affected by the metal ion concentration in the matrix (specially $Ca^{+}$). Since PBA has less free calcium ions ($Ca^{+}$) in comparison to cement, the increase in cement replacement with PBA likely decreased the chemical interaction at the fiber/matrix ITZ; thus, weakening the chemical bond. This mechanism was likely effective for all mixtures, including C-40. However, it is hypothesized that PBA's pozzolanic and/or filler effect further enhanced the pore structure at the ITZ between the fiber and matrix; thus, improving the frictional bond. For C-40, any decrease in the chemical bond may have been outweighed by the frictional bond's enhancement, thus resulting in the overall increase in the tensile strength. However, the decrease in the chemical bond may have become a dominant factor at higher cement replacement levels with PBA, thus producing the tensile strength decrease. Furthermore, it is important to mention that at 60% cement replacement level, even after the maximum dosage of HRWR (i.e., 1.5% by cement weight) was used, significant fiber clumping was observed due to lack of proper workability. This in turn, might also partially explain the marked decrease in tensile strength observed for C-60.

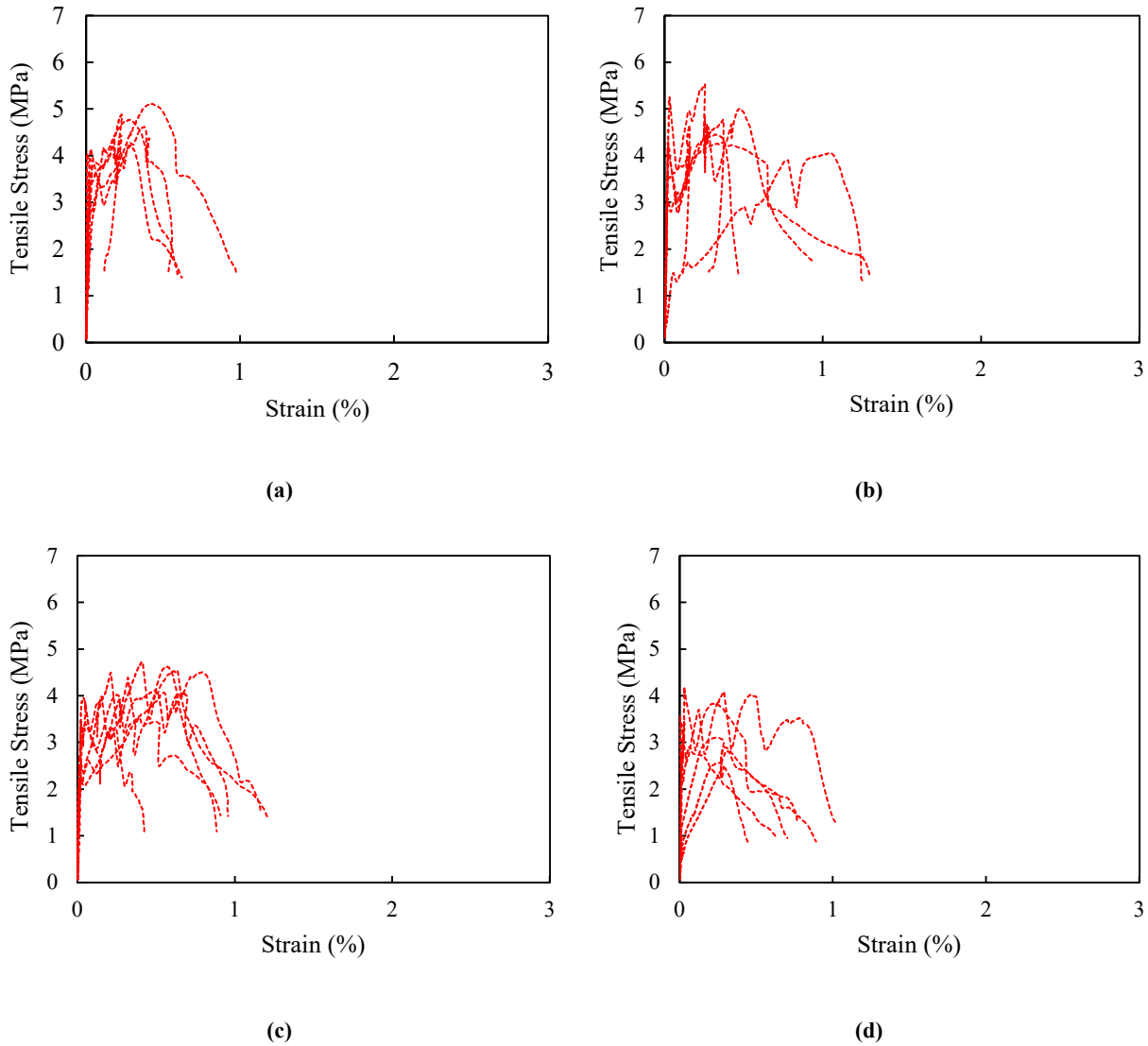


**Figure 32. Tensile stress-strain curves for class C ECC mixtures: (a) C-0, (b) C-40, (c) C-50, and (d) C-60**

The average tensile strain capacity for all class C mixtures is presented in Figure 33b. The results show that all PBA admixed ECC mixtures exhibited higher tensile ductility than the control mixture. The increments relative to the control mixture (with 0.27% tensile strain capacity) were of 7.4% for C-40 (i.e., 0.29% strain capacity), 85.2% for C-50 (i.e., 0.50% strain capacity), and 3.6% for C-60 (i.e., 0.28% strain capacity). However, the ANOVA analysis showed no statistically significant differences in the average tensile strain capacities of the ECC mixtures evaluated (*p*-value = 0.062). It is important to mention that these tensile strain capacity values are smaller than the typical tensile strain capacity for ECC mixtures (i.e., tensile strain capacity ranges from 1% to 8%). Nevertheless, the tensile strain capacity of the best performing class C mixture (C-50), in terms of ductility, was 0.50%, which is 50 times higher than that of regular concrete. It is important to mention that the low tensile ductility observed in the control mixture was due to the absence of the pozzolanic SCMs in its composition. This resulted in a high concentration of $Ca^{+}$ ions in the matrix and formed a strong chemical bond; thus, eliminating the possibility of exhibiting pseudo-strain hardening behavior.

For class C mixtures, the increase in tensile ductility for PBA admixed ECC materials is likely attributed to the decrease in the chemical bond. The decrease in the chemical bond allows more fibers to enter the pullout stage; thus, increasing $J_b'$. In addition, previous studies have shown that the increase in the content of the pozzolanic materials, such as fly ash, tends to decrease $J_{tip}$ (*53*, *57*). As such, it is hypothesized PBA also had an effect in decreasing $J_{tip}$. Consequently, it is believed that the potential increase in $J_b'$ and decrease in $J_{tip}$ are responsible for the improvement in the tensile ductility observed. However, as previously mentioned, an important loss in workability was observed at 60% cement replacement level with PBA, which produced fiber clumping. This, in turn, likely led to the reduction in tensile ductility for C-60 in comparison to C-50.

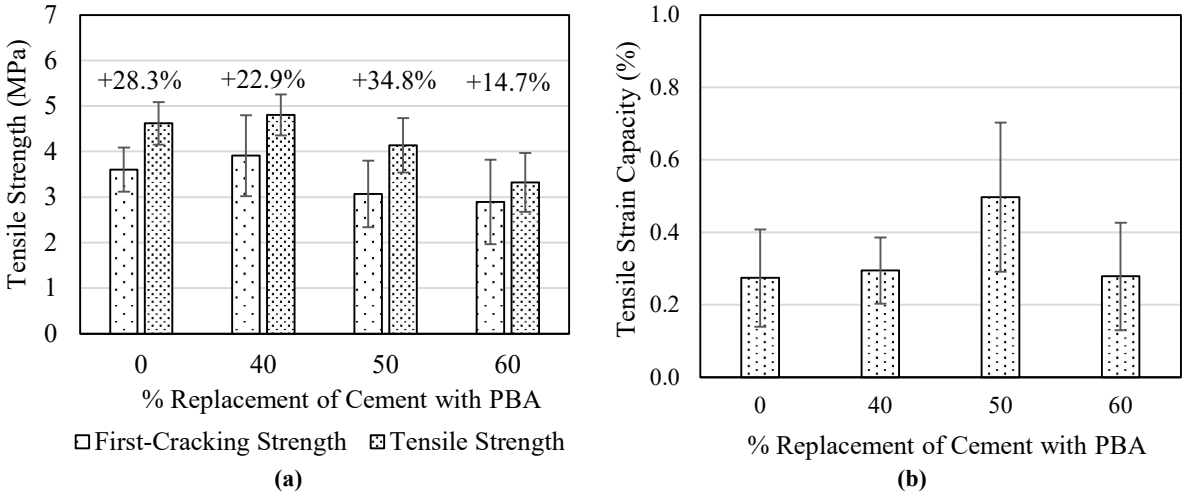


**Figure 33. Uniaxial tensile test results: (a) First-cracking strength and tensile strength and (b) Strain at peak strength**

### *5.3.4. Surface Resistivity*

#### *5.3.4.1 Class S Mixtures*

Figure 34a presents the surface resistivity (SR) values for class S mixtures. The experimental results show a progressive decrease in SR values with an increase in sand replacement level with RBA. For the control mixture, the SR value (i.e., 23.9 KΩ-cm) fell in the category of low chloride ion penetrability (CIP) per AASHTO T358 (i.e., SR values between 21 – 37 kΩ-cm, as per Table 6). In the case of S-25, the surface resistivity value decreased to 21.8 KΩ-cm (i.e., 8.8% decrease compared to control). Nevertheless, S-25 remained in the low CIP category with the control mixture. However, an increase in sand replacement with RBA beyond 25% led to a more pronounced decrease in SR with mixtures falling in the moderate CIP category (i.e., surface resistivity values between 12 – 21 kΩ-cm). Relative to the control mixture, the surface resistivity values decreased by 18.9% (i.e., 19.4 kΩ-cm) for S-50, 31.1% (i.e., 16.4 kΩ-cm) for S-75, and 43.4% (i.e., 13.5 kΩ-cm) for S-100. The decrease in SR may be primarily attributed to the increased air content with the increment of sand replacement with RBA, as discussed earlier. In turn, the increase in the number of air voids in the matrix can increase the permeability of the material and reduce the SR. It is worth mentioning that the high carbon content of RBA may have also influenced the obtained SR values since carbon may affect the electrical conductivity of the material. Furthermore, it is important to acknowledge that RBA's porous nature may increase the total porosity of the ECC materials; thus, contributing to the SR decrease. Future studies should

be conducted to evaluate the durability potential of these mixtures using direct permeability assessment methods (such as rapid chloride ion penetrability test) and evaluate whether SR is a reliable indicator of the CIP in RBA admixed ECC materials.

#### *5.3.4.2 Class C Mixtures*

For class C mixtures, a significant increase in surface resistivity with the increase in PBA content is observed. Relative to control (with SR value of 6.2 kΩ-cm), the increase in SR values for C-40, C-50, and C-60 were 43.7% (i.e., 8.9 kΩ-cm), 72.1% (i.e., 10.7 kΩ-cm ), and 71.8% (i.e., 10.6 kΩ-cm), respectively. However, surprisingly, all class C mixtures exhibited exceptionally low SR values, i.e., all materials fell into the high CIP category. This is attributed to the lack of fly ash utilization in these mixtures, which likely negatively affected the microstructure of the composite. On the other hand, the enhancement in the SR of the PBA admixed materials was attributed to the potentially improved pore structure provided by PBA's filler/pozzolanic effect. Yet, it is recognized that this effect was significantly less influential as that of fly ash since even at 60% cement replacement with PBA, SR values were low compared to those observed for class S mixtures, which did implement fly ash. It is worth mentioning that at later curing ages, the SR may significantly increase due to the matrix's densification (credited to the formation of secondary hydration products through the pozzolanic reaction). Future studies should be conducted to evaluate the durability potential of these mixtures using more direct permeability assessment methods (such as rapid chloride ion penetrability test ) and evaluate if the differences in matrix and fiber conductivity influence the surface resistivity readings for both class S and class C mixtures.

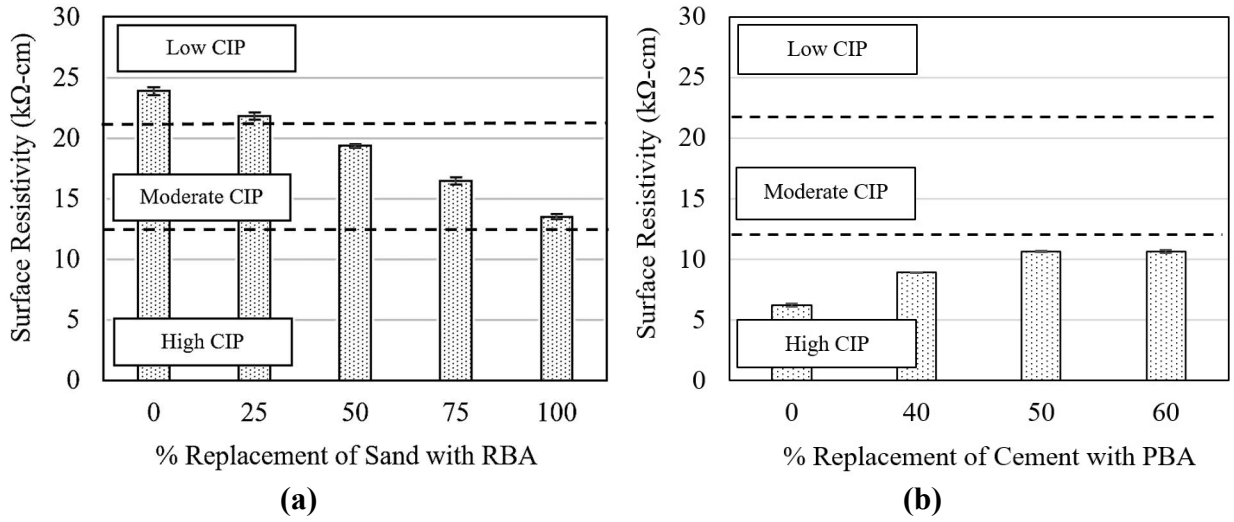


**Figure 34. Surface resistivity for ECC materials: (a) Class S mixtures and (b) Class C mixtures.**

### *5.3.5. Shrinkage*

#### *5.3.5.1 Class S Mixtures*

The shrinkage during the curing phase for class S mixtures at 7, 14, and 28 days of curing are presented in Figure 33a. The reported values are the average of four replicas. It is observed that the shrinkage during curing for class S mixtures is relatively low (in the range from 25 $\mu$m to 167.5 $\mu$m). For class S mixtures, all RBA admixed ECCs (except for S-25 at 28 days of curing) showed

an increased shrinkage during curing compared to the control mixture at all ages of curing. The greatest shrinkage increase reported at 28 days was for S-50 with an increase of 34% compared to the control mixture (i.e., from 125 $\mu\varepsilon$ to 167.5 $\mu\varepsilon$). However, an evident relationship was not observed between the RBA content and shrinkage. The higher shrinkage for RBA admixed ECC mixtures compared to control may be credited to the restraining action of aggregate. From previous literature, it is well documented that the restraining action of aggregate increases with the increase in aggregate particle size (*41*, *91*). As such, since RBA particles are significantly finer than those of the fine river sand being replaced, this is likely the main cause of the increment in shrinkage observed.

#### *5.3.5.2 Class C Mixtures*

The shrinkage for all class C mixtures at 7, 14, and 28 days of curing are presented in Figure 34b. Generally, it was observed that the shrinkage values were significantly higher than those observed for class S mixtures. Furthermore, it was observed that at all curing ages, the shrinkage for PBA admixed mixtures were higher than the control, except for C-50 at seven days of curing. At 28 days of curing, the maximum increase in relative length change compared to control was of 24.4% (i.e., from 900 $\mu\varepsilon$ to 1120 $\mu\varepsilon$) for C-60. In contrast to class S mixtures, in class C mixtures, a distinctive positive relation was encountered between the shrinkage and PBA content at 14 and 28 days of curing. However, it is important to notice that these differences were not significant. Previous studies have demonstrated fly ash's effect in reducing the shrinkage of ECC materials (*57*, *92*). As such, the dramatic increase in shrinkage for class C mixtures (compared to class S mixtures) is attributed to the fact that these materials did not implement fly ash in its composition.

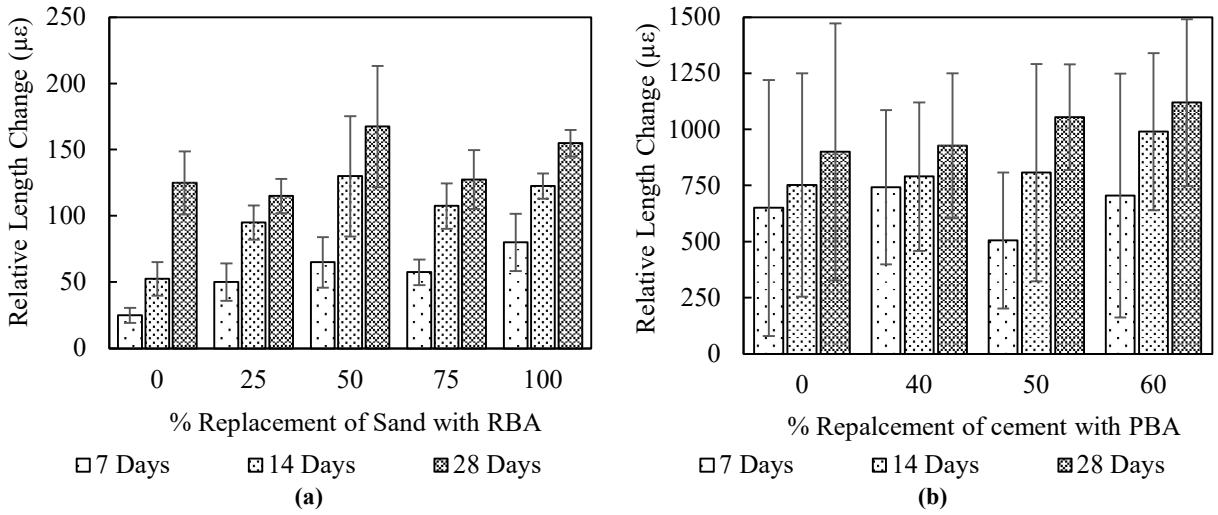


**Figure 35. Length change during curing: (a) Class S mixtures and (b) Class C mixtures**

### *5.3.6. Crack Width Analysis*

Unlike concrete materials, ECCs exhibits high ductility by the formation of multiple tight microcracks (typically in the range of 60-100 $\mu$m). Figures 36a and 36b presents the average residual crack width and number of cracks observed in dog-bone shaped specimens upon completion of the uniaxial tensile test. It is worth mentioning that three specimens were investigated per mixture design under the light microscope.

From Figure 36a, it is observed that the widths of the cracks were tight and did not exceed an average width of 58.2 $\mu$m for any of the produced mixtures. However, the use of RBA produced a slight increase in the average crack width. Compared to control, at 25, 50, 75, and 100% sand replacement with RBA, the average residual crack width increased by 11.2, 13.6, 4.6%, and 0.7%, respectively. This was attributed to a potential decrease in the fiber/matrix chemical bond due to RBA implementation. From Figure 36b, it is observed that the number of cracks increased with the increment in the sand replacement level with RBA. This, in turn, is in agreement with the enhancements in tensile ductility reported in the uniaxial tensile test section. Figure 36c and 36d present a specimen of the S-0 and S-100 ECC mixture, respectively. While the S-0 specimen only exhibited a few cracks, a robust multiple-cracking behavior with tight cracks is evident for S-100 specimen. From the results presented, class S ECC material has the potential to produce structures with excellent durability since crack widths below 100 µm do not significantly increase concrete permeability (*93*). Furthermore, it is important to mention that cracks under 50 $\mu$m in width have been reported to significantly benefit from robust autogenous healing, therefore class S ECC material may benefit from substantial self-healing capabilities; thus, enhancing the resiliency of these composites (*94*).

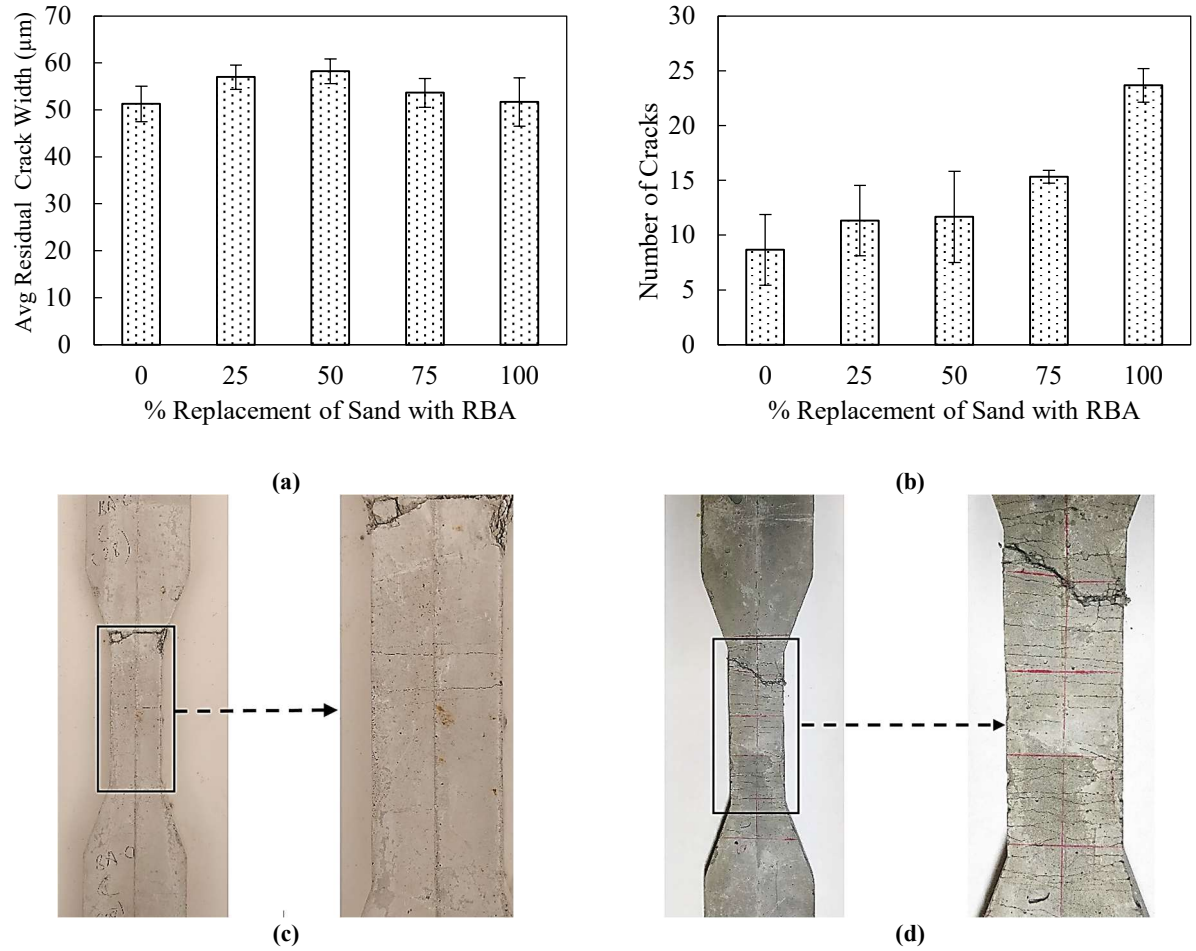


**Figure 36. Characterization of ECC cracking for class S mixtures: (a) Average residual cracks, (b) Number of cracks in class S mixtures, (c) S-0 dog-bone shaped, and (d) S-100 dog-bone shaped sample after tested in uniaxial tension.**

### *5.3.7. Slant Shear Test*

Figure 37a presents the average slant shear bond strength for the S-75/concrete and C-50/concrete composite cylinders after 28 days of curing (for the top layers, i.e., SCBA admixed ECC mixtures). The S-75 mixture was selected for the slant shear test since it produced good mechanical strength, high tensile ductility, and proper fresh state workability. On the other hand, C-50 was selected since it was the composite exhibiting the highest tensile ductility from all the class C mixtures. The calculated bond strength for the class S mixture was 13.1 MPa (1905 psi), while for the class C mixture, it was 13.5 MPa (1963 psi). It is important to mention that these bond strengths are minimum bond strength values since failure did not occur in the slant surface. Figures 37b, 37c, and 37d show the composite cylinders for the class S and class C mixtures after failure, respectively. It is observed that the cylinders failed in the top layer for class S specimens (i.e., failure of the class S mixtures). This was the case since the concrete substrate exhibited higher compressive strength than the S-75. In the case of the class C mixture, two failure modes occurred, failure at the substrate layer (Figure 37c) and top/bottom layer mixed failure (Figure 37d). The concrete used as a substrate had a 28-day compressive strength of 38.0 MPa, while the S-75 and C-50 mixtures used as top layers had a 28-day compressive strength of 29.8 MPa and 43.6 MPa, respectively. It is important to highlight that the concrete substrate was allowed to cure for 28-days prior to the pour of the top ECC layer. As such, when the composite cylinder was tested, the concrete substrate had 56 days of curing. For this reason, the concrete substrate did exhibit a higher compressive strength during the slant shear test than the 28-day strength reported above. This in turn, explain the different types of failure observed for the class C mixture as the compressive strength of the substrate was likely very close to that of the top ECC layer during the SST. Since the failure mode of both SCBA admixed ECC materials was not observed at the slant surface, this implies that the materials exhibit excellent bond characteristics. However, the class C mixture exhibited a higher bond strength than the class S mixture. This was the case since the class C composite exhibited a higher compressive strength. Nevertheless, both class mixtures present excellent potential to be used as a repair material.

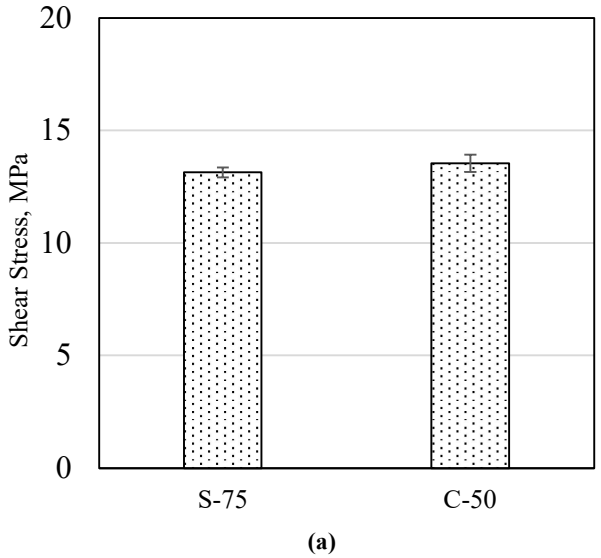


(a)

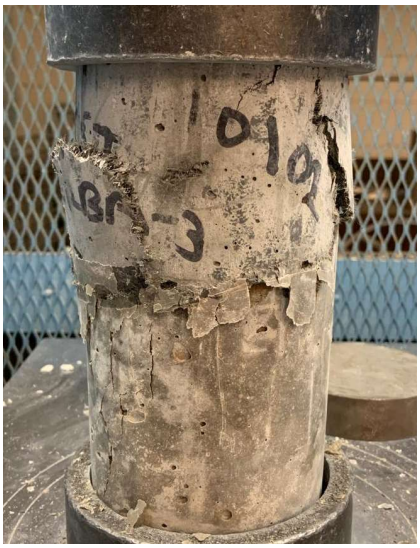

(b)

(c)

(d)

**Figure 37. Slant shear test: (a) Average shear stress at failure, MPa, (b) Class S composite cylinder failure mode, (c) Class C composite cylinder substrate failure mode, (d) Class C composite cylinder mixed failure mode**

### *5.3.8. Coefficient of Thermal Expansion*

The coefficient of thermal expansion (CTE) for class S and C mixtures is presented in Figure 38a and 38b, respectively. For class S mixtures, replacement of sand with RBA increased the CTE, i.e., all RBA admixed ECC mixtures exhibited higher CTE than the control mixture. Among all class S mixtures, S-50 exhibited higher CTE. Relative to the control mixture with CTE of 5.4 microstrain per °C, the increase in CTE for S-50 was 43.4% (i.e., CTE of 7.7 microstrain/°C). The CTE for RBA admixed ECC mixtures ranged from 6.7 to 7.7 microstrain/°C. It is worth mentioning that the CTE of PCC ranges between 7.4 to 13 microstrain/°C (*95*). As such, all RBA admixed ECC CTE values were comparable to that of concrete. The CTE of cementitious materials is influenced by several factors, including aggregate type (i.e., concrete using limestone has a lower CTE than concrete using siliceous aggregate), cement content and fineness, W/C ratio, cement and SCMs composition, and age (*95*). Since RBA addition increases the CTE of the mixture, it is hypothesized that the CTE of RBA is higher than that of silica sand.

For class C mixture, the CTE decreased with the increase in cement replacement level with PBA. For instance, the CTE of the control mixture was 13.2 microstrain/°C, which decreased up to 10.6 microstrain/°C for C-50 (i.e., a decrease of 19.7%). The CTE for PBA admixed ECC materials ranged from 11.2 to 10.6 microstrains/°C. It is important to mention that the control mixture exhibited slightly higher CTE than typical values for PCC. Since the CTE of cement paste is higher (i.e., 18 to 20 microstrain/°C) (*95*) than a typical concrete mixture, the high CTE for the class C mixture may be attributed to the higher content of cement. Furthermore, PBA decreased the CTE of ECC mixtures, indicating PBA admixed ECC has a lower potential for thermally induced dimensional changes.

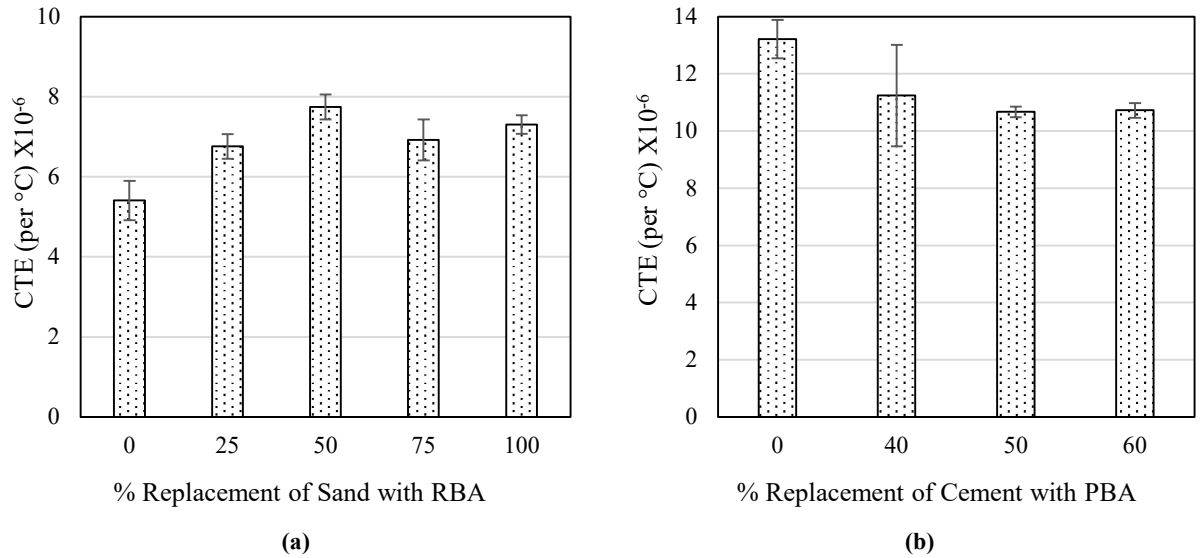


**Figure 38. Coefficient of thermal expansion: (a) Class S mixtures and (b) Class C mixtures**

## 5.4. Testing of Ecuador SCBA Admixed ECC Mixtures

### *5.4.1. Compressive Strength*

The compressive strength of all class S-E mixtures at 7 and 28 days of curing is presented in Figures 39a and 39b, respectively. A distinctive trend of increase in compressive strength with the increase in the sand replacement level with EBA is observed at both curing ages (except for S-E-100 compared to S-E-75). For instance, the increase in compressive strength for S-E-25, S-E-50, S-E-75, and S-E-100 at 7 days of curing compared to control (with compressive strength of 17.15 MPa) was 16.5, 23.8, 20.7, and 19.1%, respectively. On the other hand, the increase in compressive strength at 28 days of curing for S-E-25, S-E-50, S-E-75, and S-E-100 compared to control (with compressive strength of 26.69 MPa) was 8.8, 12.9, 21.0, and 12.3%, respectively. As such, the increase in compressive strength with EBA addition was similar at both curing ages. It is worth mentioning that the EBA enhanced the compressive strength, which contrasts with the influence of RBA on compressive strength. Since EBA exhibited high SAI and met the SAI requirement to be classified as a pozzolan, the increase in compressive strength can be associated with its pozzolanic activity and/or filler effect.

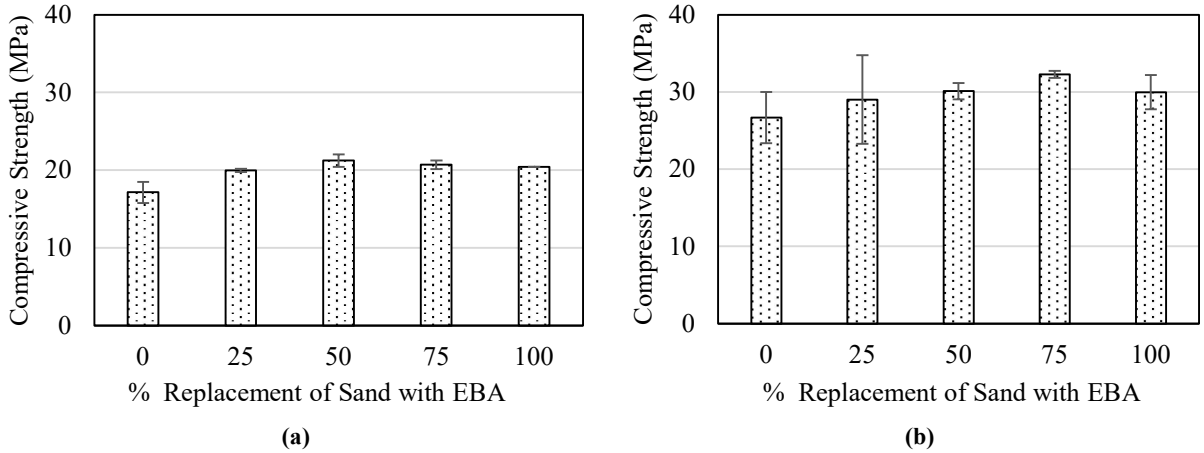

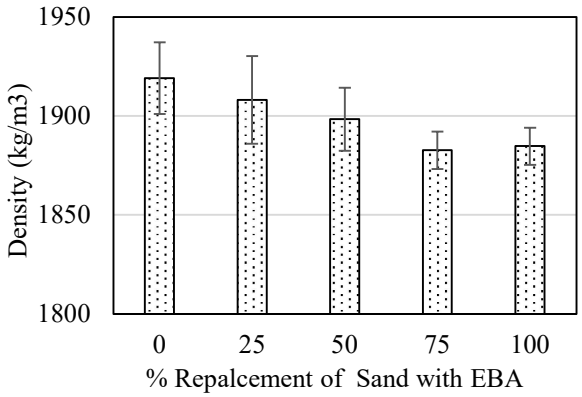


(c)

**Figure 39. EBA admixed ECC properties: (a) Compressive Strength at 7 days, (b) Compressive strength at 28 days, and (c) ECC Hardened Density at 28 Days**

Figure 39c presents the hardened densities of all class S-E mixtures. As seen in the figure, the density of the ECC mixtures decreased with the increase in the sand replacement level with SCBA. This was expected since SCBA exhibits a lower specific gravity than river sand.

### *5.4.2. Flexural Strength Test*

The flexural strength of class S-E mixtures at 7 and 28 days of curing are presented in Figure 40a and 40b, respectively. A distinctive trend of increase in flexural strength with the increase in the sand replacement level with EBA is observed at both curing ages (except for S-E-100 compared to S-E-75 at 7 days of curing). For instance, the increase in flexural strength for S-E-25, S-E-50, S-E-75, and S-E-100 at 7 days of curing compared to the control mixture (with a flexural strength of 3.3 MPa) was 10.4, 14.4, 9.5, and 20.5%, respectively. Similarly, the increase in flexural strength for S-E-25, S-E-50, S-E-75, and S-E-100 at 28 days compared to control (with a flexural strength of 4.5 MPa) was 7.9, 9.6, 19.1, and 21.5%, respectively. It is worth mentioning that the flexural strength of cementitious composites is controlled by their tensile failure mode (*96*). As such, it is hypothesized that the pozzolanic and/or filler effect of EBA increased fiber/matrix frictional bond; thus, increasing the fiber-bridging capacity. Consequently, the enhanced fiber-bridging capacity due to EBA addition resulted in a higher flexural strength of ECC mixtures.

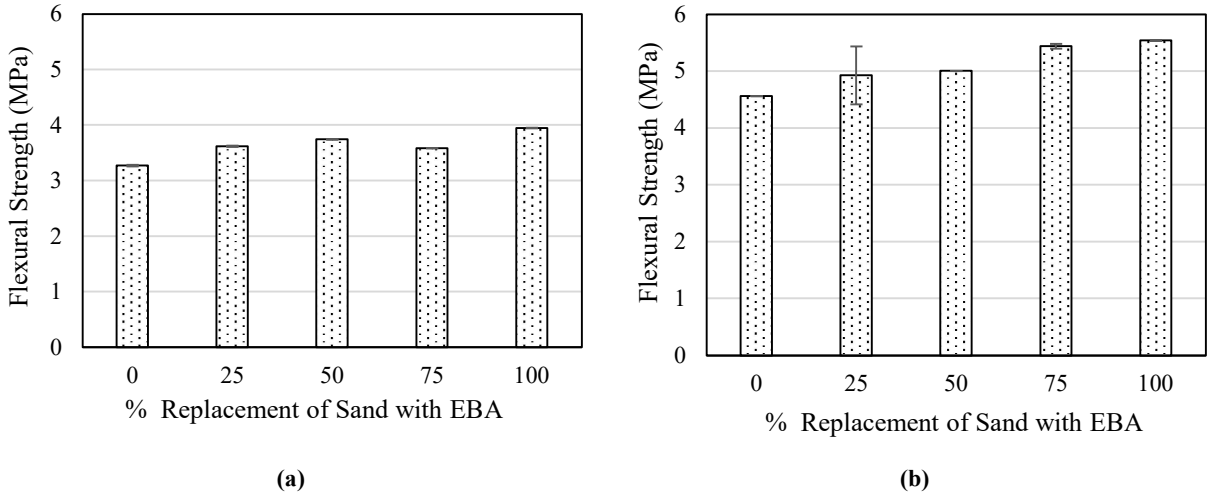


**Figure 40. EBA admixed ECC properties: (a) Flexural strength 7 days and (b) Flexural strength 28 days**

# 6. CONCLUSIONS

This study evaluated the effects of raw SCBA (RBA) as a partial and complete replacement of sand (i.e., class S mixtures) and post-processed SCBA (PBA) as a partial replacement of cement (i.e., class C mixtures) on the mechanical and physical properties of ECC materials. Both RBA and PBA were produced in Louisiana. In addition, the study also evaluated the effect of raw SCBA (EBA) produced in Ecuador as a substitute to silica sand in ECC mixtures (i.e., class S-E mixtures). Based on the experimental findings and analysis, the following conclusions can be drawn:

- RBA met the minimum pozzolanic component requirement (i.e., a minimum of 50% per ASTM C618) to be classified as class C pozzolan; however, it presented an unsatisfactory SAI of 71.2%, failing to meet the minimum SAI requirement (i.e., 75%) to be classified as a SCM. Consequently, RBA cannot be used as an SCM in concrete materials. The low SAI of RBA was mainly attributed to its high carbon content and relatively large particle size compared to cement. Nevertheless, compared to conventional fine aggregate, RBA exhibited a small particle size (i.e., mean particle size of 256 $\mu$m), which makes it an excellent candidate to be used as fine aggregate in the manufacture of ECC materials.

- The post-processing of RBA by further burning and grinding to produce PBA significantly increased the SAI of the SCBA to 78.8%; thus, allowing it to exceed the minimum SAI requirement to be classified as a pozzolan. Furthermore, PBA did also meet ASTM C618 minimum pozzolanic component requirement (i.e., 70%) to be classified as a class F or N pozzolan. The enhancement in PBA's pozzolanic activity was mainly attributed to the finer particle size and removal of carbon due to the burning and grinding process. The mean particle size of the final ground PBA product was 28 $\mu$m, which is comparable to that of the fly ash used in this study (i.e., 22.8 $\mu$m).

- Compared to RBA, EBA exhibited significantly higher SAI, i.e., 91.1%; thus, meeting the minimum SAI requirement to be classified as a pozzolan. However, like RBA, EBA exhibited large particle size (i.e., mean particle size of 248 $\mu$m) relative to cement and high carbon content. Therefore, use of RBA as SCM is not advised. Instead, RBA presented the

potential to be an excellent substitute to silica sand in ECC mixtures. The significant difference in pozzolanic properties of RBA and EBA highlights the effect of SCBA source on the material properties. This discrepancy may also arise due to the difference in the burning methodology of sugarcane bagasse fibers at respective sugar mills, which influences the SCBA chemical composition.

- The increase in sand replacement with RBA caused a small reduction in the compressive strength of class C ECC materials at 28 days of curing. The maximum strength decrease observed was of 11% for the ECC mixture using 75% of sand replacement with RBA. This strength reduction was attributed to the increase in air content observed with the increase in RBA dosage, which was associated with the necessary increase in HRWR required to produce a workable mixture. Nevertheless, the decreases in compressive strength observed for the amount of additional air content reported (compared to control) were lower than expected. This was credited to RBA's pozzolanic and/or filler effect, which likely mitigated the compressive strength decrease. For the case of cement replacement with PBA, increasing replacement of cement with PBA caused important reductions in compressive strength. The maximum decrease in compressive strength observed of 39.1% occurred at the maximum cement replacement level evaluated of 60% by weight. The significant decrements in compressive strength observed were attributed to the fact that the cylinders were evaluated at 28 days of curing; thus, substantially limiting the contribution of the pozzolanic reaction of PBA to the strength gain of the ECC mixtures. However, it is expected that at later ages of curing, the PBA admixed ECC materials should exhibit smaller differences in compressive strength compared to the control ECC mixture.

- The implementation of RBA as sand replacement in ECC materials (i.e., class S mixtures) dramatically improved the tensile strain capacity of the composites. Compared to the control ECC, the maximum tensile strain capacity enhancement reported was 311%, which occurred for the ECC mixture implementing a 100% replacement of sand with RBA. Furthermore, the tensile strength of all RBA admixed ECCs did also improve compared to control, with the maximum reported increase of 22.3% occurring at 25% of sand replacement with RBA. The increase in the tensile ductility was attributed to the combined effect of a reduction in $J_{tip}$ (due to the decrease of the aggregate particle size), an increase in $J_b'$ (due to the decrease in the chemical bond from the potential fiber carbon coating effect produced by RBA), and an enhanced fiber dispersion (achieved due to RBA's small particle size compared to the fine river sand used in this study). On the other hand, the tensile strength enhancement observed was attributed to RBA's filler and/or pozzolanic effect, which likely resulted in an improvement in the fiber/matrix frictional bond. For the case of cement replacement with PBA (i.e., class C mixtures), the addition of PBA did also produce an enhancement in the tensile ductility of all the PBA admixed ECC materials. Compared to control, an increase in the tensile strain capacity of up to 85% was observed for the ECC mixture utilizing 50% cement replacement with PBA. These observations were primarily attributed to a reduction in $J_{tip}$ (due to the weakening of the cementitious matrix with PBA addition) and a possible increase in $J_b'$ (associated with the decrease in the fiber/matrix chemical bond due to the reduction in the concentration of calcium ions in the matrix by PBA addition), leading to an increase in the PSH energy index ($J_b'/J_{tip}$). Regarding the tensile strength of class C mixtures, when 40% of cement was replaced with

PBA, a marginal enhancement in tensile strength of 4.1% was observed compared to the control mixture. However, the mixtures using 50% and 60% of cement replacement with PBA exhibited lower tensile strengths compared to control. The maximum decrement in tensile strength of 28.1% was reported for the ECC mixture implementing 60% cement replacement with PBA.

- For class S-E mixtures, the implementation of sand replacement with EBA produced an increase in compressive strength of ECC mixtures at 7 and 28 days of curing. At 28 days, the maximum increase in compressive reported of 21.0% occurred at a sand replacement level of 75% by volume. The improvements observed in the compressive strength were attributed to the high SAI exhibited by EBA. Similar improvements were observed in the flexural strength of EBA admixed ECC materials. An enhancement of up to 21.5% in flexural strength was reported for the ECC mixture using 100% of sand replaced with EBA at 28 days of curing. These improvements were attributed to EBA's pozzolanic activity and/or filler effect, which likely enhanced the fiber bridging capacity of the EBA admixed ECC mixtures.

- The surface resistivity of ECC materials showed a progressive decrease with the increase in sand replacement level with RBA. However, both the control mixture and the ECC mixture using 25% of RBA as a substitution to sand fell in the category of low CIP. With regard to the ECC mixtures implementing 50, 75, and 100% RBA as a sand replacement, these fell in the category of medium CIP. The decrease in surface resistivity with RBA addition was attributed to the increase in air content (associated with the increasing contents of HRWR dosage), RBA's porous nature, and the high carbon content of RBA (which may have affected the electrical conductivity of the materials). For mixtures implementing PBA as cement replacement (i.e., class C mixtures), the surface resistivity increased with the increase in cement replacement with PBA. However, all class C mixtures, including control, fell into the category of high CIP. This was attributed to the fact that class C mixtures did not implement fly ash in its composition. Furthermore, the progressive enhancement in surface resistivity with PBA addition was attributed to PBA's filler/pozzolanic effect. However, it is acknowledged that this effect was much less influential as that of fly ash since even at 60% cement replacement with PBA, SR values for class C mixtures were low compared to those observed for class S mixtures, which did implement fly ash.

- For class S mixtures, excepting S-25 at 28 days of curing, all RBA admixed ECC showed an increase in shrinkage during curing compared to the control mixture at all ages of curing. The higher shrinkage observed for RBA admixed ECC mixtures was credited to a reduction in coarser sand particles due to the replacement of fine river sand with RBA. However, an evident relationship between RBA content and shrinkage was not distinguished. The greatest shrinkage increase reported at 28 days of curing was 34% for S-50 (compared to the control). For class C mixtures, it was observed that the shrinkage values were significantly higher than those observed for class S mixtures. This was attributed to the lack of fly ash in the composition of class C mixtures. Moreover, it was observed that the shrinkage for PBA admixed mixtures was higher than control at all curing ages, except for C-50 at 7 days of curing. Furthermore, a distinctive positive relation was encountered

between the shrinkage and PBA content at 14 and 28 days of curing. At 28 days of curing, the maximum increase in shrinkage reported compared to control was of 24.4% for C-60.

- Upon completion of the uniaxial tensile test, the average residual crack width for all class S ECC materials ranged from 51.3 to 58.2 μm. The tight crack width reported suggests that ECC mixtures implementing RBA as a sand replacement may provide with low permeability and significant autogenous healing capabilities; thus, translating into an excellent durability potential.

- The failure mode of ECC mixtures S-75 and C-50 subjected to slant shear test on a concrete substrate did not occur in the slant surface; thus, indicating excellent bond characteristics of these materials.

# 7. REFERENCES


1. Mindess, S., J. F. Young, and D. Darwin. *Concrete*. Prentice Hall, Pearson Education, Inc. Upper Saddle River, NJ 07458, U.S.A., 2003.

2. Yang, E. Designing Added Functions in Engineered Cementitious Composites. 2008, p. 276.

3. Fischer, G., and V. C. Li. Effect of Fiber Reinforcement on the Response of Structural Members. *Engineering Fracture Mechanics*, Vol. 74, No. 1–2, 2007, pp. 258–272.

4. Li, V. C. *Engineered Cementitious Composites (ECC) – Material, Structural, and Durability Performance*. 2008.

5. Li, V. C. *Engineered Cementitious Composites (ECC): Bendable Concrete for Sustainable and Resilient Infrastructure,* Springer-Verlag GmbH Germany. 2019, 286-290.

6. Şahmaran, M., and V. C. Li. Suppressing Alkali-Silica Expansion. *Concrete International*, Vol. 38, No. 5, 2016, pp. 47–52.

7. Liu, H., Q. Zhang, V. Li, H. Su, and " C. Gu. Durability Study on Engineered Cementitious Composites (ECC) under Sulfate and Chloride Environment. *Construction and building materials*, Vol. 133, 2017, pp. 171–181.

8. Yang, Y., M. D. Lepech, E. H. Yang, and V. C. Li. Autogenous Healing of Engineered Cementitious Composites under Wet-Dry Cycles. *Cement and Concrete Research*, Vol. 39, No. 5, 2009, pp. 382–390.

9. Nematollahi, B., J. Sanjayan, and F. U. Ahmed Shaikh. Tensile Strain Hardening Behavior of PVA Fiber-Reinforced Engineered Geopolymer Composite. *Journal of Materials in Civil Engineering*, Vol. 27, No. 10, 2015, pp. 1–12. https://doi.org/10.1061/(ASCE)MT.1943-5533.0001242.

10. Li, V. C. On Engineered Cementitious Composites (ECC). A Review of the Material and Its Applications. *Journal of Advanced Concrete Technology*, Vol. 1, No. 3, 2003, pp. 215–

230.

11. Qian, S., M. D. Lepech, Y. Y. Kim, and V. C. Li. Introduction of Transition Zone Design for Bridge Deck Link Slabs Using Ductile Concrete. *ACI Structural Journal*, Vol. 106, No. 1, 2009, pp. 96–105.

12. Ozyildirim, H. C., and G. M. Moruza. High-Performance Grouting Materials in Shear Keys between Box Beams. *Transportation Research Record*, Vol. 2577, No. 2577, 2016, pp. 35–42.

13. American Sugar League *Industry Information,* American Sugar League, Thibodaux, LA, 2019.

14. American Sugar Cane League. *Louisiana Sugarcane Industry Production Data from 1975 to 2016*. American Sugar League, Thibodaux, LA, 2019.

15. U.S. Department of Energy. *U.S. Billion-Ton Update: Biomass Supply for a Bioenergy and Bioproducts Industry.* RD Perlack and BJ Stokes (Leads) Oak Ridge National Laboratory, Oak Ridge, TN, 2011. Available from: http://bioenergykdf.net Accessed on Jan. 18, 2019

16. Ganesan, K., K. Rajagopal, and K. Thangavel. Evaluation of Bagasse Ash as Supplementary Cementitious Material. *Cement and Concrete Composites*, Vol. 29, No. 6, 2007, pp. 515–524.

17. Payá, J., J. Monzó, M. V. Borrachero, L. Díaz-Pinzón, and L. M. Ordónez. Sugar-Cane Bagasse Ash (SCBA): Studies on Its Properties for Reusing in Concrete Production. *Journal of Chemical Technology and Biotechnology*, Vol. 77, No. 3, 2002, pp. 321–325.

18. Cordeiro, G. C., R. D. Toledo Filho, L. M. Tavares, and E. M. R. Fairbairn. Pozzolanic Activity and Filler Effect of Sugar Cane Bagasse Ash in Portland Cement and Lime Mortars. *Cement and Concrete Composites*, Vol. 30, No. 5, 2008, pp. 410–418.

19. Srinivasan R., Sathiya K. Experimental Study on Bagasse Ash in Concrete. *International 44 Journal for Service Learning in Engineering, Humanitarian Engineering and Social Entrepreneurship*. 2018;5(2):60–6..

20. Cordeiro, G. C., R. D. Toledo Filho, L. M. Tavares, and E. de M. R. Fairbairn. Ultrafine Grinding of Sugar Cane Bagasse Ash for Application as Pozzolanic Admixture in Concrete. *Cement and Concrete Research*, Vol. 39, No. 2, 2009, pp. 110–115.

21. Subedi, S., G. Arce, M. Hassan, N. Kumar, M. Barbato, and M. T. Gutierrez-wing. Influence of Production Methodology on the Pozzolanic Activity of Sugarcane Bagasse Ash. No. 271, 2019, pp. 1–5.

22. Ma, H., S. Qian, Z. Zhang, Z. Lin, and V. C. Li. Tailoring Engineered Cementitious Composites with Local Ingredients. *Construction & Building Materials*, Vol. 101, 2015, pp. 584–595.

23. Li, V. C. Postcrack Scaling Relations for Fiber Reinforced Cementitious Composites. *Journal of Materials in Civil Engineering*, Vol. 4, No. 1, 1992, pp. 41–57.

24. Li, V. C. Engineered Cementitious Composites ( ECC ) – Material, Structural, and

Durability Performance. In *Concrete Construction Engineering Handbook*, pp. 1–15.

25. Marshall, D. B., & Cox, B. N. A J-integral Method for Calculating Steady-State Matrix Cracking Stresses in Composites. *Mechanics of Materials*, Vol. 7, No. 2, 1988, pp. 127–133.

26. Li, V. C., C. Wu, S. Wang, A. Ogawa, and T. Saito. Interface Tailoring for Strain-Hardening Polyvinyl Alcohol- Engineered Cementitious Composite. *Material Journal*, Vol. 99, No. 5, 2003, pp. 463–472.

27. Pan, Z., C. Wu, J. Liu, W. Wang, and J. Liu. Study on Mechanical Properties of Cost-effective Polyvinyl Alcohol Engineered Cementitious Composites (PVA-ECC). *Construction and building materials*, Vol. 78, 2015, pp. 397–404.

28. Kanda, T., and V. C. Li. Practical Design Criteria for Saturated Pseudo Strain Hardening Behavior in ECC. *Journal of Advanced Concrete Technology*, Vol. 4, No. 1, 2006, pp. 59–

29. Kanda, T., and V. C. Li. New Micromechanics Design Theory for Pseudostrain Hardening Cementitious Composites. *Journal of Engineering Mechanics*, Vol. 125, No. April 1999, pp. 373–381.

30. Noorvand, H., G. Arce, M. Hassan, and T. Rupnow. Investigation of the Mechanical Properties of Engineered Cementitious Composites with Low Fiber Content and with Crumb Rubber and High Fly Ash Content. *Transportation Research Record*, Vol. 2673, No. 5, 2019, pp. 418–428.

31. Modani, P. O., and M. R. Vyawahare. Utilization of Bagasse Ash as a Partial Replacement of Fine Aggregate in Concrete. *Procedia Engineering*, Vol. 51, No. 0, 2013, pp. 25–29.

32. Sua-Iam, G., and N. Makul. Use of Increasing Amounts of Bagasse Ash Waste to Produce Self-Compacting Concrete by Adding Limestone Powder Waste. *Journal of Cleaner Production*, Vol. 57, 2013, pp. 308–319.

33. Sales, A., and S. A. Lima. Use of Brazilian Sugarcane Bagasse Ash in Concrete as Sand Replacement. *Waste Management*, Vol. 30, No. 6, 2010, pp., 1114–1122.

34. Martins, C. H., T. R. de Castro, and C. C. Gallo. Characterization of Mixed Mortars with Partial Replacement of Sand with Sugarcane Bagasse Ash (SCBA). *Journal of Civil Engineering*, Vol. 6, 2016, pp. 410–419.

35. Bahurudeen, A., and M. Santhanam. Influence of Different Processing Methods on the Pozzolanic Performance of Sugarcane Bagasse Ash. *Cement and Concrete Composites*, Vol. 56, 2015, pp. 32–45.

36. Arce, G., M. Hassan, M. T. Gutierrez-wing, and M. Barbato. *Use of Bagasse Ash as a Concrete Additive for Road Pavement Application*. Tran-SET Project No. 18CLSU03, Transportation Consortium of South-Central States, 2019, pp 1-63.

37. Amin, N. Use of Bagasse Ash in Concrete and Its Impact on the Strength and Chloride Resistivity. *Journal of Materials in Civil Engineering*, Vol. 23, No. 5, 2010, pp. 717–720.

38. Montakarntiwong, K., N. Chusilp, W. Tangchirapat, and C. Jaturapitakkul. Strength and

Heat Evolution of Concretes Containing Bagasse Ash from Thermal Power Plants in Sugar Industry. *Materials and Design*, Vol. 49, 2013, pp. 414–420.

39. Bahurudeen, A., A. V. Marckson, A. Kishore, and M. Santhanam. Development of Sugarcane Bagasse Ash Based Portland Pozzolana Cement and Evaluation of Compatibility with Superplasticizers. *Construction and Building Materials*, Vol. 68, 2014, pp. 465–475.

40. ASTM C618-12a. Standard Specification for Coal Fly Ash and Raw or Calcined Natural Pozzolan for Use. ASTM International, West Conshohocken, PA, 2010, pp. 3–6.

41. Mustafa, Ş., M. Lachemi, K. M. A. Hossain, R. Ranade, and V. C. Li. Influence of Aggregate Type and Size on Ductility and Mechanical Properties of Engineered Cementitious Composites. *ACI Materials Journal*, Vol. 106, No. 3, 2009, pp. 308–316.

42. Lepech, M. D., V. C. Li, R. E. Robertson, and G. A. Keoleian. Design of Green Engineered Cementitious Composites for Improved Design of Green Engineered Cementitious Composites for Improved Sustainability. No. March 2017, 2019.

43. Hungria, R., G. Arce, M. Hassan, M. Anderson, M. Mahdi, T. Rupnow, and S. M. Bogus. Evaluation of Novel Jointless Engineered Cementitious Composite Ultrathin Whitetopping (ECC-UTW) Overlay. *Construction and Building Materials*, Vol. 265, 2020, p. 120659.

44. Wang, S., and V. C. Li. Engineered Cementitious Composites with High-Volume Fly Ash. *ACI Materials Journal*, Vol. 104, No. 3, 2007, pp. 233–241.

45. Lehne, J., and F. Preston. *Making Concrete Change Innovation in Low-Carbon*. Chatham House Report, Energy Environment and Resources Department: London, UK, 2018.

46. Yu, K. Q., Z. D. Lu, J. G. Dai, and S. P. Shah. Direct Tensile Properties and Stress-Strain Model of UHP-ECC. *Journal of Materials in Civil Engineering*, Vol. 32, No. 1, 2020, pp. 1–13.

47. Costa, F. B. P. d., D. P. Righi, A. G. Graeff, and L. C. P. d. Silva Filho. Experimental Study of Some Durability Properties of ECC with a More Environmentally Sustainable Rice Husk Ash and High Tenacity Polypropylene Fibers. *Construction and Building Materials*, Vol. 213, 2019, pp. 505–513.

48. Huang, X., R. Ranade, V. C. Li, and F. ASCE. Feasibility Study of Developing Green ECC Using Iron Ore Tailings Powder as Cement Replacement. Vol. 25, No. July 2013, pp. 923–931.

49. Zhou, J., S. Qian, M. G. Sierra Beltran, G. Ye, K. van Breugel, and V. C. Li. Development of Engineered Cementitious Composites with Limestone Powder and Blast Furnace Slag. *Materials and Structures*, Vol. 43, No. 6, 2010, pp. 803–814.

50. Nematollahi, B., J. Sanjayan, and F. U. A. Shaikh. Strain Hardening Behavior of Engineered Geopolymer Composites: Effects of the Activator Combination. *Journal of the Australian Ceramic Society*, Vol. 51, No. 1, 2015, pp. 54–60.

51. Kan, L. li, W. song Wang, W. dong Liu, and M. Wu. Development and Characterization of Fly Ash Based PVA Fiber Reinforced Engineered Geopolymer Composites Incorporating Metakaolin. *Cement and Concrete Composites*, Vol. 108, No. April 2020.

52. Ling, Y., K. Wang, W. Li, G. Shi, and P. Lu. Effect of Slag on the Mechanical Properties and Bond Strength of Fly Ash-Based Engineered Geopolymer Composites. *Composites Part B: Engineering*, Vol. 164, No. February 2019, pp. 747–757.

53. Wang, S., and V. C. Li. Engineered Cementitious Composites with High-Volume Fly Ash. *ACI Materials Journal*, Vol. 104, No. 3, 2007, pp. 233–268.

54. Wang, Y., Z. Zhang, J. Yu, J. Xiao, and Q. Xu. Using Green Supplementary Materials to Achieve More Ductile ECC. *Materials*, Vol. 16, No. 6, 2019.

55. American Coal Ash Association. Production and Use Reports. *American Coal Ash Association*. https://www.acaa-usa.org/publications/productionusereports.aspx. Accessed Aug. 8, 2020.

56. Li, V. C., S. Wang, and C. Wu. Tensile strain-hardening Behavior or Polyvinyl Alcohol Engineered Cementitious Composite (PVA-ECC). *ACI Materials Journal*, Vol. 98, No. 6, 2001, pp. 483–492.

57. Yang, E., Y. Yang, and V. C. Li. Use of High Volumes of Fly Ash to Improve ECC Mechanical Properties and Material Greenness. *ACI Materials Journal*, Vol. 104, No. 6, 2007, pp. 620–628.

58. Yu, J., J. Lin, Z. Zhang, and V. C. Li. Mechanical Performance of ECC with High-Volume Fly Ash after Sub-Elevated Temperatures. *Construction and Building Materials*, Vol. 99, 2015, pp. 82–89.

59. Amin, M. N., M. Ashraf, R. Kumar, K. Khan, D. Saqib, S. S. Ali, and S. Khan. Role of Sugarcane Bagasse Ash in Developing Sustainable Engineered Cementitious Composites. Vol. 7, No. April 2020, pp. 1–12.

60. ASTM C 150/ C150M. Standard Specification for Portland Cement. *ASTM International, West Conshohocken, PA.*, 2017, pp. 1–8.

61. ASTM C778. Standard Specification for Standard Sand. *ASTM International, West Conshohocken, PA*, Vol. 14, 2017, pp. 1–3.

62. Degen, T., M. Sadki, E. Bron, U. König, and G. Nénert. The High Score Suite. *Powder Diffraction*, Vol. 29, No. May 2014, pp. S13–S18.

63. ASTM Standard C188-09. Standard Test Method for Density of Hydraulic Cement. *ASTM International*, No. C, 2009, pp. 1–3.

64. C128, A. S. Standard Test Method for Density, Relative Density (Specific Gravity), and Absorption of Fine Aggregate. *ASTM International, West Conshohocken, PA*, Vol. i, 2012, pp. 1–6.

65. Quarcioni, V. A., F. F. Chotoli, A. C. V. Coelho, and M. A. Cincotto. Indirect and Direct Chapelle's Methods for the Determination of Lime Consumption in Pozzolanic Materials. *IBRACON Structures and Materials Journal*, Vol. 8, No. 1, 2015, pp. 1–7.

66. Associação Brasileira de Normas Técnicas. NBR 15895 (2010). *Materiais Pozolanicos: Determinação Do Teor de Hidróxido de Cálcio Fixado—Método Chapelle Modificado*. Rio

de Janeiro, 2010.

67. ASTM Standard C311/C311M. *Standard Test Methods for Sampling and Testing Fly Ash or Natural Pozzolans for Use*. ASTM International, West Conshohocken, PA, 2017.

68. ASTM Standard C778. *Standard Specification for Standard Sand.* ASTM International, West Conshohocken, PA, 2017, pp. 1–5.

69. ASTM C109/109M. *Standard Test Method for Compressive Strength of Hydraulic Cement Mortars (Using 2-in. or [50-Mm] Cube Specimens).* ASTM International West Conshohocken, PA, 2016, pp. 1–10.

70. ASTM C311/C311M. *Standard Test Methods for Sampling and Testing Fly Ash or Natural Pozzolans for Use in Portland-Cement Concrete*. ASTM International, West Conshohocken, PA, 2005, pp. 204–212.

71. ASTM Standard C511. *Standard Specification for Mixing Rooms, Moist Cabinets, Moist Rooms, and Water Storage Tanks Used in the Testing of Hydraulic Cements and Concretes*. ASTM International, West Conshohocken, PA, 2019.

72. ASTM Standard C157/ C157M. *Standard Test Method for Length Change of Hardened Hydraulic-Cement Mortar and Concrete.* ASTM International, West Conshohocken, PA, 2017, pp 1-7.

73. ASTM C39/C39M. *Standard Test Method for Compressive Strength of Cylindrical Concrete Specimens.* ASTM International, West Conshohocken, PA, 2016, pp. 1–7.

74. Japan Society of Civil Engineers. Applications and Recommendations for Design and Construction of High-Performance Fiber Reinforced Cement Composites with Multiple Fine Cracks (HPFRCC) Testing Method. *Concrete Engineereing Series*, Vol. 82, 2008, pp. 6–10.

75. AASHTO T 358. S*tandard Method of Test for Surface Resistivity Indication of Concrete's Ability to Resist Chloride Ion Penetration*. American Association of State Highway and Transportation Officials, Washington, D.C., U.S.A, 2017.

76. ASTM C531-00. *Standard Test Method for Linear Shrinkage and Coefficient of Thermal Expansion of Chemical-Resistant Mortars, Grouts, Monolithic Surfacings, and Polymer Concretes*. ASTM International, West Conshohocken, PA, 2000.

77. ASTM 192/192M. *Standard Practice for Making and Curing Concrete Test Specimens in the Laboratory.* ASTM International, West Conshohocken, PA, 2018, pp. 1–8.

78. ASTM Standard C109/109M. *Standard Test Method for Compressive Strength of Hydraulic Cement Mortars ( Using 2-in . or [ 50-Mm ] Cube Specimens )*. ASTM International, West Conshohocken, PA, 2016.

79. ASTM C293/ C293M-16. *Standard Test Method for Flexural Strength of Concrete (Using Simple Beam With Center-Point Loading)*. ASTM International, West Conshohocken, PA, 2016.

80. ASTM Standard C192/C192M. *Standard Practice for Making and Curing Concrete Test*

*Specimens in the Laboratory*. ASTM International, West Conshohocken, PA, 2016.

81. Xu, Q., T. Ji, S. J. Gao, Z. Yang, and N. Wu. Characteristics and Applications of Sugar Cane Bagasse Ash Waste in Cementitious Materials. *Materials*, Vol. 12, No. 1, 2018, pp. 1–19.

82. ASTM C618. *Standard Specification for Coal Fly Ash and Raw or Calcined Natural Pozzolan for Use in Concrete.* ASTM International, West Conshohocken, PA, 2010, pp. 3–6.

83. Cordeiro, G. C., T. R. Barroso, and R. D. Toledo Filho. Enhancement the Properties of Sugar Cane Bagasse Ash with High Carbon Content by a Controlled Re-Calcination Process. *KSCE Journal of Civil Engineering*, Vol. 22, No. 4, 2018, pp. 1250–1257.

84. ASTM Standard C618. *Standard Specification for Coal Fly Ash and Raw or Calcined Natural Pozzolan for Use in Concrete*. ASTM International, West Conshohocken, PA, 2017.

85. Huang, F., H. Li, Z. Yi, Z. Wang, and Y. Xie. The Rheological Properties of Self-Compacting Concrete Containing Superplasticizer and Air-Entraining Agent. *Construction and Building Materials*, Vol. 166, 2018, pp. 833–838.

86. Łaźniewska-Piekarczyk, B. The Methodology for Assessing the Impact of New Generation Superplasticizers on Air Content in Self-Compacting Concrete. *Construction and Building Materials*, Vol. 53, 2014, pp. 488–502.

87. ACI Committee 212. *ACI 212.3 R-16 Report on Chemical Admixtures for Concrete*. American Concrete Institute, Farmington Hills, Michigan, 2016

88. Moseley, M. D., R. P. Ojdrovic, and H. J. Petroski. Influence of Aggregate Size on Fracture Toughness of Concrete. *Theoretical and Applied Fracture Mechanics*, Vol. 7, No. 3, 1987, pp. 201–210.

89. Nallathambi, P., B. L. Karihaloo, and B. S. Heaton. Effect of Specimen and Crack Sizes, Water / Cement Ratio, and Coarse Aggregate Texture upon Fracture Toughness of Concrete. *Magazine of Concrete Research*, Vol. 36, No. 129, 1984, pp. 227–236.

90. Li, M., and V. C. Li. Rheology, Fiber Dispersion, and Robust Properties of Engineered Cementitious Composites. *Materials and Structures*, Vol. 46, No. 3, 2013, pp. 405–420.

91. Liu, J., F. Han, G. Cui, Q. Zhang, J. Lv, L. Zhang, and Z. Yang. Combined Effect of Coarse Aggregate and Fiber on Tensile Behavior of Ultra-High Performance Concrete. *Construction and Building Materials*, Vol. 121, 2016, pp. 310–318.

92. Zhu, Y., Y. Z. Yang, and Y. Yao. Effect of High Volumes of Fly Ash on Flowability and Drying Shrinkage of Engineered Cementitious Composites. *Materials Science Forum*, Vol. 675 677, 2011, pp. 61–64.

93. Lepech, M. D., and V. C. Li. Water Permeability of Engineered Cementitious Composites. *Cement and Concrete Composites*, Vol. 31, No. 10, 2009, pp. 744–753.

94. Li, V. C., and E. H. Yang. *Self Healing in Concrete Materials*. Springer, Dordrecht, 2007.

95. Federal Highway Administration Research and Technology. *Thermal Coefficient Of Portland Cement Concrete*. Washington, D.C., U.S, 2016.

96. Mohamed Maalej, V. L., and Mohamed Maalej and Victor C. Li. Flexural/Tensile-Strength Ratio in Engineered Cementitious Composites. *Journal of Materials in Civil Engineering,* Vol. 6, No. 4, 1994, pp. 513–528.

# APPENDIX A: STATISTICAL ANALYSIS FOR COMPRESSIVE STRENGTH

## A.1 Statistical Analysis for Class S Mixtures

**Table A1. Class S concrete cylinders 28 days compressive strength one-way ANOVA results**

| Source | DF | Sum of Squares | Mean Square | F Value | Pr > F |
|---|---|---|---|---|---|
| Model | 4 | 787747.0667 | 196936.7667 | 12.99 | 0.0006 |
| Error | 10 | 151596.6667 | 15159.6667 | | |
| Corrected Total | 14 | 939343.7333 | | | |

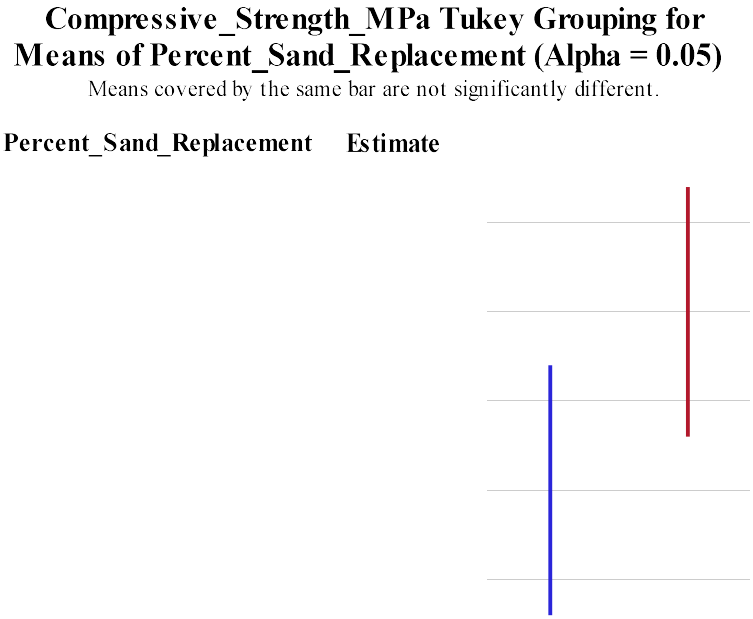


**Figure A1. Class S concrete cylinders 28 days compressive strength Tukey grouping for means of index ($\alpha$ = 0.05)**

## A.2 Statistical Analysis for Class C Mixtures

**Table A2. Class C concrete cylinders 28 days compressive strength one-way ANOVA results**

| Source | DF | Sum of Squares | Mean Square | F Value | Pr > F |
|---|---|---|---|---|---|
| Model | 4 | 777.9003 | 194.4750 | 471.10 | <.0001 |
| Error | 10 | 4.1280 | 0.4128 | | |
| Corrected Total | 14 | 782.0283 | | | |

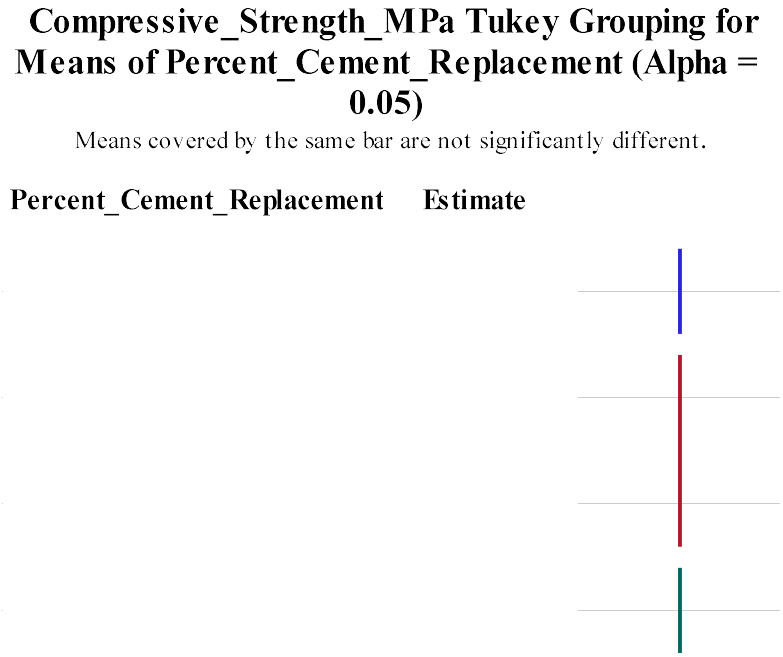


**Figure A2. Class C concrete cylinders 28 days compressive strength Tukey grouping for means of index ($\alpha$ = 0.05)**

# APPENDIX B: STATISTICAL ANALYSIS FOR TENSILE STRENGTH AND TENSILE STRAIN CAPACITY

## B1. Statistical Analysis for Tensile Strength of Class S Mixtures

**Table B1. Class S mixtures 28 days tensile strength one-way ANOVA results**

| Source | DF | Sum of Squares | Mean Square | F Value | Pr > F |
|---|---|---|---|---|---|
| Model | 4 | 2.31698347 | 0.57924587 | 4.18 | 0.0099 |
| Error | 25 | 3.46096733 | 0.13843869 | | |
| Corrected Total | 29 | 5.77795080 | | | |

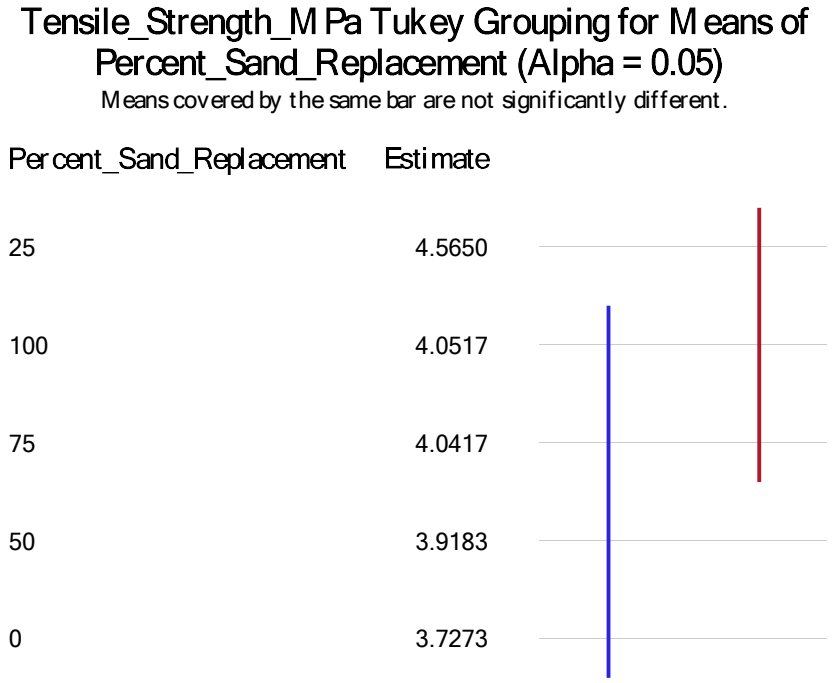


**Figure B1. Class S mixtures 28 days tensile strength Tukey grouping for means of index ($\alpha$ = 0.05)**

## B2. Statistical Analysis for Tensile Strain Capacity of Class S Mixtures

**Table B2. Class S mixtures 28 days tensile strain capacity one-way ANOVA results**

| Source | DF | Sum of Squares | Mean Square | F Value | Pr > F |
|---|---|---|---|---|---|
| Model | 4 | 34.0483467 | 8.5120867 | 3.16 | 0.0311 |
| Error | 25 | 67.2868833 | 2.6914753 | | |
| Corrected Total | 29 | 101.3352300 | | | |

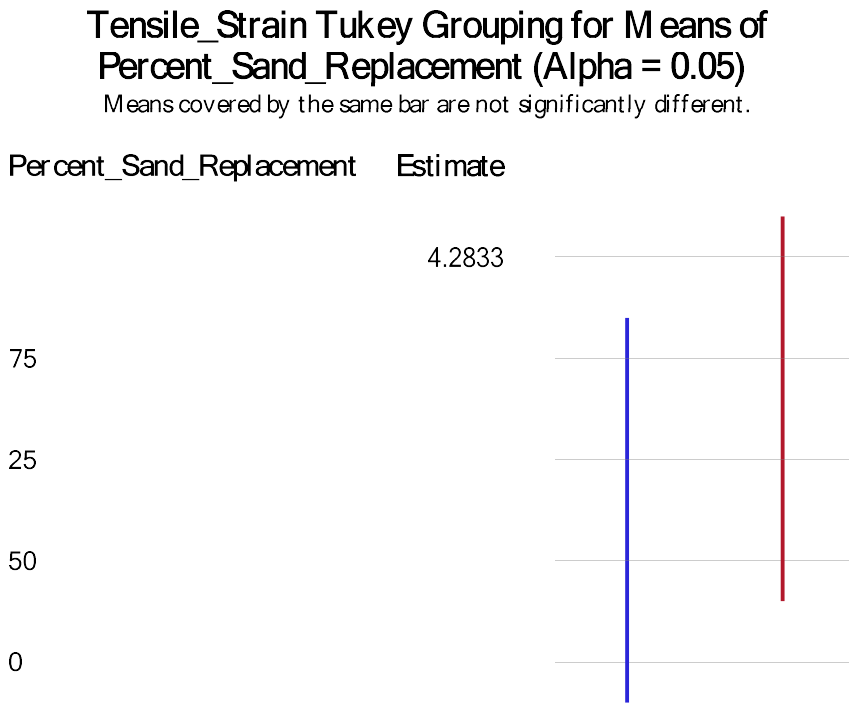


**Figure B2. Class S mixtures 28 days tensile strain capacity Tukey grouping for means of index ($\alpha$ = 0.05)**

## B3. Statistical Analysis for Tensile Strength of Class C Mixtures

**Table B3. Class C mixtures 28 days tensile strength one-way ANOVA results**

| | | | | | |
|---|---|---|---|---|---|
| Model | 3 | 7.53313861 | 2.51104620 | 8.30 | 0.0010 |
| Error | 19 | 5.74846000 | 0.30255053 | | |
| Corrected Total | 22 | 13.28159861 | | | |

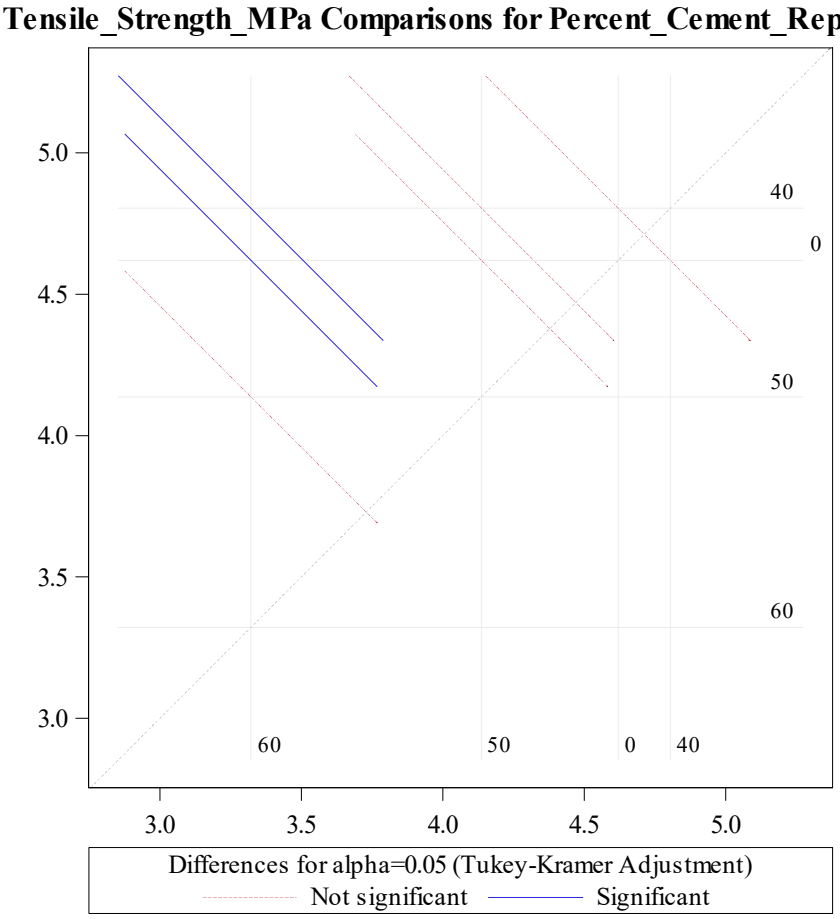


**Figure B3. Class C mixtures 28 days tensile strength Tukey grouping for means of index ($\alpha$ = 0.05)**

## B4. Statistical Analysis for Tensile Strain Capacity of Class C Mixtures

**Table B4. Class C mixtures 28 days tensile strain capacity one-way ANOVA results**

| | | | | | |
|---|---|---|---|---|---|
| Model | 3 | 0.20514377 | 0.06838126 | 2.88 | 0.0627 |
| Error | 19 | 0.45038667 | 0.02370456 | | |
| Corrected Total | 22 | 0.65553043 | | | |

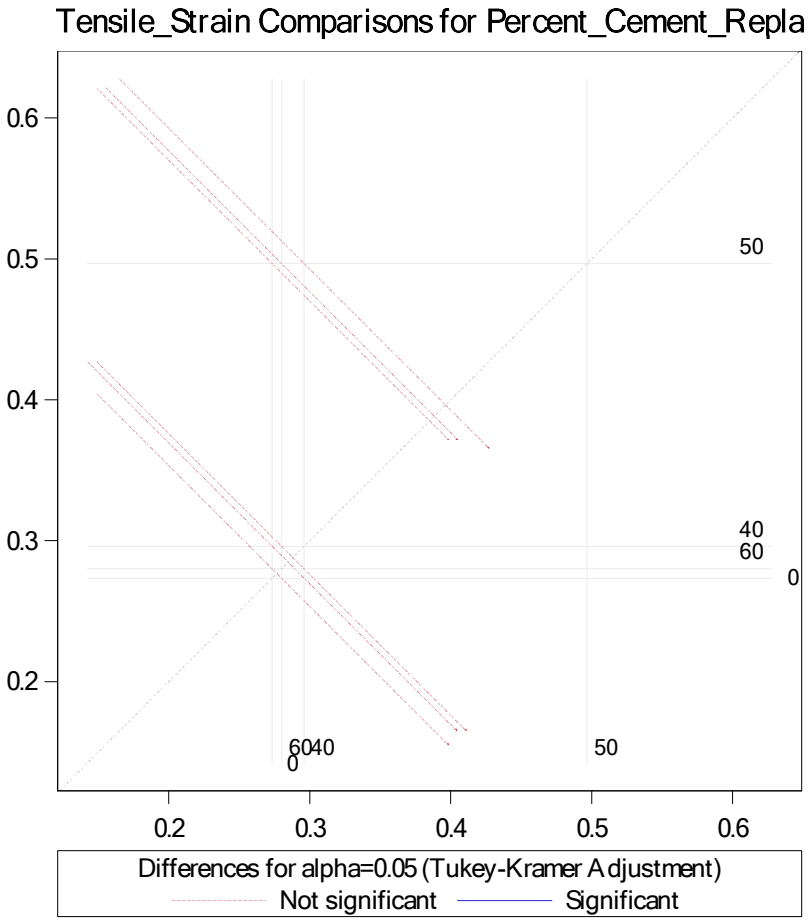


**Figure B4. Class C mixtures 28 days tensile strain capacity, Tukey grouping for means of index ($\alpha$ = 0.05)**